Probabilistic-based method for realizing safe and reliable mechatronic systems

Von der Fakultät für Ingenieurwissenschaften,

Abteilung Maschinenbau und Verfahrenstechnik der

Universität Duisburg-Essen

zur Erlangung des akademischen Grades

eines

Doktors der Ingenieurwissenschaften

Dr.-Ing.

genehmigte Dissertation

von

Kai-Uwe Dettmann
aus
Düsseldorf

Gutachter: Univ.-Prof. Dr.-Ing. Dirk Söffker
Univ.-Prof. Dr.-Ing. Claus-Peter Fritzen
Tag der mündlichen Prüfung: 21. Dezember 2011

Acknowledgements

The research which yielded the results presented in this thesis was carried out at the Chair of Dynamics and Control (SRS) at the University of Duisburg-Essen. I would like to acknowledge my debt to those who have helped me - directly and indirectly - on my path towards completing this work and towards finding solutions to other important things in life.

In particular, I would like to thank my supervisor Univ.-Prof. Dr.-Ing. Dirk Söffker for offering me the opportunity to work at his chair. As research sometimes works in mysterious ways and the way towards the goal is not always straight, his motivation, visionary ideas, and knowledge have opened up new paths towards novel insights and enabled me "to boldly go where no man has gone before." I am very grateful for his enthusiasm, support, and guidance, all of which make him a great mentor.

I would also like to thank Univ.-Prof. Dr.-Ing. Claus-Peter Fritzen from the University of Siegen for taking the place of my second supervisor. His interest and immense insightful knowledge in the area of structural health monitoring helped to improve the value of this thesis.

I want to thank Univ.-Prof. Dr.-Ing. Klaus Solbach for enhancing my electrical knowledge, especially in the field of high frequency applications and piezo-electric ceramics.

I would also like to thank my colleagues Dr.-Ing. Elmar Ahle, Dr.-Ing. Dennis Gamrad, Dipl.-Ing. Frank Heidtmann, Dipl.-Ing. Marcel Langer, M.Sc. (USA), Dr.-Ing. Yan Liu, and Lou'i Al-Shrouf, M.Sc. - not only for the interesting discussions, valuable contributions, coffee breaks, and philosophies, but also for contributing to such an inspiring and pleasant working atmosphere.

I would like to thank my students who supported my work, Dipl.-Ing. (FH) Bärbel Egenolf-Jonkmanns, M.Sc., Dipl.-Ing. Sebastian Esch, cand. ing. Georg Hägele, Dipl.-Ing. Xin Jin, Felix Kleinherbers, B.Sc., Jenni Ravelin, B.Sc., cand. ing. Oliver Sacher, and Dipl.-Ing. Xuexuan Xu.

Thanks to Yvonne Vengels and Doris Schleithoff who made all administrative issues very easy. Likewise, I would like to thank Kurt Thelen for his support with fundamental, non-scientific work. In addition, I really enjoyed the non-scientific conversations.

In addition, I would like to thank Dipl.-Übersetzerin Esther Wiemeyer for proofreading relevant parts of my manuscript.

I thank my mother Regina for her faith and love. She provided me with the roots to grow and always supported my decisions.

And, last but not least, I am very thankful to my patient and loving wife, Isabel, who tolerated my moods, supported me at any time and gave me the strength and belief to finish this work. ¡Te quiero muchísimo, mi vida! Y, Gracias por Pablo!

"Sólo tu corazón caliente, y nada más.", *Deseo* [GLGP08]

Duisburg, January 2012.

Contents

1 Introduction

For many years now, machineries have been used in industrial processes and detached humans from the direct production process. Modern machines are used for a broad range of tasks, from simple to highly complex. While automation of technical processes used to be exclusively mechanically based in the past, novel machines incorporate the fields of applied mechanics, electronics, and informatics.

Mechatronics, a cross-discipline branch of engineering, combines these three traditional approaches (see Figure 1.1 for a schematic overview).

Various definitions of Mechatronics have been developed over time, each of which emphasizes a slightly different origin and aim. In [Aus96], Mechatronics is "the application of complex decision making to the operation of physical systems". One fact that is underlined is that Mechatronics is more than a simple reaction to stimuli. It involves complex decision-making processes, for example by artificial neural networks or fuzzy approaches. The aspect that the mechanical and electrical part of the system need to be developed simultaneously is discussed in [Ise99]. In analogy to [Aus96], the ability to integrate sophisticated information processing techniques is presented. The novel aspect of including fault detection and diagnosis features directly in the system is explained in detail.

Since a mechatronic system is thus capable of perceiving, processing, and responding to external stimuli, further development efforts focus on detecting and reacting appropriately to changes in systems' behavior. This aspect is addressed in [FK09], "where sensor networks, actuators and computational capabilities are used to enable a structure to perform a self-diagnosis with the goal that this structure can release early warnings about a critical health state, locate and classify damage or even to forecast the remaining life-time."

Thus, existing (usually mechanic) systems are extended to mechatronic systems in order to improve their functionality. The informational infrastructure is then used for sophisticated strategies, such as avoiding major damage to the system, environment, and operator by fault diagnosis methods. The results of the subsequent fault diagnosis are commonly used for preventive maintenance measures and only rarely for targeted compensation by appropriate countermeasures. Furthermore, the additional electronic and informational components directly lead to an increased complexity on multiple levels due to additional sensors, numerous inner and outer dependencies, etc., and thus to a higher error-proneness.

1.1 Motivation

Due to increasing economic, ecological and safety requirements, a highly reliable operation in conjunction with high availability has become the predominant goal in industry. Mechatronic systems are therefore developed in order to improve the efficiency of the process without compromising for reliability.

Depending on the industrial sector and product, nowadays maintenance strategies consider worst-case scenarios for the occurrence of (premature) failures. Maintenance works are carried out at predetermined intervals (periodical inspections) and are intended to reduce

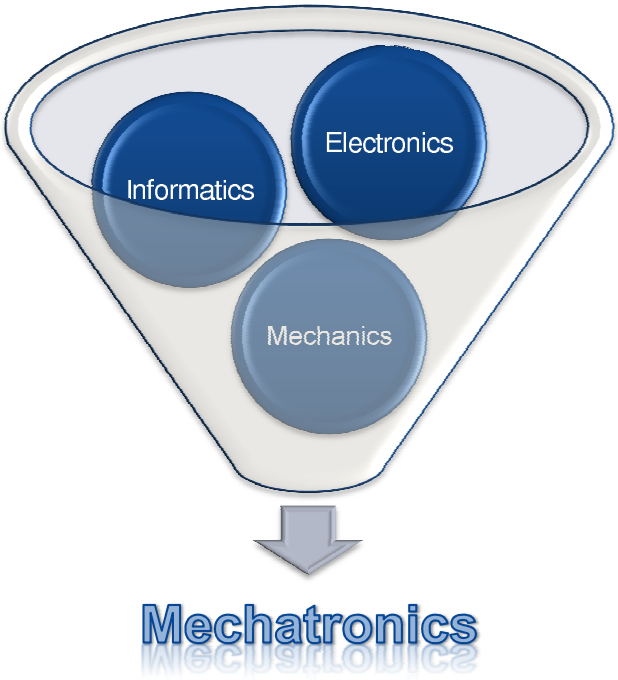

Figure 1.1: Scheme of Mechatronics

the probability of failure or the degradation of the functioning of an item [IEC 60050-191]. Consequently, systems tend to have an excessive safety margin and/or need to be maintained before they approach their planned (individual) end of life. In fact, healthy and costly components are replaced and put out of service. These preventive maintenance strategies (Reliability Centered Maintenance, RCM) are time-consuming. In most cases, RCM is used especially for systems where failures lead to human casualties and/or immense financial losses. While a highly reliable and safe operation is guaranteed, the life-cycle costs are increased and the availability is reduced due to frequent inspection intervals and down-times.

In case of less safety-relevant systems, novel maintenance strategies replace a critical system as close to (or even after) its (individual) failure as possible. One main issue is to make a timely maintenance decision, based on the on-line deterioration information. This concept is called Condition-Based Maintenance (CBM) and aims at calculating relevant information about the actual deterioration and further reliability characteristics, such as actual damage, probability of failure, remaining useful life, etc. The added value is that real, actual field operation is considered on-line. In [Fri10] this fact is proposed to offer "many opportunities for prolonging the life of a structure by the early detection of damage."

The goal of all maintenance strategies is to realize a reliable operation of a system, usually by replacing critical components.

The long-term vision is to operate a system in such a way that the deterioration is reduced, the useful life and availability is increased (maximized), and maintenance actions are only performed if necessary. In order to address these competing objectives (enhanced safety, improved reliability, reduced life-cycle costs), a holistic view of the deterioration behavior due to the operation of the (individual) system needs to be developed. This method has to include two aspects: estimating the effect of operational parameters on the individual

state-of-deterioration and the state-of-deterioration itself.

In [WS04, WS05] a generic simulation model is presented that calculates the reliability of a component on the basis of its utilization and incorporates assumptions about its future utilization. This is particularly important as the deterioration due to operation can vary depending on the actual state-of-deterioration, initial deterioration, etc. Thus, both the history of stress and actual and future operation have to be taken into account to predict the deterioration development under possible operation scenarios. Based on literature data, the simulation results indicate that reliability can be improved by modifying the operation in a deterioration-adaptive way.

This thesis gives a detailed explanation of this aspect, which helps to ensure an optimal, safe, and reliable operation of mechatronic systems by reliability-enhancing strategies. Thus, this thesis realizes the vision of a deterioration-adaptive algorithm by means of two real, different comprehensive systems.

1.2 Structure of Thesis

The Chapter 2 contains the reliability-related, relevant definitions. Special attention is given to probabilistic aspects, as these reflect the stochastic nature of failure. Afterwards, the common idea of fault detection, fault diagnosis, and fault prognosis are introduced.

In Chapter 3, the generic Safety and Reliability Control Engineering (SRCE)-concept [RS96, SR97] is introduced in detail. Based on this concept and preliminary works on it, the single modules are developed and discussed in detail. The adaptive probabilistic-based deterioration model realizes the continuously adaptive, time-variant, probabilistic correlation between deterioration-proportional information and the most probable deterioration. Appropriate strategies for modifying the operation of the systems (by limiting disproportionately high damaging situations, proposing alternative strategies etc.) are derived and proposed on the basis of the obtained deterioration estimations.

The application of the developed modules is the core issue of this thesis. It is introduced and discussed in Chapter 4 for a mechanical system failing due to mechanical wear (abrasive wear) and in Chapter 5 for an electro-chemical system failing due to capacity fade.

In Chapter 4, the main focus is on the newly developed measurement chain and related evaluation of deterioration-inherent quantities. As the deterioration process is highly nonlinear, solely signal-based fault detection and diagnosis approaches are discussed and appropriate, deterioration-specific countermeasures for reliability improvements are shown.

In Chapter 5, a model-based fault detection and diagnosis strategy is developed and novel aspects for appropriate deterioration countermeasures are explained in detail.

Finally, Chapter 6 reviews the newly developed solutions and gives an outlook on future work.

2 Theoretic Background

In this chapter, the main terms and most important methods as well as their theoretical foundations in relation to reliability engineering are introduced and embedded in the research context. The main objectives of this thesis are to analyze actual reliability and to act appropriately to improve the overall reliability of the considered system.

In Section 2.1, basic definitions from international standards are given to provide a uniform basis of terminology.

Following the description of the main characteristics, several quantitative measures for the reliability of non-repairable systems are detailed in the subsequent sections. In addition, the common methods for reliability analysis are proposed in Section 2.2. The main aim of these methods is to identify the main causes of failure, as influenced by the operation of the particular system. Special attention is given to probabilistic approaches due to the stochastic nature of failures and/or operational conditions.

Subsequently, methods for fault detection and diagnosis are discussed. In Section 2.4, the relevant methods for fault detection are introduced. Afterwards, general ideas for fault diagnosis are introduced and combined with the detection algorithms. Once the relevant aspects of reliability are evaluated, strategies for the investigation of future progress are introduced in Section 2.6.

2.1 Definitions

To unify the manifold understandings of relevant terms used throughout this work, the definitions for the most important terms are given. As this thesis reports on technical systems, the reliability of software and/or humans is not considered.

Load and Stress
In this thesis, load is understood as a measurable quantity, acting on a system. In subsequent sections, loading is used as a synonym for the operational conditions, controlling the operation of the particular system. The individual reaction on loading is denoted by the term stress, which is an individual quantity and hence, system- and time-dependent.

Maintenance
"The combination of all technical and administrative actions, including supervision actions, intended to retain an item in, or restore it to, a state in which it can perform a required function", [IEC 60050-191]. The scope of this thesis is to develop a strategy to reduce preventive maintenance measures by operating the considered system deterioration-optimal. As this is not part of the (classical) definition, maintenance itself is not discussed in detail but is the subsequent step in a holistic view of all availability-improving strategies.

Failure
In [IEC 60050-191], a failure is defined as "the termination of the ability of an item to perform a required function", or (more general) the "permanent interruption of a system

ability to perform a required function under specific operating conditions", [BKLS06]. The cause for the interruption due to aging is covered by these definitions but neglected in this thesis. Only failures due to loading are considered in the following. The more relevant term of a wear-out failure is defined by [EN 13306] as "a failure whose probability of occurrence increases with the operating time or the number of operations of the item and the associated applied stress [load]." The hazard function during wear-out is increasing, the remaining useful life (RUL) is decreasing [Ban09].

Damage, Degradation, and Deterioration
In [WDB04], the term damage is defined as a state "when the structure is no longer operating in its ideal condition but can still function satisfactorily, i.e. in a sub-optimal manner." The definition is particularized by [SFH+04] as "damage is not meaningful without a comparison between two system states, one is often an initial or undamaged state." The term degradation is defined by [IEC 60050-191, EN 13306] as "a detrimental change in physical condition, with time, use or external cause. Degradation may lead to a failure." The term deterioration is analogous defined as a "diminish or impair in quality" and used synonymical for degradation.

Fault
In [VDI 3452], a fault "of an item can be considered to be a state in which at least one parameter of an item lies outside of the specified tolerance." By neglecting faults induced during the design phase, construction phase, manufacturing phase, etc., faults do only occur due to deterioration and hence due to operation. In this thesis, a fault is understood as a direct consequence of a deterioration process.

Reliability
"The ability of an item to perform a required function under given conditions for a given time interval", [IEC 60050-191]. According to [Nac05], reliability is the "probability that a device properly performs its intended function over time when operated within the environment for which it was designed." The main difference to [IEC 60050-191] is that [Nac05] stresses the stochastic aspect of the term reliability. In this thesis, the definition given by [Nac05] is extended such that reliability is understood as the probability that a device properly performs its intended function over a given time interval when operated under given, technically permitted conditions within the environment for which it was designed for.

Redundancy
In engineering sense, "the existence of more than one means for performing a required function", [EN 13306]. Redundancy is the simplest way to increase the reliability of a system. A distinction is made between active redundancy (pure and shared parallel structures), k-out-of-n systems, and standby redundancy. The latter category is subdivided into cold (stand-by, passive) ([Coi01, IEC 60050-191]), warm and hot redundancy [FCGC01]. The main drawbacks of redundant mechatronic systems are higher costs and weight due to doubly present components. Even redundant software needs an appropriate hardware infrastructure (higher computing performance, redundant power supply, etc.). In this thesis, redundancy is not considered as a reasonable method for reliability improvement as the deterioration and hence the failure cause is not considered and appropriately reduced.

Availability
"The ability of an item to be in a state to perform a required function under given conditions at a given instant of time or over a given time interval [...]", [IEC 60050-191, EN 13306]. As an increasing reliability is accompanied by an increasing availability, the latter characteristic is not explicitly followed up.

Dependability
Dependability is defined in [IEC 60050-191] as "the ability to perform as and when required". The standard [EN 13306] subsequently states that dependability covers its influencing factors "reliability, fault-tolerance, recoverability, integrity, security, maintainability, durability, and maintenance support." The term therefore is a generic term that summarizes different quantities, namely reliability (referring to "as required"), maintainability and availability ("when required"). Throughout this thesis, only reliability-relevant aspects are analyzed. Other failure-preventive strategies are not considered, e. g., scheduled maintenance.

Safety
According to [MIL-STD], safety is defined as the absence of conditions "that can cause death, injury, occupational illness, or damage to or loss of equipment or property, or damage to the environment." In this thesis, only safety aspects are considered that are directly influenced by operation. Faults due to these operation are forced and desired but must not lead to any casualties or potential threats to health, life, and environment. Hazard to the operational safety, e. g., by disregarding of barriers, safety regulations, etc., are excluded from the following considerations. Hence, a safe operation is obtained if the operating conditions do lead to a controlled fault without causing any harm to human and machine.

2.2 Reliability Analysis

According to [VDI 4008], reliability analysis is the generic term for several methods (based on logical and/or mathematical models) that reveal, e. g., enhancement potentials about reliability characteristics. As introduced, a reliable (non-repairable) system is obtained if it performs its intended function over a given time interval at a high probability. Since reliability is concerned with probabilities, the relevant aspects of probability are introduced at the outset. Based on this, the mathematical description of reliability-related characteristics and common methods for reliability analysis of technical systems are discussed in Section 2.2.2.

2.2.1 Probability Distribution

The probability denotes the belief that an outcome of an experiment will occur. The individual outcome (result of an experiment) is denoted by x_i. All possible realizations (output quantities) of x_i are indicated by the sample space $\Omega = \{x_1, x_2, ..., x_n\}$. As all outcomes x_i are real-valued, positive (life time is described by a real value), and finite, so the sample space Ω is. In [BSMM05], the theory of probabilities is detailed.

For many applications, the evaluation of the probability that a realized quantity X, defined on the sample space Ω, is within a predefined range, is of interest. The probability distribution of the real-valued random variable X in dependency on the upper interval limit

x is given by

$$\Pr(X \leq x) = F(x) \text{ , with } -\infty \leq x \leq +\infty \text{ .} \tag{2.1}$$

For practical calculation, the frequency distribution of all possible (experimentally derived) realizations x_i of the sample space Ω is required. This distribution is denoted by $f(\,\cdot\,)$ and named as the Probability Density Function (PDF).

In combination with Equation (2.1), the Cumulative Distribution Function (CDF) is expressed as

$$\Pr(X \leq x) = F(x) = \int_{-\infty}^{x} f(\tau) d\tau \text{ .} \tag{2.2}$$

In this context, the mean (or expected) value of the random variable X is defined as

$$\mathrm{E}(X) = \mu = \int_{-\infty}^{+\infty} x f(x) dx \text{ .} \tag{2.3}$$

In addition, the variance is defined as

$$\sigma^2 = \int_{-\infty}^{+\infty} (x-\mu)^2 f(x) dx \text{ .} \tag{2.4}$$

To evaluate the probability of an outcome X, an appropriate PDF has to be fitted (from experiments, etc). For many applications and quantities, the obtained distribution function reveals a characteristic shape. The majority of different experiments and outcomes can therefore be covered by standard distribution functions, adapted in shape by specific parameters. The main representatives of typical distribution functions are detailed in the following.

Normal Distribution

If the outcome X is distributed according to

$$\Pr(X \leq x) = F(x) = \frac{1}{\sigma\sqrt{2\pi}} \int_{-\infty}^{x} \exp\left(-\frac{(\tau-\mu)^2}{2\sigma^2}\right) d\tau \text{ ,} \tag{2.5}$$

then X is normally distributed.

The mean value of the distribution is defined by the parameter μ, according to Equation (2.3). The parameter σ^2 represents the variance of the outcome X.

The PDF of the normal distribution is

$$f(\tau) = \frac{1}{\sigma\sqrt{2\pi}} \exp\left(-\frac{(\tau-\mu)^2}{2\sigma^2}\right) . \tag{2.6}$$

For the special case with $\mu = 0$ and $\sigma = 1$, the Gauss distribution

$$f(\tau) = \frac{1}{\sqrt{2\pi}} \exp\left(-\frac{\tau^2}{2}\right) . \tag{2.7}$$

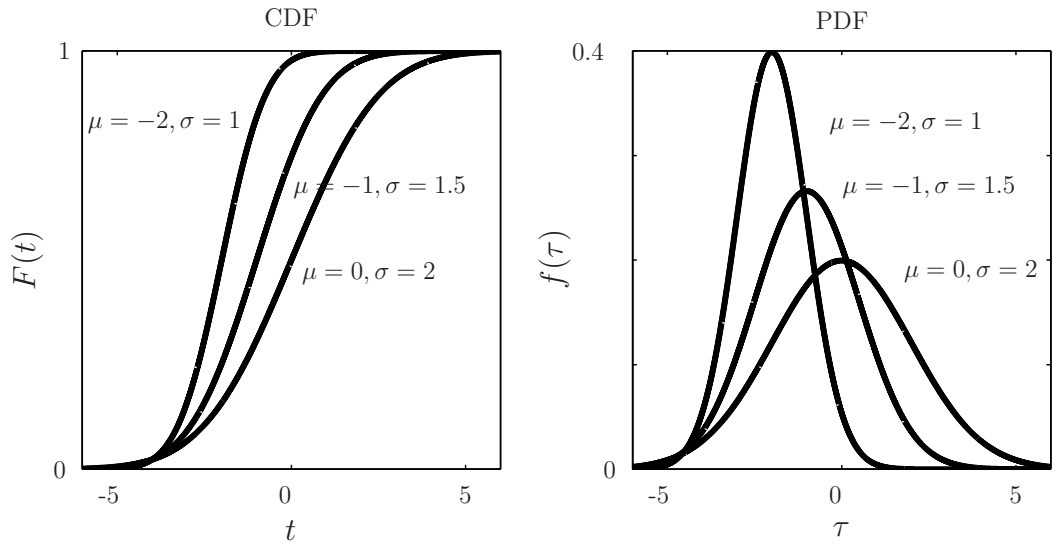

Figure 2.1: Different shapes of normal distribution function in dependency on parameters μ and σ

is obtained.

The principle shapes of the CDF and the corresponding PDF in dependency on different parameters μ and σ are depicted in Figure 2.1.

Weibull Distribution

In [Wei51], a distribution function for describing the life time of technical systems, especially for systems under fatigue, is introduced. The distribution function with the two parameters α and β is

$$F(x) = 1 - \exp\left(-\frac{x}{\beta}\right)^{\alpha} \quad x \geq 0, \alpha > 0, \beta > 0 \tag{2.8}$$

with β as the scale parameter and α describing the shape parameter or Weibull modulus (for material strength investigations). By choosing the parameter α appropriate, other distribution functions are obtained, e. g., for $\alpha = 1$ the exponential distribution, where $\alpha = 2$ reveals the Rayleigh distribution, as depicted in the left plot of Figure 2.2.

The PDF of the two parameter Weibull distribution is described by

$$f(\tau) = \frac{\alpha}{\beta}\left(\frac{\tau}{\beta}\right)^{\alpha-1} \exp\left(-\frac{\tau}{\beta}\right)^{\alpha} \tag{2.9}$$

as depicted in the right plot of Figure 2.2.

The modal value

$$\widehat{f}(x) = \beta\frac{\alpha - 1}{\alpha}^{\frac{1}{\alpha}} \tag{2.10}$$

describes the maximum value of the considered PDF.

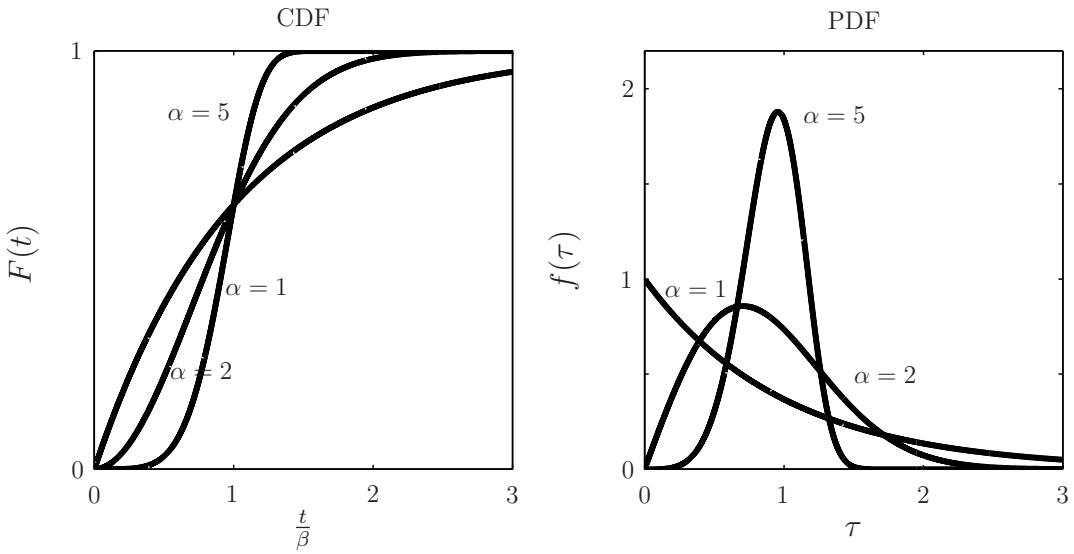

Figure 2.2: Different shapes of two parameter Weibull function in dependency on parameter α; $\beta = 1$

Beside the Weibull distribution with two parameters, a third parameter γ can be introduced to adapt the distribution additionally in location. The CDF with three parameters is described by

$$F(x) = 1 - \exp\left(-\frac{x-\gamma}{\beta}\right)^{\alpha} \quad x \geq 0, \alpha > 0, \beta > 0, -\inf < \gamma < \inf \ . \tag{2.11}$$

Accordingly, the PDF for three parameters is given by

$$f(\tau) = \frac{\alpha}{\beta}\left(\frac{\tau-\gamma}{\beta}\right)^{\alpha-1} \exp\left(-\frac{\tau-\gamma}{\beta}\right)^{\alpha} \ . \tag{2.12}$$

Miscellaneous
Apart from the above mentioned functions, the Γ distribution, the (log)normal distribution, the χ^2 distribution, and exponential distribution (Weibull distribution with $\alpha = 1$) are other important functions. Further details are given in [BSMM05, RH04].

2.2.2 Reliability Characteristics

From the definition given in Section 2.1, the mathematical formulation of reliability is given as

$$R(t) + F(t) = 1 \ , \tag{2.13}$$

with t denoting the (period of) time, and $F(t)$ denoting the complementary function to reliability, which describes the failure distribution (probability of failure, see Section 2.2.1). The values of $R(t)$ and $F(t)$ lie within the interval $[0, 1]$, where a value of 0 for $R(t)$ indicates a never-working system and $R(t) = 1$ a never-failing system [DW92, Wol08].

Hence, the reliability depends on the considered time interval $[0, t]$ and on the particular failure distribution function $F(t)$, which in turn depends on the operating conditions. The failure rate

$$\lambda(t) = \frac{f(t)}{R(t)} \,, \tag{2.14}$$

is therefore considered to describe the change of the reliability with time and operating conditions.

Rewriting Equation (2.14) with regard to Equation (2.13) and according to the relation of Equation (2.2), the failure rate is

$$\begin{aligned} \lambda(t) &= \frac{\frac{d}{dt}F(t)}{R(t)} \\ &= \frac{\frac{d}{dt}(1 - R(t))}{R(t)} \\ &= -\frac{d}{dt} \ln R(t) \,. \end{aligned} \tag{2.15}$$

In turn, the reliability is obtained as

$$R(t) = \exp\left(- \int_0^t \lambda(\tau) d\tau \right) \,. \tag{2.16}$$

In analogy to the correlation between the particular probability distribution function $f(t)$ and the cumulative density function $F(t)$, the cumulative failure rate

$$\Lambda(t) = \int_0^t \lambda(\tau) d\tau \tag{2.17}$$

is obtained.

To describe the depicted behavior mathematically (typically by the Weibull distribution), a piecewise description is chosen. In dependency on the particular phase, a specific set of parameters for α and β is chosen. In Equation 2.18 the phase-specific formulae are given.

$$\lambda(t) = \begin{cases} \frac{\alpha}{\beta}\left(\frac{t}{\beta}\right)^{\alpha-1} & t \leq t_1, \alpha < 1 \\ \text{const.} & t_1 < t < t_2 \\ \frac{\alpha}{\beta}\left(\frac{t}{\beta}\right)^{\alpha-1} & t \geq t_2, \alpha > 1 \end{cases} \tag{2.18}$$

According to [DW92], a typical representative of an exemplary, empirically failure rate $\lambda(t)$ is depicted in Figure 2.3 as the so called bathtub curve. It is commonly used to exemplary visualize the three major phases of system failure. Within region I, systems have a high probability to fail. This region is called the early failure region or run-in phase. In region II the useful life is obtained; later in Chapter 3, this phase will be denoted as the phase of

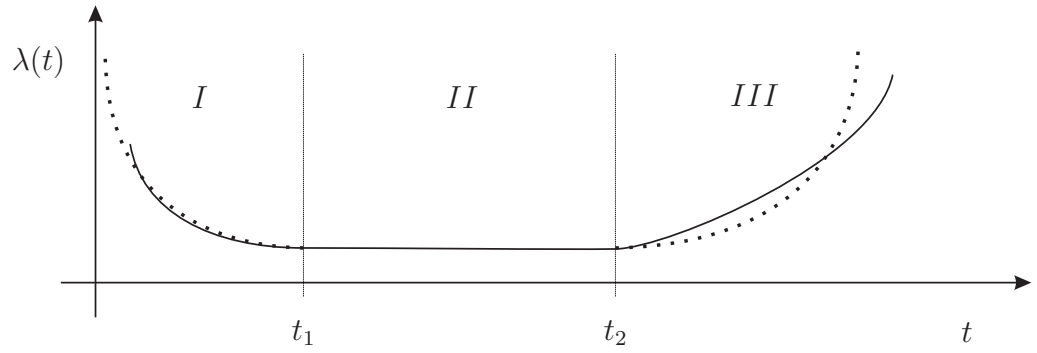

Figure 2.3: Bathtube curve

permanent wear. The failure rate within this region is ideally constant until the wear-out failure region *III* begins. Within the last region, the systems fail due to the exceedance of their designated life time. For the given figure, the result of the approximation are indicated by dotted lines for each phase. In dependency on the considered system and/or domain, the failure rate and thus, the curve shape changes significantly. Hence, the observed failure rate of an entire population of systems over time has to be approximated by the set of parameters.

In summary, reliability states an estimate about the probability of failure within a considered time interval, based on the distribution of measured failures and assumptions about the future usage.

The individual distribution is obtained by comprehensive tests or existing data bases (from literature). The military handbook [MIL-HDBK] offers a data base to describe the failure rate of electronic components. In [MIL-NSWC], the results of comprehensive studies (reliability prediction analysis) with mechanical systems are given. Subsidiary information (from manufacturer, expert knowledge, burn-in tests, environmental stress screening) about the failure distribution of the considered system complete the foundation of further investigations.

The aspect about the future usage is handled by various considerations, e. g., prospective system operation under standard, worst-case, or best-case operating conditions, etc. Beside the specification of the exact trajectory of the operating parameters, sophisticated information about the future usage can be stated, e. g., requirements for minimum life time, maximum reliability until a time instant, maximum availability, etc.

2.2.3 Reliability Methods

Based on these information, appropriate methods are available to investigate the future reliability of a system. The common way in reliability analysis starts with a model of the interdependencies (consisting of its function-relevant components). Subsequently, the individual failure distributions are estimated, based on the above mentioned strategies for failure distributions. For repairable components, Markov methods are commonly used. For non-repairable components, the Reliability Block Diagram (RBD) is usually more suitable to describe the function of a system. The symbols, terms and definitions are chosen according to [DIN EN 61078]. The RBD of a sample system, consisting of an architecture with components in serial and parallel connection, is depicted in Figure 2.4.

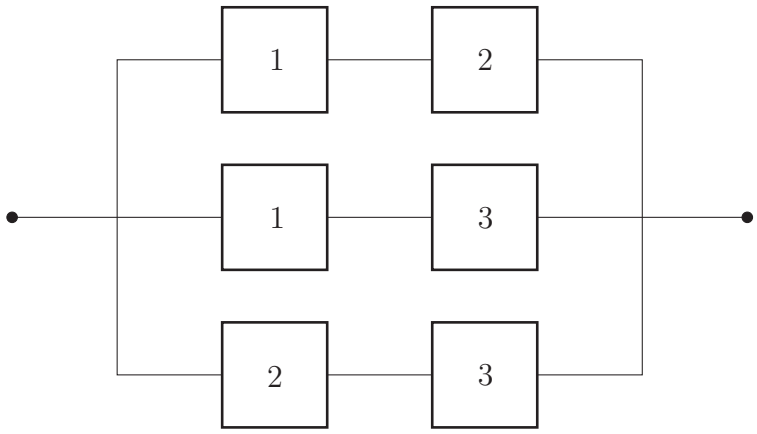

Figure 2.4: Reliability Block Diagram for a sample system

From this representation, the critical path, the most unreliable component, etc. can be identified. The exemplary calculation of a non-repairable system depicted in Figure 2.4 according to [RH04] is briefly shown in the following to illustrate the general scheme of reliability calculation.

The structure function of the depicted 2-out-of-3 structure is

$$\begin{aligned} \phi(p(t)) &= p_1(t)p_2(t) \cup p_1(t)p_3(t) \cup p_2(t)p_3(t) \\ &= p_1(t)p_2(t) + p_1(t)p_3(t) + p_2(t)p_3(t) - 2p_1(t)p_2(t)p_3(t) \ , \end{aligned} \tag{2.19}$$

with p_i denoting the individual failure probability of each component i, $p_i = 1$ denoting a fully functioning component, whereas $p_i = 0$ denotes a failed component at the considered time instant t. Hence, the structure function $\phi(p(t))$ is equal to 0 if at least 2 components failed.

The survival function results to

$$R_S(t) = R_1(t)R_2(t) + R_1(t)R_3(t) + R_2(t)R_3(t) - 2R_1(t)R_2(t)R_3(t) \ . \tag{2.20}$$

For simplicity, the reliability of each component is assumed as identical $R_i(t) = R(t)$ for $i = 1 \ldots 3$. With Equation (2.16), the reliability of the 2-out-of-3 system is

$$R_S(t) = 3\exp(-2\lambda t) - 2\exp(-3\lambda t) \ . \tag{2.21}$$

Hence, suggestions about improvements are derived in terms of more reliable components, redundancy structures, less components, etc. The effect of these actions can be calculated and appropriate measures for reliability improvements can be initiated. These suggestions are basically helpful during the design phase, revision activities ("facelift" in automotive sector), or maintenance planning. For an existing system, only the latter aspect forms a feasible solution for classical reliability improvement. In [VDI 4008, RH04], a comprehensive introduction to the most relevant reliability methods are given, namely Fault Tree Analysis (FTA), Markov chain, and Bayesian models. For comprehensive studies on reliability determination and novel scientific applications, the European Safety and Reliability Association (ESRA) reveals an exhaustive collection of further methods and approaches to reliability

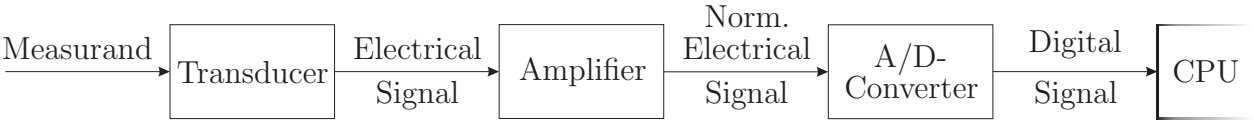

Figure 2.5: Basic components of general measurement chain

engineering and related topics in their annual conferences ESREL. Additionally, the International Journal of Reliability, Quality and Safety Engineering (IJRQSE) is a relevant source for reliability-concerned issues.

2.3 Measurement Chain for Acquiring Deterioration-Inherent Signals

The challenge of measuring continuously (deterioration-inherent) signals with a non-destructive concept is detailed in the following. In general, the measurement chain provides the interface between the (physical, electrical, etc.) quantities and their digital correspondents (signals) and covers all relevant measurement components. In analogy to [DIN 1319], the general measurement chain is depicted in Figure 2.5.

At the outset of developing a novel measurement chain, the relevant measurands (physical properties) are identified. This is realized by material examinations, field failure examinations, expert judgments, heuristic knowledge about the physics of failure, etc. The aim is to identify the physical, deterioration-concerned properties that cause the fault and failure, respectively. The measurement itself must not influence the measurement result and/or system. If the physical properties are directly measurable, the deterioration itself is directly measurable. Hence, appropriate transducers are applied to convert the deterioration into a digital signal. In general, the sensitivity of the measurement chain to marginal damages is a challenging task [Fri10].

In the common case, the deterioration properties are locally distributed (e. g., surface roughness of plate) and/or are not directly measurable (e. g., chemical reaction in accumulator). Then, surrogate properties are measured that correlate with the real deterioration properties. The indirect measurements presuppose that the surrogate quantities contain deterioration-relevant information. The connection between the surrogate quantities and the real properties is realized by a filter. In summary, relevant physical properties (either direct or surrogate quantities) are measured by appropriate transducers (or complete sensors) to transform these into electrical signals.

In general, a sensor is a functional element which connects a (non-)technical process (e. g., technical, chemical, biological) with an information processing unit (e. g., CPU). The principle of measurement assumes the existence of a reproducible, known relation between the measurand (its physical effect, phenomenon) and the surrogate quantity. The linearity between both is desirable due to less effort during the filtering process. As every sensor is an energy converter, it usually consists of a transducer and an amplifier. The transducer has to respond to a physical property by converting the (non-)electrical measurand into an appropriate electrical signal. It provides directly measurable information about a measurand in terms of quantity, condition or property. The electrical signal can be a voltage, current

or charge. The amplifier has to be electrically compatible with the output signal of the transducer. Additionally, the electrical circuit of the amplifier must not change the electrical signal waveform, e. g., by a noisy power supply, nonlinear transfer behaviors, power loss, not matching input impedance, etc.

Ideally, the principle of measurement is highly sensitive to the considered measurand only. In practice, different (unknown) quantities influence the conversion process. Therefore, countermeasures for suppressing noise, reducing signal attenuation, increasing robustness, etc. are applied. Commonly, this is realized by, e. g., integrating the transducer and amplifier into a customized housing.

In general, sensors are classified according to different criterion, e. g., field of application, principle of measurement, energy consumption, costs, etc. In [DIN 1313, DIN 1319], the relevant information about the fundamentals of metrology are given.

Following [Whi87], an abridgment about a classification scheme for sensors is given in Table 2.1.

As shown in Figure 2.5, the normalized electrical signal is digitized by an analog-to-digital converter (ADC) and passed to the CPU. An ADC digitizes an analog input signal into a series of time and value-discrete values. The quantization in time denotes the resolution in time and is commonly expressed by a sample rate. The conversion is realized by keeping the analog value constant for one time step (sample-and-hold element) and passing it to an high-impedance ADC. Then, the ADC quantizes the analog value into an digital value. The resolution is generally expressed in number of bits. Again, the electrical specification (in terms of bandwidth, electrical compatibility, response time, etc.) have to be adapted to the output of the amplifier, the input of the information processing unit (CPU), and the desired resolution for further examinations (filters, etc.). The particular practical challenges are detailed in Sections 4.2 and 5.2.

As the measurement chain is the base for all subsequent investigations, special care has to be taken by choosing, applying, and operating the equipment and components. To ensure reliable and reproducible measurements, the following aspects have to be considered in advance: The measurement chain

- must not affect the process itself (no feedback),
- withstand aggressive substances, environmental conditions,
- cover deterioration-relevant signals,
- measure relevant physical/chemical/... effect(s), and
- must be robust against measurement noise.

In anticipation of Chapters 4 and 5, relevant standards for piezoelectric ceramics and their operations are [DIN 50321-1, DIN 50321-3] as well as [DIN EN 60254] and [IEC 60050-486] for electrical measurements considering accumulators.

In summary, the measurement chain provides the digitized signals (raw data) to subsequent signal processing steps, e. g., fault detection and diagnosis algorithms. Commonly, measurments are involved as process inputs (operational parameters) and outputs (deterioration-inherent signals) have to be processed. The measuring principle has to be non-destructive and the signals have to be measured continuously and with low noise.

Measurands	
Acoustic	Wave amplitude, phase, spectrum, etc.
	Wave velocity
	Other
Electric	Charge, Current
	Electric field (amplitude, phase, polarization, spectrum)
	Other
Mechanical	Position (linear, angular)
	Velocity
	Other

Detection Means used in Sensors
Electric, Magnetic, Electromagnetic Wave
Mechanical Displacement or Wave
Other

Technological Aspects of Sensors
Sensitivity
Measurand range
Stability (short-term, long-term)
Resolution
Selectivity
Others

Table 2.1: Classification aspects for sensors [Whi87]

2.4 Fault Detection

The task of fault detection is to evaluate the deterioration-related deviation from a nominal, a priori known behavior. The central prerequisite is that the deterioration mechanism effects the measured and/or numerically derived quantities. The evaluation can either be realized by model- or signal-based methods.

In general, quantities are defined according to their direction of action: an input covers everything that acts on a system, whereas an output is defined as the causal reaction of a system to an input. Hence, the system itself is driven by the inputs and reacts with corresponding outputs, as depicted in Figure 2.6. The measured inputs $\mathbf{u}$ and outputs $\mathbf{y}$ can either be continuous or discrete in time and/or values. For reasons of simplicity, the indication t for time-continuous and k for time-discrete systems are omitted in the following. Unless otherwise stated, all considerations are applicable for both, time-continuous and time-discrete approaches. Vectors and matrices are indicated by a bold notation.

In dependency on the availability and applicability of a sufficiently exact mathematical description of the system, its complexity, real-time demands, etc., an appropriate method for fault detection has to be chosen. The relevant methods are classified into two categories: model- and signal-based methods.

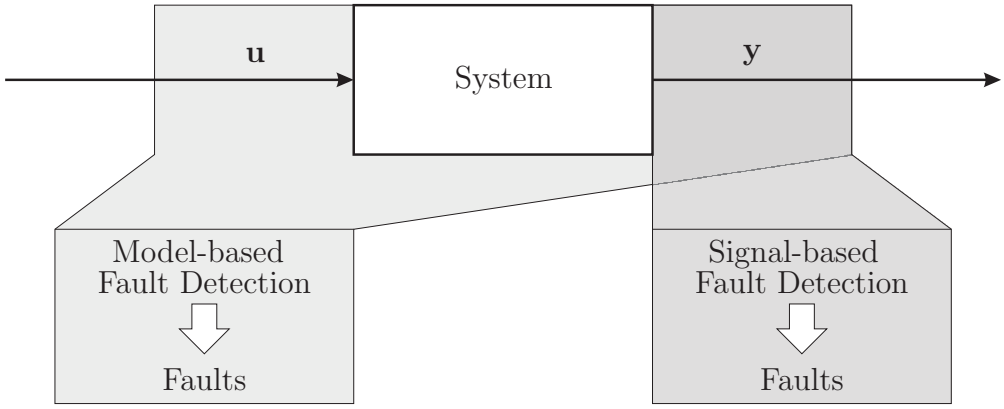

Figure 2.6: General scheme for model- and signal-based fault detection of a system with inputs **u** and outputs **y**

Model-based methods are chosen if an appropriate model of the system is available and applicable. Within this category, the input and output information as well as the system dynamics are used to calculate the model output $\hat{y}_\mathrm{i}$, the residual(s) r_i, etc. The residuals are realized by the comparison of both, fault-free (modeled) and measured quantities.

If the system dynamics can not be modeled, signal-based methods are applied that solely use the measured outputs. The realization of signal-based methods is usually time- and cost-efficient. Since signal-based methods provide only qualitative information about the system deterioration, the interpretation of the calculation results (e. g., single values, frequency spectra, etc.) requires extensive knowledge about the process. This knowledge has to be externally provided, e. g., by threshold or patterns. Hence, signal-based methods are commonly applied, if the responsible cause for deterioration and its characteristic effect are known for all valid operating conditions but can not be formulated mathematically.

2.4.1 Model-based Methods

If the mathematical formulation of the (nominal, fault-free) system behavior can be stated (e. g., derived from first principle), model-based methods are commonly chosen. The measured system's output y_i is combined with the estimated output $\hat{y}_i$ to derive the residual r_i (deviation between both). The idea is to use indirect measurement of (easy to have) quantities to conclude to the deterioration level of the considered component by observing the residual(s). The decision, whether or not a fault is present, is based upon the residual.

In general, model-based methods for fault detection are applicable if the mathematical model of the fault-affected system property can be stated and is robust against disturbances and model uncertainties, e. g., due to environmental changes, measurement noise, etc. The fulfillment of the prerequisite of mathematical modeling can become ambitious for non-linear, complex, and/or unknown deterioration behavior. Additional information can be used in a post processing step to reduce the false alarms, improve the accuracy of the model, etc.

In model-based fault detection, an adequate mathematical model, describing the input-output behavior of a system, is used to detect deviations from nominal behavior and to predict prospective behaviors. In [BKLS06], the "dynamical model of the system should

not only describe the faultless, but also the faulty system for all faults [...]." According to [MEC02], "modeling begins by developing deterministic physical/chemical models for the failure mechanisms. Then random and stochastic process distributions can be added [...] to account for important process variabilities." That means that all fault-relevant dynamics must be considered during modeling. The model accuracy is subsequently evaluated by simulation (verification) or experiments (validation).

Following [SRA+08], model-based methods are divided into two groups, law-driven and data-driven models. Other categorizations of the term model are known from literature, e. g., [Bel98].

Law-Driven Models

The following modeling techniques focus on an estimation of the measured, fault-relevant input-output behavior by appropriate mathematical models (in terms of a set of mathematical equations). These models have to represent sufficiently the system's behavior with a finite number of parameters [Nel01].

For linear, time-invariant systems with m inputs u and r outputs y, the input-output behavior can be modeled as a set of ordinary differential equations [Lun08]

$$\sum_{j=1}^{n} a_{ij} \frac{d^j y_i}{dt^j} = \sum_{k=1}^{m} \sum_{l=1}^{q} b_{kl} \frac{d^l u_k}{dt^l} \ , \quad (i = 1, 2, \ldots, r) \ , \tag{2.22}$$

with a_{ij} and b_{kl} as the time-invariant coefficients of the derivatives of the output and input, respectively. The index n denotes the system order and the maximum order of derivative of the output $y(\,\cdot\,)$ where q represents the maximum order of the derivative of the input $u(\,\cdot\,)$. The variables i, j, k, and l are continuous indices.

The initial conditions

$$\frac{d^j y_i}{dt^j}(0) = y_{0,ij} \ , \quad (i = 1, 2, \ldots, r \text{ and } j = 0, 1, \ldots, n-1)$$

have to be known.

It is obvious that the description of the input-output behavior by differential equations, especially for systems with multiple inputs and/or multiple outputs, can become very complex. Hence, the system dynamics is represented in the state space. For linear continuous systems, described in time domain, the state space description is defined as

$$\dot{\mathbf{x}} = \mathbf{A}\mathbf{x} + \mathbf{B}\mathbf{u} \ , \tag{2.23}$$

$$\mathbf{y} = \mathbf{C}\mathbf{x} + \mathbf{D}\mathbf{u} \ , \tag{2.24}$$

with $\mathbf{x}$ representing the states of the system's dynamic in dependency on the time, $\mathbf{u}$ corresponding to the inputs to the systems, and $\mathbf{y}$ describing the outputs of the system. The system matrix $\mathbf{A}$ represents the dynamics and couplings of the system. In combination with the input matrix $\mathbf{B}$, describing the influence of the input vector $\mathbf{u}$ on the system dynamics, Equation (2.23) is called the dynamical equation. The output equation (2.24) consists of the matrix $\mathbf{C}$, mapping the states $\mathbf{x}$ to the output $\mathbf{y}$, and the matrix $\mathbf{D}$, realizing the direct feed through of inputs $\mathbf{u}$ on the output $\mathbf{y}$.

In the following, the two common mathematical models for fault detection purpose are introduced. An overview about available methods is given in [Ise06].

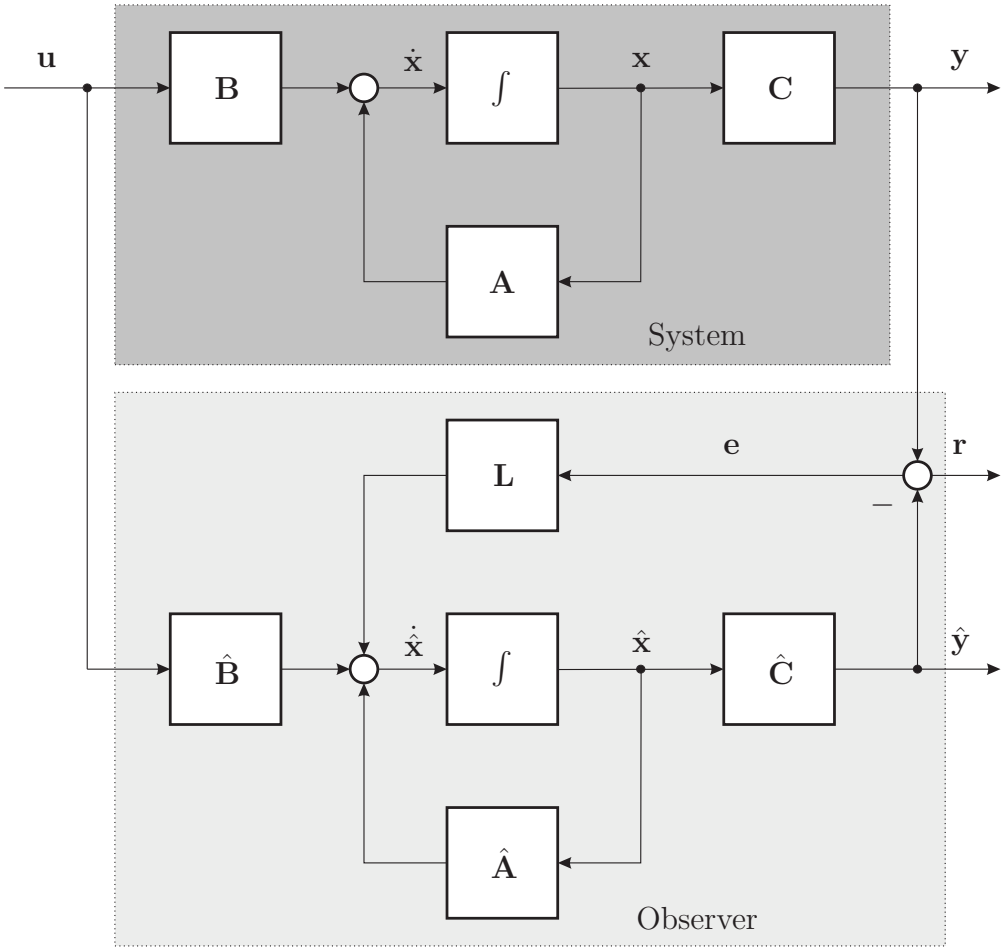

Figure 2.7: General scheme of Luenberger observer

- State Observer
  In general, a state observer reconstructs internal states from measured states on basis of a mathematical model and known model parameters. For diagnosis purpose, the observer uses measurable states (system's outputs $\mathbf{y}$) in order to conclude to internal states $\hat{\mathbf{x}}$ that are not directly measurable. In Figure 2.7, the general scheme of a system with an observer in parallel is given.

  The standard Luenberger observer [Lue64] is described by

$$\dot{\mathbf{x}} = \left(\hat{\mathbf{A}} - \mathbf{L}\hat{\mathbf{C}}\right)\hat{\mathbf{x}} + \mathbf{L}\mathbf{y}\,, \tag{2.25}$$

$$\mathbf{y} = \hat{\mathbf{C}}\hat{\mathbf{x}}\,, \tag{2.26}$$

  with $\hat{\mathbf{D}} = 0$. The hat notation indicates the observer matrices and signals.

  The mathematical prerequisite for the applicability of an observer is the observability of the considered system model, which means that immeasurable states can be reconstructed from measurement of outputs and thus, eigenmotions can be reconstructed.

For systems with few states, the observability is proven if the KALMAN criterion [Kal60]

$$\operatorname{rank}(\mathbf{Q}_o) = \operatorname{rank}\begin{bmatrix} \mathbf{C} \\ \mathbf{CA} \\ \vdots \\ \mathbf{CA}^{n-1} \end{bmatrix} \stackrel{!}{=} n \ , \tag{2.27}$$

is fulfilled.

To obtain a high observer performance, a high-gain $\mathbf{L}$ is usually chosen [Lun08, Kha02]. As a result, the residual $\mathbf{r}$ decays rapidly. The main drawbacks of this approach are a high sensitivity against measurement noise and model and/or parameter errors. Additionally, peaking is a commonly known challenge for high-gain observers that results in high corrective actions and thus, overshooting of $\hat{\mathbf{y}}$ [Kha02].

Hence, the determination of an appropriate observer gain $\mathbf{L}$ is the main challenge for the observer design. The gain has to be chosen such the observer is faster than the real system which is realized by the location of the eigenvalues of the observer. A common measure for a sufficiently fast response of the observer is obtained by placing the eigenvalues three to ten times faster than the dominating eigenmotions of the observed system [Lun08].

The model is simulated in parallel to the real system. As introduced above, the residuals $\mathbf{r}$ (deviation between measured output $\mathbf{y}$ and calculated output $\hat{\mathbf{y}}$) are used as an indicator for fault detection. A fault is defined as an intersection of the residual (one or several values) during the observation with a predefined lower or upper limit. Hence, the residual evaluation is a rule-based method in order to detect faults. The interpretation of the connection between cause and responding residual must be found.

In [HS09], an example for observer-based fault detection is proposed. The method is applied to an elastic mechanical system (cantilever beam) for the localization of cracks. A (increasing) deterioration is assumed to act as an additional input (virtual force) on the system and hence, disturbing the nominal behavior. The solution of the inverse problem reveals fault-relevant information about the unknown force and fault, respectively.

In [FK06], an observer-based method for unknown input identification is proposed. The filter (law-driven model) is an analytic model (Finite Element Model) of the structure that reconstructs external inputs (forces) to the system from measured structural responses (accelerometer and strain gauges).

- Parity Equations
  Similarly to the observer technique, the parity space equations are based on the evaluation of the computed and measured signals.

  Here, models with known structure (commonly in state space representation) but unknown parameters are used. The parameters of the model are estimated based on the measured input and output data. Subsequently, the estimated parameters are used to simulated the model behavior, based on measured inputs. The general scheme is similar to the one, shown in Figure 2.7 except for the feed back of the error $\mathbf{e}$ to the

observed state $\hat{\mathbf{x}}$. As this branch is omitted, no considerations about observability and stability have to be carried out. Only the parameters of the model have to be identified which is typically formulated as an optimization task. Typical methods for parameter estimations are the Least Squares Estimation (LSE) and the Maximum Likelihood Estimation (MLE), detailed in Section 3.4.

In [Kas06], parity equations and an observer are used in parallel as virtual sensors to supervise a system. By merging these information to so called symptoms, the fault detection sensitivity is improved. The post processing step (subsequent filter) can be realized by a fuzzy-based method.

Both law-driven models base on a mathematical model, commonly derived from first principle. From a diagnostic point of view, the main difference between the proposed approaches is the importance of the parameters. The parameters of the observer are derived from measurement and satisfy the physical equations (in terms of units, physically correct values, etc.). If the system is observable, the observer gain $\mathbf{L}$ has to be designed such that the observer reacts sufficiently fast and stable in order to calculate the output (placement of eigenvalues). This numerically complex procedure can be avoided by using the parity equations. Within this approach, the parameters are estimated by standard algorithms in order to reproduce the input-output behavior. The drawback is that the estimated parameters have no physical meaning but only satisfy the optimization task. Hence, a cross-link between estimated parameters and physical quantities is only possible by using an observer technique.

Data-Driven Models

In contrast to law-driven approaches, the data-driven models do not depend on predefined mathematically formulated laws but derive the input-output relation from observations (e. g., measurements). As stated in [YPL96], these models "can describe reality with a minimum of adjustable parameters." Furthermore, data-driven models are commonly used in the domain of non-linear systems, where most systems and/or behaviors occurring in nature are non-linear. A non-linear system performance is present if either the principle of superposition and/or the principle of homogeneity are not fulfilled and/or do not apply. The non-linearity can occur in the function(s) and/or the arguments. Non-linear models need an infinite number of parameters, in order to describe a system and/or its dynamics (see [Nel01]). Such models are realized typically by means of interpolation data, set of curves, characteristic diagrams, neural or Wavelet nets, etc. These models require preliminary information neither about the physical behavior of the considered system nor about its physical parameters.

- Artificial Neuronal Net (ANN)
  An ANN is composed of inputs that are connected via numerous individual neurons with the output(s). The information transfer is realized by a directed communication between the individual neurons. By connecting and organization these neurons into groups, so called (input, hidden, and output) layers of the ANN are obtained. A comprehensive introduction into ANN is given, e. g., in [Bis94].

  The ANN has to be trained first to reproduce the input-output behavior (supervised learning). Subsequently, the training result is tested on the basis of different (untrained) inputs. If the calculation results correspond sufficiently with a representative number of untrained input-output behaviors, the net is used for detection purposes.

Otherwise, the net must be further trained or additional layers and/or activation functions etc. have to be added/modified. An ANN can be adapted to almost every system whether it is linear or non-linear without phrasing the inner (fault) dynamics mathematically. The disadvantage of this method is that the generated model has no physical equivalent; the layers can not be interpreted and correlated with physical parameters.

- Fuzzy Logic
  Where the well-known Boolean Logic only discriminates between two states, 0 (false) and 1 (true), the Fuzzy Logic extends the discrimination to a continuous range between 0 and 1. Fuzzy Logic is commonly applied if a continuous quantity has to be assigned to different states. This assignment is realized by (overlapping) membership functions.

  For fault detection purposes, Fuzzy Logic is usually applied to evaluate residuals. However, the Fuzzy Logic (basically if-then rules) can be trained by numerical data and the support of ANNs. The advantage over the ANN method is that the model can be both, accurate enough and interpretable. In dependency on the degree of complexity, the Fuzzy Logic can combine the ability to learn from measured data and to reveal relevant input-output connections. Hence, an insight into the unknown inner structure (physical behavior) of the supervised system can be obtained [Mor05].

  In [MMS+03], a state of damage of a combustion engine is based on the measured lubrication contamination by wear debris. The deterioration is subsequently estimated by a mathematical data-driven Fuzzy Logic that assigns the measured debris concentration to a level of deterioration.

Subsequently, the validation proofs the validity of the derived model within predefined limits. Normally this is done by propagating uncertainties in the input values, model parameters, etc. through the model. Typical simulation methods are either Monte-Carlo simulation (assuming distributed input parameters, derived from observation and/or estimation) or Bayesian analysis. By evaluating the deviation of the estimated and observed outputs, information about the fault's confidence (interval) are obtained.

2.4.2 Signal-based Methods

For systems with simple or highly complex (non-linear) inner dynamics, unknown inputs, etc. signal-based methods are used that do not base on the exact, mathematically formulated input-output behavior of the system. The calculation results vary from single values to frequency spectra. Thus, the subsequently introduced methods are subdivided into two major categories: time domain methods and (time-)frequency domain methods.

Time Domain Methods

For many safety relevant systems, supervision of a threshold value is required to realize an emergency stop function. In [JW06], the temperature of an accumulator is supervised by a sensor. A rapid change of the cell temperature and threshold crossing is interpreted as a failure and the operation of the cell is terminated immediately. Here, the supervision of one measurand is sufficient to conclude qualitatively to an extensive deterioration. The knowledge about this correlation is derived from an heuristic knowledge base. A model-based method could be applied here as well, but the signal-based method is more robust,

easy to have, and reliable. The interpretation of a variation of temperature from nominal behavior requires a knowledge base, which can be provided as a look-up table derived from baseline tests, etc. The temperature development over system usage can then be used as a deterioration indicator for fault detection. Commonly, solely signal-based methods are limited to stationary processes. Otherwise, thresholds have to adapted for varying working points, operating conditions, etc.

In dependency on the particular domain, the following methods are commonly applied.

- Threshold Monitoring
  The threshold value analysis is the simplest method for fault detection. A fault is detected as soon as a predefined limit is intersected. For the threshold value analysis there is a multiplicity of typical application possibilities, like the monitoring of temperature, current flow, pressure, force etc.

- Trend Estimation
  For a system under constant operation, this method is applied to reveal the tendencies within the considered time data. In combination with statistical measures, signals from random and faulty behavior can be separated from each other.

  The cycle-counting algorithm by [DS82], rainflow-counting algorithm by [ME68], etc. are algorithms to count the occurrence of events versus an operation phase. The obtained histogram (e. g., rainflow-matrix), can found the base for separating normal and abnormal behaviors. Especially for the analysis of fatigue data, the rainflow-counting algorithm is used.

  Beside the direct evaluation of time data, statistical quantities can be supervised by the method as well. This is relevant for systems under repetitive operation, where trends between results at identical set point operations can be compared.

(Time-)Frequency Domain Methods

The (Time-)Frequency analysis is performed if deterioration-relevant information are assumed to characteristically and uniquely influence the frequency spectrum and "are used to analyze non-stationary events", [Fri10]. All following methods decompose periodic and non-periodic signals into single harmonic sinusoid functions.

- Fourier Transformation (FT)
  The Fourier Transformation $\mathcal{F}$ of a signal $y(t)$ is expressed by [BSMM05] as

$$F(\omega) = \mathcal{F}\{y(t)\} = \int_{-\infty)}^{+\infty} y(t)e^{-i\omega t}dt \ . \tag{2.28}$$

  As the frequency content of non-stationary signals will be examined later on, the time-discrete realization of the Fourier Transformation is given by

$$y_D(i\omega) = \sum_{k=0}^{N-1} y(kT_0)e^{-i\omega kT_0} \tag{2.29}$$

where N describes the number of samples at discrete time instants (e. g., measurements, data points, etc.) and T_0 represents the sampling interval [Ise06]. Therefore, the continuous sequence $y(t)$ is split into several sequences, each of identical length N. To avoid aliasing effects, appropriate non-overlapping window functions are applied. These window function modify the signal such that the signal is reduced to zero at its interval boundaries $k = [0, N-1]$. Thus, no discontinuities arise from the windowing.

In the case of a present fault, the evaluation of fault-sensitive signals reveals the deviation from the nominal behavior and is thus applicable for fault detection purposes.

- Short Time Fourier Transformation (STFT)
  The consecutive calculation of the FT results in a temporal succession of spectra from short time intervals. This kind of transformation is called Short Time Fourier Transformation (STFT) and preserves the time information within the frequency analysis. In dependency on the chosen overlapping strategy, the single Fourier Transformation are lines up or overlapping. The advantage of the STFT in comparison to a FT is that also transient signals can be transferred into a time-dependent frequency spectrum. A window w function, commonly a Hann window, is introduced in Equation (2.28) and the STFT is obtained as

$$y_{STFT}(i\omega) = \int_{-\infty)}^{+\infty} y(t)w(t-\tau)e^{-i\omega t}dt \ . \tag{2.30}$$

  The parameter τ indicated the time instant of interest.

  Unfavorable is that the detectability of a transient signal is depended with regard to the chosen length N of discrete values. High frequencies (relative to the fundamental frequency) appear less dominant in the spectrum than lower frequencies.

In summary, fault detection evaluate the deterioration-related deviation from a nominal, a priori known behavior. The decision, whether a model- or signal-based method is applicable is only depending on the feasibility of setting up a model for the deterioration-affected input-output behavior or deterioration mechanism, respectively. If the inputs can be assigned by a mathematically formulated model to the deterioration-affected outputs, then model-based methods are chosen as these reveal direct deterioration-proportional faults and allow higher level reasoning. If this requirement is not fulfilled or the system dynamics are too complex (e. g., non-linear), signal-based methods are applied. The obtained faults yield raw information about upward/downward trends of values, changed frequency contents, etc.

2.5 Fault Diagnosis

The task of fault diagnosis is to evaluate the detected fault in order to determine the origin of deviation and thus, correlating the fault to the resulting state-of-deterioration. Hence, the fault diagnosis is the subsequent step to fault detection; the relation between both is depicted in Figure 2.8. The required knowledge to interpret the fault has to be provided, e. g., in dependency on the performance of the fault, available information, etc. According to the source of knowledge, the fault diagnosis methods are divided into two categories.

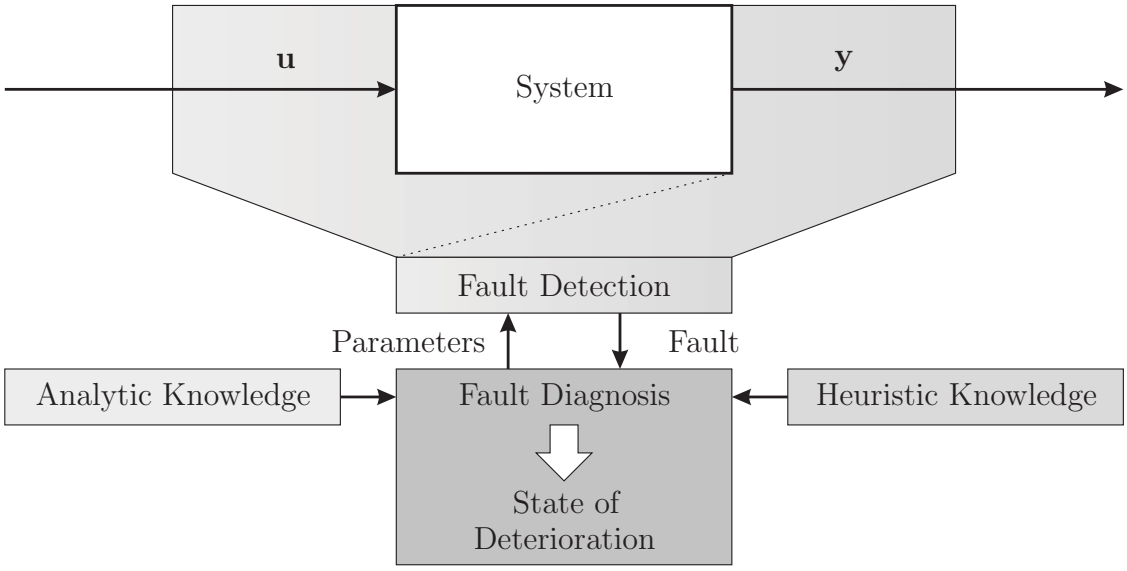

Figure 2.8: General scheme of fault diagnosis

2.5.1 Analytic Knowledge

In the case that a model-based fault detection method is applied, the knowledge is build up by aligning varying and deterioration-affected physical parameters of the model and their effect on the modeled system behavior to the observed faults. As the knowledge about the faulty behavior and causal model parameters is thus derived from analytic considerations, this category is denoted as analytic knowledge. The prerequisite to reveal and validate the analytic knowledge are that the deterioration has to be quantitatively measurable at arbitrary instants of time, usage, etc. (e. g., by crack length measurements, characteristic fault behaviors (patterns) under special operating conditions, etc.) and the deteriorating event sustainable and characteristically modifies the fault. If confirmed, the performance of both, fault and deterioration, are compared to each other in order to reveal a characteristic correlation. This connection is commonly used to adapt the parameters of model-based fault detection methods such that the calculated information vanishes and the state-of-deterioration is derived from the chosen parameter set, etc. (model updating method).

Typical examples for systems with measurable state-of-deterioration are accumulators, where the State-of-Health (SoH) is usually stated in dependency on the nominal capacity, e. g., [JW06]. By aging the accumulator, the capacity diminishes due to an increasing (measurable) internal resistance. This capacity fade can be monitored by standard measurements (special charge-discharge profiles) and hence, compared to nominal values. The analytic knowledge is represented as physical parameters (resistance, capacity, etc.) for nominal and various states-of-deterioration until failure. The actual state-of-deterioration is then derived from the actual valid set of parameters to obtain the vanishing of the fault.

For a mechanical component, failing due to fracture, propagating cracks lead to a reduced stiffness and subsequent failure. Hence, the a Finite Element Model (FEM) for the dynamical behavior (structural stiffness, etc.) reveals indicators for the actual state-of-deterioration, e. g., [Fri05]. By appropriate mathematical approaches (e. g., model updating), the mea-

sured (locally) reduced stiffness can be traced back to localize and quantize the state-of-deterioration. A similar idea of solving the inverse problem of calculating from measured effect to cause can be realized by an observer, as described in [HS09]. This process uses techniques based on observed (known) input-output correlations (law-driven models).

Furthermore, other methods for interpreting the connection between fault and (deterministic) deterioration are known in literature, e. g., neural nets (see Section 2.4.2), Bayesian nets, etc.

2.5.2 Heuristic Knowledge

In the case that the deterioration behavior is not available in analytic terms, a heuristic approach is chosen to assign the faults to the state-of-deterioration. Especially, if stochastically occurring deteriorating events (temporarily) effect the (deterioration-inherent) fault, but a direct correlation between a state-of-deterioration and a shift, trend, or exact (absolute) value of fault is not possible since immeasurable, fault diagnosis based on heuristic knowledge is applied. The relationship between deteriorating event and fault performance are then derived from continuous supervision of fault shifts, etc.

By designing appropriate test runs, heuristic knowledge is empirically derived from observed failures. In dependency on the particular domain (mechanical, electrical, etc.) and (dominant) failure mechanism, a priori assumptions are used to support the evaluation of the measurements (known physical principles, etc.). Based on this knowledge, general load-failure connections (models) are established in order to approximate the deterioration behavior (deterioration-proportional information).

Therefore, the effect of the deterioration mechanism on the failure is investigated empirically and an heuristic knowledge (assumed effect of deterioration on failure) is build up which incorporates information from process histories and failure statistics. Thus, the diagnosis bases on empirical data that reveal the correlation between the state-of-deterioration and the detected failure.

As the calculation can not be correlated with the real state-of-deterioration, the assumptions about the deterioration mechanism determine the calculation result. Due to the various sources of uncertainties or limited number of measurements, the deterioration model can still be invalid or at least incomplete. To deal with these probabilities, probabilistic-based assumptions and validation test runs play a major role.

2.6 Failure Prognosis

The preceding sections deal with the challenges in determining the actual state-of-deterioration. In failure prognosis, the prospective deterioration is considered and hence to support the choice of deterioration-optimal parameters. “The highest and most sophisticated level [of damage assessment] is the prognosis of the remaining useful life” [Fri10], where the Remaining Useful Life (RUL) is “the operating time between a certain time instant and an unacceptable level of degradation”, [Sye10].

In contrast to fault diagnosis, the prognosis extends the consideration to the task of correlating the operational parameters with the resulting state-of-deterioration. In order to maximize the remaining useful life and hence, minimize the deterioration of a system, surrogate models are used to estimate the most probable deterioration behavior of a system

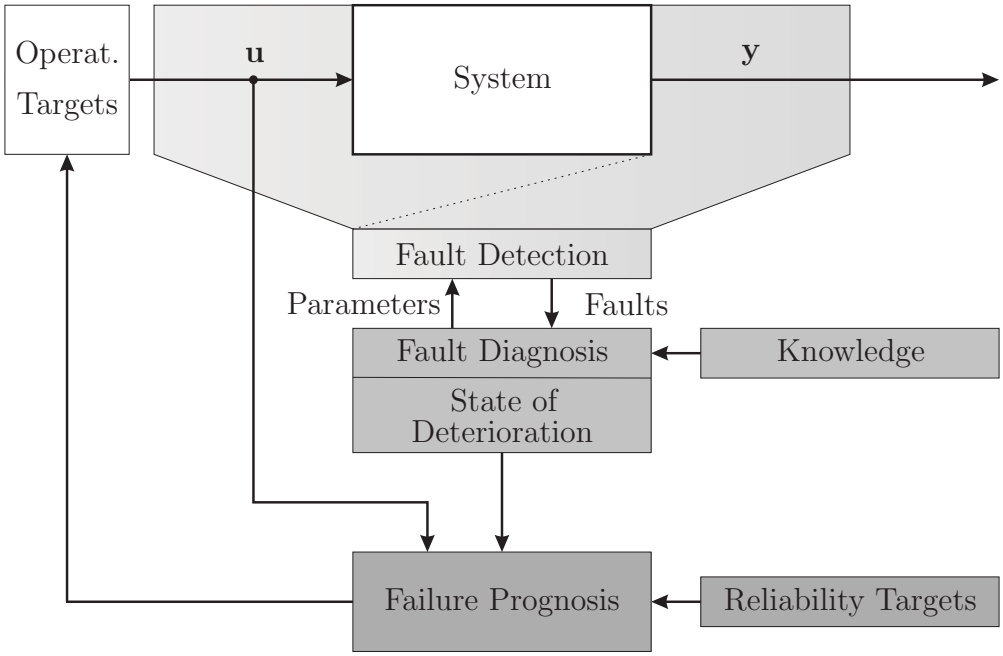

Figure 2.9: General scheme for a reliability-supervised system

for a given (known) input trajectory (operational parameters). These models have to consider the actual state-of-deterioration, assumptions about the future deterioration (behavior) within predefined confidence limits, the past and prospective operational conditions, and the required reliability targets. Several methods, describing an input-output behavior, are introduced above and applicable here (e. g., Neural Nets, (Neuro-)Fuzzy approaches, ARMAX models, etc.).

The novel aspect of approximating the propagation (time evolution) of faults and hence, instant of failure as a consequence of the prospective deterioration behavior is addressed in this section. The scheme of diagnostic-based failure prognosis and control is depicted in Figure 2.9.

This chapter comprises the key challenges for failure prognosis and introduces the theoretical foundations for multi-dimensional models to approximate the response of a system (life time, deterioration, etc.) due to the applied (independent) operational parameters. It is assumed in the following that statistically sufficient samples of failure data sets (past operational profiles and associated deterioration) are available to support the training of the models.

First, the idea is illustrated of how to design appropriate test runs that reveal the required information of appropriate operational parameters for each identified operational (deterioration) phase. Then, a functional relationship is identified that ties together the loading and the aging and hence closes the gap between deterioration measurement and deterioration control.

Length of Test Specimen [mm]	ξ_1	250	350
Amplitude of Load Cycle [mm]	ξ_2	8	10
Load [N]	ξ_3	40	50
Normalized Factors	x_i	-1	$+1$

Table 2.2: Operational parameters of a sample system and assignment to normalized factors [BDHH07]

2.6.1 Design of Experiment (DoE)

The primer task of test design is addressed by the Design of Experiments (DoE) [Mon09, BHH05, BDHH07] in order to obtain the required test results within a minimum number of test runs. The secondary aim of DoE is to avoid redundant, meaningless tests, and long test periods by appropriately designing the test matrices and procedures. The important factors (operational parameters) that have a major influence on the deterioration are known from previous investigations. Additional methods, e. g., sensitivity analysis can be applied to support this investigation step and to focus on the significant (in terms of usage control) parameters (factors). A first approach is the observation of typical parameter sets and their number of occurrence during a representative test period.

At the exploratory stage of the test design, a parameter sub-space of the possible parameter space (spanned by all independent operational parameters) is selected to reveal significant results about the relationship between load and deterioration. Subsequently, the relevant range (value limits) of each parameter is determined. Again, the search space is restricted to an explicit sub-space of operational parameters in order to rapidly reveal a first insight into the system behavior. Based on the obtained results and conclusions, adjacent investigations augment the test matrices and thus, the parameter sub-space.

In the following, a system with three independent operational parameters $\mathbf{u}$ is considered that is operated under various operational conditions until failure. In Table 2.2, the operational parameters with their relevant limits are given.

As the method of DoE is independent of the type and source of operational (physical) parameters $\mathbf{u}$ (quantitative and/or qualitative sources can be mixed), normalized factors $\mathbf{x}$ are used instead, which are linear transformations of the original measure. The transformations for the operational parameters of the sample system are realized by

$$x_1 = \frac{u_1 - 300\text{mm}}{50\text{mm}}\,, \qquad x_2 = \frac{u_2 - 9\text{mm}}{1\text{mm}}\,, \text{and} \qquad x_3 = \frac{u_3 - 45\text{N}}{5\text{N}}\,. \tag{2.31}$$

For the above introduced example with three independent factors x_1, x_2, and x_3, a test matrix with eight comparable systems, realizing all possible combinations of the normalized factors, is selected. The aging results are given in Table 2.3.

Based on the results, subsequent test runs are designed appropriately. In dependency on the aim of investigation, other parameter sets (extended limits, intermediate values, etc.) can be tested as well as additional operational parameters can be varied in order to extend the data base.

In summary, the method of DoE is a guideline to focus on the relevant test runs. In combination with few but relevant failure tests, constituting the data base for deteriora-

Operational Parameters			Normalized Factors			Cycles to Failure
u_1	u_2	u_3	x_1	x_2	x_3	
250	8	40	−1	−1	−1	674
350	8	40	+1	−1	−1	3636
250	10	40	−1	+1	−1	170
350	10	40	+1	+1	−1	1140
250	8	50	−1	−1	+1	292
350	8	50	+1	−1	+1	2000
250	10	50	−1	+1	+1	90
350	10	50	+1	+1	+1	360

Table 2.3: Test matrix with operational (physical) parameters, normalized factors and resulting cycles to failure [BDHH07]

tion prognosis, a method is introduced in the following that supports the approximation of optimal parameter values.

2.6.2 Response Surface Method

The Response Surface Method (RSM), firstly described by [BW51], is applied to estimate the response of a system by using a censored data base. In this thesis, the method is used to calculate the response of a system (deterioration) to several (independent) factors x_i (operational parameters $\mathbf{u}$). A comprehensive introduction to the topic of RSM is given in [BDHH07]. Here, the general scheme is introduced and relevant aspects for failure prognosis are emphasized.

According to [BDHH07], the functional relation between an expected response $\mathrm{E}(y)$ and several factors $\mathbf{x}$ is mathematically expressed as

$$\mathrm{E}(y) = \eta = f(\mathbf{x}) \,, \tag{2.32}$$

where y denotes the observed response of an experiment and f the real, globally valid functional relationship between multiple factors and response. Thus, the discrepancy due to scattering outcomes between the observed value y and the mean (hypothetical) value η is addressed by this consideration.

The deterioration due to the operation with different operational parameter sets constitute the data base for deterioration prognosis. The supporting points are determined by DoE, as described in Section 2.6.1, and the empirically evaluated test runs reveal the results (e. g., cycles to failure y). Based on this supporting tuples $(\mathbf{x}, y)$, an appropriate approximation of the real response function f is required to determine the most probable responses due to untested values of the considered factors.

Polynomial Functions for Response Surface Approximation

The approximation of the functional relation is denoted by the function g in the following, which is only locally valid within the considered sub-space. The response function g is described by general polynomial functions. In general, first-order or second-order models

are assumed to describe the response surface. Although higher-order models are possible as well, these are seldom applied as the number of parameters increases significantly.

The first-order model is described as

$$\begin{aligned} y &= g(\mathbf{x}) \\ &= \beta_0 + \beta_1 x_1 + \beta_2 x_2 + \ldots + \beta_k x_k + \epsilon \\ &= \beta_0 + \sum_{i=1}^{k} (\beta_i x_i) + \epsilon \,, \end{aligned} \tag{2.33}$$

with k denoting the number of inputs and β_i the parameters to be identified by appropriate methods.

The second-order model for the locally valid response function g is expressed as

$$\begin{aligned} y &= \beta_0 + \beta_1 x_1 + \beta_2 x_2 + \ldots + \beta_k x_k + \ldots \\ &\quad \beta_{1,1} x_1^2 + \beta_{2,2} x_2^2 + \ldots \beta_{k,k} x_k^2 + \ldots \\ &\quad \beta_{1,2} x_1 x_2 + \ldots \beta_{1,k} x_1 x_k + \ldots \beta_{k-1,k} x_{k-1} x_k + \epsilon \\ &= \beta_0 + \sum_{i=1}^{k} (\beta_i x_i) + \sum_{i=1}^{k} \left(\beta_{i,i} x_i^2\right) + \sum_{i=1}^{k} \sum_{j=i+1}^{k} (\beta_{i,j} x_i x_j) + \epsilon \,. \end{aligned} \tag{2.34}$$

The parameters of g are evaluated over the considered limits by appropriate approximation procedures for fitting the empirical function g to the supporting tuples, e. g., by polynomial fitting by maximum-likelihood, least squares, etc. According to [BDHH07], the true (unknown) underlying response function f can be approximated within this limited region sufficiently. Hence, it is possible to represent the relevant connection between factors (operational parameters) and response (resulting deterioration). "Although the approximation can be far from perfect" [BDHH07], qualitative information can be derived from the revealed function (e. g., influence of single factors on deterioration, etc.), e. g., the direction (in terms of gradients) of factor modification in order to obtain a response-optimal value.

Application of First-Order Model to Sample Data

For relationships with up to three inputs ($k = 3$), the (piecewise, locally valid) function g is graphically represented as a curve (two dimensional) or a plane (three dimensional), respectively to approximate the untested data points. For the higher-dimensional case (more than three inputs $\mathbf{u}$), geometric representations are not available to visualize the relation and is thus, realized numerically.

Considering the data from Table 2.3, the parameters of the first-order polynomial from Equation (2.33) are evaluated by the method of least squares such that

$$y = 1045.3 + 738.8 x_1 - 605.3 x_2 - 359.8 x_3 + \epsilon \,. \tag{2.35}$$

The surface for a constant value for the cycles to failure (exemplary assumed as 1000 cycles to failure, colored in light-gray) is depicted in Figure 2.10.

As narrow limits are chosen for the operational parameters, the approximation by a first-order functional relationship can be sufficient to conclude to optimal operational parameters (in terms of maximum system usage).

For deterioration prognosis, Equation (2.35) reveals the important information. As the cycles to failure are investigated, the parameter set has to be determined that maximizes

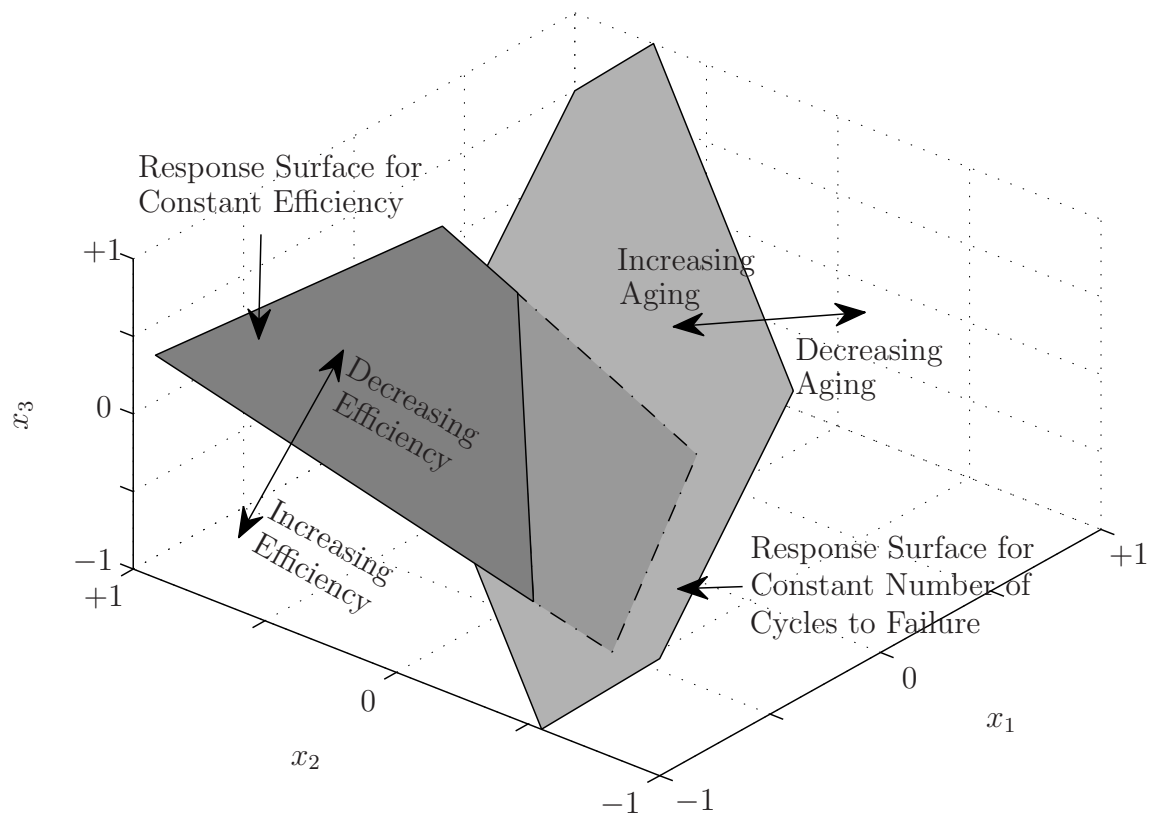

Figure 2.10: Surfaces of deterioration (light gray) and efficiency (dark gray) response

the response y. It can easily be seen from the equation that the factor x_1 has the largest impact on the response. Hence, increasing x_1 directly leads to an rapidly increasing number of cycles to failure. Especially for systems with more independent operational parameter than three (as considered here in this example), this information is essential to adjust the most sensitive operational parameters in the intended direction.

The ultimate challenge to solve is, in which extend a modification (here: maximization of factor x_1) is contrary to additional conditions, e. g., process efficiency, product quality, etc. Hence, the objectives of the system (high throughput, minimum energy, minimum amount of material, reduced idle modes, etc.) have to be included in this considerations to adequately modify the operation of the system and fulfill in parallel the objectives (of production, functionality, etc.) Therefore, the response (here: efficiency) is derived by using the same operational parameters. The resulting plane is depicted in Figure 2.10 by the dark-gray colored plane. The intersection of both planes, representing the optimal parameter set on the one hand in terms of deterioration, on the other hand in terms of operation, reveals the parameter constellation that comprises for both, deterioration and functionality.

From this figure it is obvious that the operation is not optimal in terms of deterioration but can be varied in order to increase the number of cycles to failure (decrease aging) by

adjusting the parameters such that the aging plane is moved to the right until only one intersecting point of both planes is obtained.

In general, the optimum for each response may reveal conflicting setting. Hence, a balance between the aging and the efficiency has to be found that reveals the most appropriate values for all responses.

Finally, the number of occurrence (of parameter sets) can be incorporated in this investigation as well (selection of sub-space, see Section 2.6.1). Thus, the distribution of typical operational parameter sets is evaluated. By fusing all this information, a comprehensive overview is obtained that forms the base for optimization.

In summary, the method of RSM in combination with DoE provides a powerful measure for optimizing the deterioration of a system by varying the relevant (or typical) operational parameters and fulfilling in parallel production targets. The explicit formula, derived from experiments, is differentiable. Hence, the response can be maximized or minimized according to gradient examinations. This aspect is especially important to reveal an optimal trajectory of inputs in accordance with an optimal response. Furthermore, detailed information about additional, not yet accomplished test runs can be derived from this investigations to complete the data base.

The location of the experimental region of most interest is identified and subsequent test runs can economically fit a more elaborate model (in terms of degree of complexity, parameters, etc.) between the inputs and the response. This is especially important for the design of further experiments. Conflicting goals (increasing input one leads directly to an unwanted decrease of input two) can be found within the investigation. Finally, the investigations can be supported by inputs, limited to predefined limits. An optimization strategy can subsequently be applied to reveal the appropriate input settings for a given goal of response.

3 Novel Probabilistic-based Method for Modeling and Controlling Systems' Deterioration

Research within classical fault-tolerant control architectures addresses mainly the re-configuration of the controller with regard to the functionality of the system. One example for this interpretation of Fault Tolerant Control (FTC) is given in [BIMP04], where FTC for "a reconfiguring unit [...] adjusts the structure and the tuning of the controller in order to preserve specified performances also for the faulty system." A typical example of the common interpretation of fault-tolerant control is given by [BKLS06]. A model-based fault diagnosis approach is "used to find remedial actions that adapt the control algorithms to the faulty conditions in order to keep the system in operation." The actual state-of-deterioration (classical SHM strategy) is thus estimated only with the help of model-based approaches, based on heuristic knowledge. Depending on the analyzed fault, the controller parameters and/or configuration are changed "to on-line re-design the controller" in order to adapt to the faulty situation. The strategy of the control reconfiguration concentrated exclusively on maintaining the functionality of the system to "satisfy the performance specifications". This reactive strategy does not incorporate alternative operational strategies in order to prevent fault development, but focuses on the "reconfigurability of the system or the search for redundant sensors and actuators, which can replace faulty components." The sophisticated aspect of controlling fault propagation is not addressed by this approach. Hence, a reliability-controlled system, based on the derived deterioration information, is not realized. The novel interpretation of fault-tolerant control selects appropriate operational parameters with regard to an extension of the life time and reduction of further deterioration.

Generally, the life-time trajectory of a system is composed of a sequence of non-overlapping, distinct phases with particular deterioration behaviors. If the deterioration behavior depends on the actual state-of-deterioration, these systems are called phased mission systems. Typical phases are the run-in phase, the permanent-wear phase, and the wear-out phase, as described by [San08] for fracture mechanics and [Jon09] for accumulators. Generally speaking, other classifications are possible; see, for example, [AB09], who divides the mission of an aircraft into the phases take-off, cruise, and landing. Other systems switch between operational and maintenance phases, for example power plants.

The challenge is to develop methods that consider the actual state-of-deterioration, the previous loading history, the particular operational phases, and the time instant of investigation.

The idea behind finding an adaptive compromise between safety, reliability, and costs over the life time during field usage of a phased mission system is to control the affecting input signals (operational parameters) adequately. In this thesis, this key feature is subdivided into three tasks which are based on one another: First, the connection between loading and deterioration needs to be determined and expressed in an adequate mathematical model. Based on this knowledge, the operational parameters which affect the deterioration have to be adapted in a deterioration-optimal way (while maintaining the functionality), and

finally, the appropriate countermeasures have to be initiated to reduce the probability of fault occurrence.

Besides the classical challenges of SHM, the novel aspect developed in this thesis is a method to estimate the optimal operational parameters (determined by the actual state-of-deterioration) and their subsequent use for controlling the life time. The underlying, promising SRCE-concept [SR97] is explained in detail in the following section. Afterwards, the probabilistic part of the SRCE-concept, introduced by [Wol08], and its essential results, as derived from numerical studies, are briefly discussed.

This thesis broadens the preliminary work by introducing novel aspects of appropriate strategies for addressing and improving systems' reliability. Additionally, the conceptual ideas of the SRCE concept are brought into practice for the first time. The open tasks to realize the SRCE concept are refined in Section 3.2. They are divided into three modules, which will be adapted to special technical applications in Chapter 4 and Chapter 5. Particular emphasis is put on modules 2 and 3, which realize the failure prediction, based on an insufficient data base, and form the base for control strategies. The latter module in particular is important for controlling the deterioration by adaptive operational strategies. In the following, only the most critical (unreliable) component with one dominant failure mode is investigated. Additionally, deterioration due to rusting, weathering, etc. is neglected, as countermeasures are easy to take.

3.1 Safety and Reliability Control Engineering Concept (SRCE)

A sophisticated concept for reliability and safety consideration is introduced by [RS96, SR97] as the Safety and Reliability Control Engineering (SRCE)-concept.

The idea is to calculate continuously (over the complete system usage) relevant reliability characteristics. Within the SRCE-concept, the reliability characteristics are depended on time, actual loading and past loading history (operational conditions). Especially the latter is novel in the field of reliability theory [Wol08]. Subsequently, the difference between the actual and the reference reliability is estimated. Based on these estimations and appropriate fault detection and diagnosis methods, the reliability becomes the reference value of the life time control-loop. Especially the measures for optimization of systems' life time are then conceptually realized by a "control unit integrating inner control-loop control, maintenance- and repair strategies" [SR97]. Thus, the reliable operation of the considered system until a predefined usage is guaranteed within an ensured reliability. The approach bases on the idea of modifying the operational parameter such that the deterioration is reduced but the operation is ensured.

The global concept incorporates ideas about CBM strategies during the design phase and especially monitoring concepts for the field usage. The main scientific achievements within this concept describe the idea of extending the possible utilization by reducing the performance but keeping the minimum needed functionality.

The SRCE-concept can be applied to different systems, no matter which domain or degree of complexity. The concept is depicted in Figure 3.1. In analogy to Figure 2.9, the SRCE-concept reflects the proposed idea of failure prognosis.

The SRCE-concept guarantees a maximum amount of utilization by probabilistic methods. As depicted, the operational conditions (in terms of loading) as well as stress information

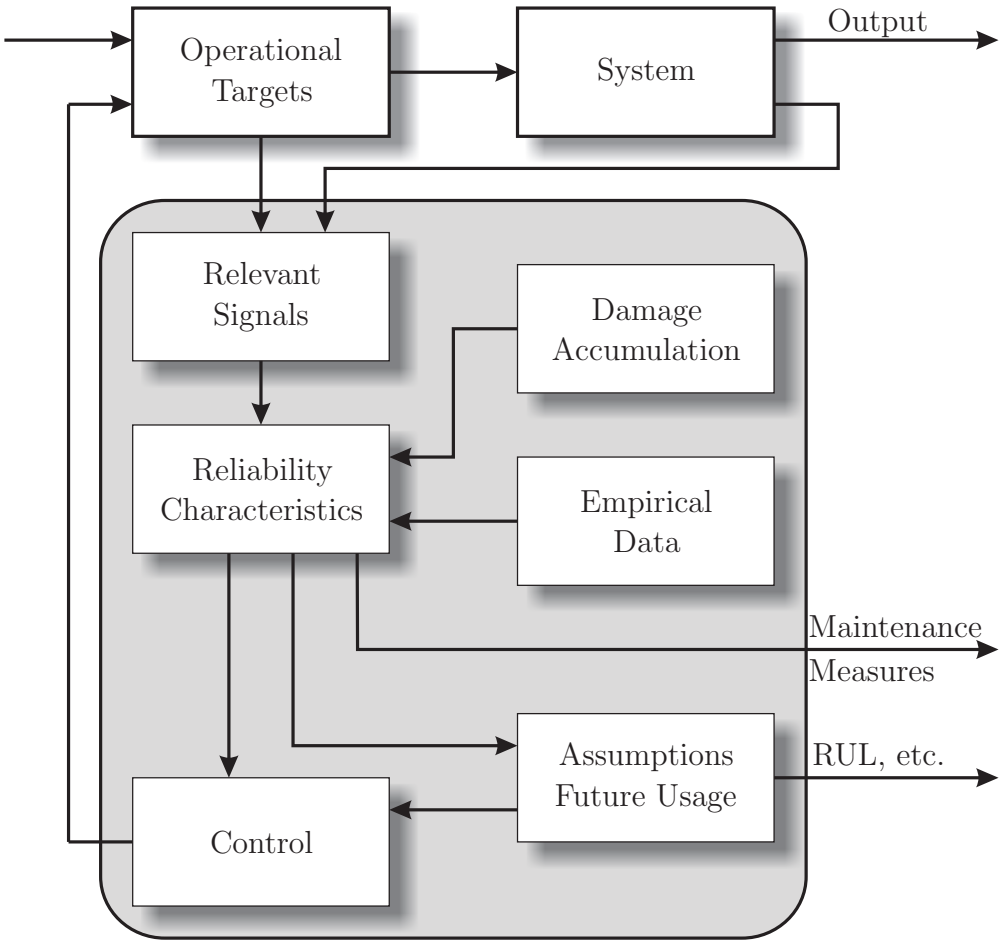

Figure 3.1: SRCE concept

(in terms of a reaction of the component to the load) have to measured and provided to the algorithm. These relevant signals are subsequently transformed into reliability characteristics by analytic and/or heuristic knowledge. The measurement of relevant signals in combination with appropriate filtering techniques are the most challenging requirements.

Once these information are available, probabilistic-based methods for calculating the reliability characteristics become applicable and are briefly reviewed in the next section.

The aspect of controlling the RUL of a system is a promising idea to realize to above mentioned goals of adjusting the operation of a system adaptively to the actual condition (state-of-deterioration). This idea is subsequently introduced in Section 3.2.

3.1.1 Preliminary Work

In [Wol08], a complete analytic description and detailed calculation of the utilization-depended Reliability Characteristics (RC) is given. The inner stochastic connections between loading and RUL, in combination with various assumptions about the future usage U, are considered. The formalisms to estimate the probabilistic instant of failure (intersection of actual reliability RC_i with critical reliability RC_{crit}, see Figure 3.2) under consideration of different operation scenarios U are set up. For the simulation, reference data from [SH87]

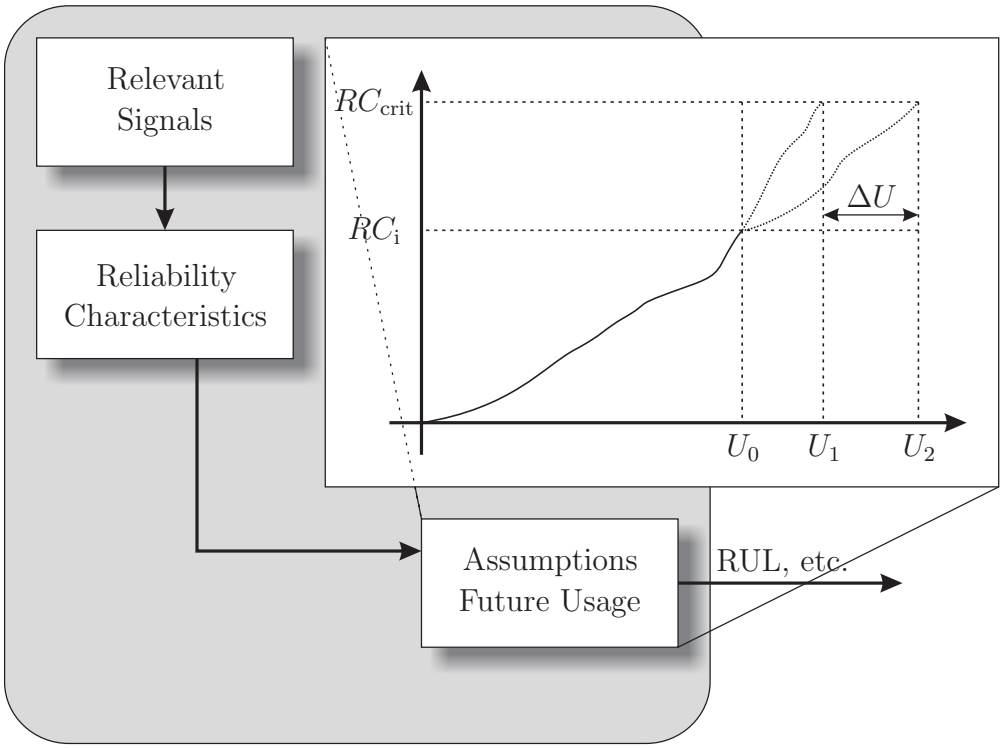

Figure 3.2: Realized components of SRCE-concept, according to [Wol08]

were investigated.

The simulation reveal how the current probability of failure of a unit under different operational conditions U_{i} can be determined and its dependency on the applied loading is shown. Different scenarios can be simulated and the probability of failure (in dependency of different simulated loading) can be estimated. The resulting difference between the deterioration due to different operational parameters is denoted by ΔU. Information about the actual and expected probability of failure and the maximum service life with different prognosis scenarios can be derived from the simulation.

In Figure 3.2, the realized components of the SRCE-concept are depicted. The generic concept's functionality is detailed by the RC's trajectory; as depicted, different trajectories are obtained due to varied operation.

Suitable deterioration models, measured operational conditions and system responses (output) and explicit adaptive, prospective deterioration behaviors are not discussed in [Wol08].

3.2 Extension and Realization of SRCE-Concept

In order to realize the Safety and Reliability Control Engineering concept, it is first modularized and then extended by a probabilistic-based deterioration estimation approach. In Figure 3.3 a graphical representation of the modular, extended SRCE-concept is given.

Appropriate knowledge (for example a mathematical model) of the loading-deterioration connection is a prerequisite of deterioration-optimal operation. As shown in Section 2.5, this knowledge can be derived either from analytic models or heuristic data. Both knowledge

sources are based on measuring deterioration-inherent quantities to relate the applied loading to the caused deterioration and to estimate the sensitivity of loading on deterioration. The relevant measurands are processed by a suitable measurement chain, as introduced in Section 2.3. As qualitative information about the deterioration process and the main influencing factors is usually available, the main prerequisite of measuring the deterioration-inherent signals can be met by appropriate sensors and specially designed test runs (Section 2.6.1). A pragmatic approach is to conduct accelerated tests by varying different operational parameters in a targeted manner, determining their impact on life time and then fitting the life time model. Since this testing covers only few variations (tests need to be completed within a reasonable time frame), the estimation of field reliability is based on extrapolation without any verification (comparatively low confidence).

To determine the central information about the loading-deterioration relation, the operational parameters are kept constant to yield reasonable estimates of the system's life under nominal operational conditions and comparable deterioration behaviors until failure. The realization of specialized measurement chains will be considered by means of two completely different systems in Sections 4.2 and 5.2. As a result, the deterioration-inherent signal is available, based on an appropriately chosen and validated measurement chain.

The task of fault detection and fault diagnosis is realized in module 1 by selecting and adapting the filtering techniques to transform the measured quantities into deterioration(-proportional) information. The filters are optimized on the basis of expert and heuristic knowledge, failure probabilities, post mortem analysis of each failed system, etc. The problem of test censoring addressed by [MM10, Run10] is avoided by operating all systems until failure, which is (by definition) due to the same mechanism for all experiments. To avoid redundant, obsolete, time- and/or cost-intensive experiments, an appropriate Design of Experiments (DoE) (see Section 3.4) as well as representative loading and systems are chosen. Hence, the selection and adaption of suitable filtering techniques plays the major role, as it connects the deterioration-inherent signal with the deterioration(-proportional) information.

In Section 3.4, module 2 is introduced, which realizes the novel probabilistic-based general deterioration model. As the deterioration(-proportional) information from module 1 does not reveal a deterministic relation between loading and assumed real deterioration, the scattering effect is addressed here. The idea is to derive an approximation about the average deterioration progression. Therefore, module 2 consists of an updating framework based on loading and deterioration(-proportional) information at constant loading conditions, and is adapted to the system-specific conditions.

Finally, module 3 bridges the gap between fault diagnosis and life-time control by realizing a multidimensional deterioration model. The missing information about the deterioration progress at unmeasured operational parameters will be addressed as well as varying operational parameters. In conjunction with module 2, module 3 is continuously updated by novel on-line measurement results (failures), so that it adapts continuously to novel situations. This gives an experiments-based relation between (relevant) operational parameters and their contribution to the deterioration. This module provides insight into reasonable, phase-specific operational parameters and thus leads to optimal deterioration. As a side-effect, the sensitivity of the system's deterioration to different loads due to chosen operation parameters at different operational phases is obtained. In addition to the information about phase-specific optimal operational parameters, the probable RUL (controlled by loading) can be calculated (as shown in [Wol08]), if the relevant loading (inputs), the deterioration (out-

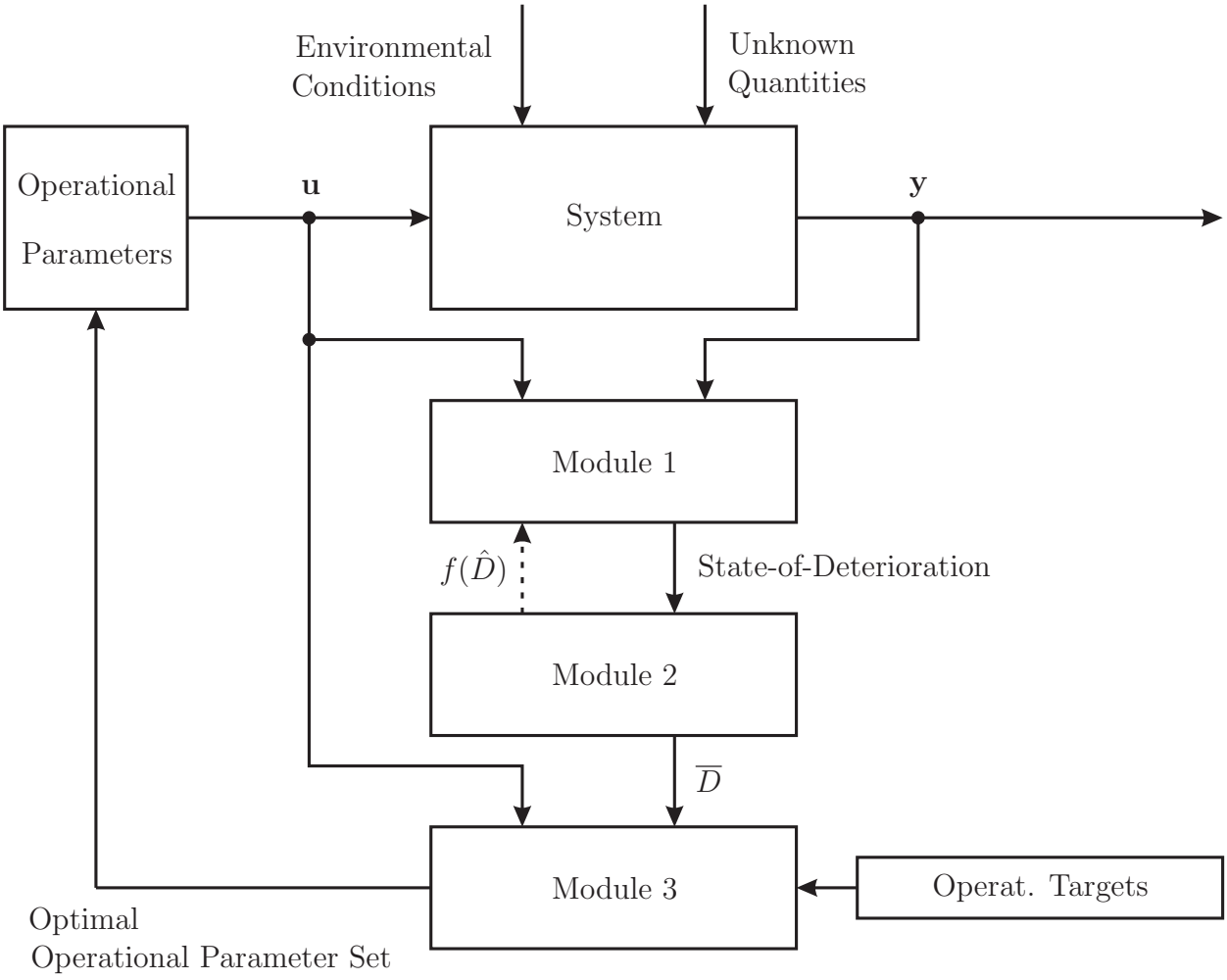

Figure 3.3: Overview

put), as well as valid information about the future usage (loading trajectory) are adequately determinable. In this thesis, the optimization goals, such as maximum life time, maximum performance, or maximum energy withdrawal, are formulated mathematically in terms of restricted regions and are considered in an appropriate control scheme.

3.3 Module 1: Deterioration Estimation

The deterioration-inherent signals are provided by the measurement chain. Thus, the purpose of module 1 is to establish a correlation between these signals and the state-of-deterioration. In module 1, two consecutive processing steps are handled to reveal such correlation.

First, a signal conditioning (reduction of noise, band-pass filtering of relevant frequency contents, compensation of transducer transfer characteristics, etc.) of the provided digitized signals (measured operational (and environmental) parameters and output signals) is performed, which is not depicted in the following schemes. As this process is signal- and application-specific, the particular approaches are discussed in the experimental parts of this thesis.

The more important second step in deterioration estimation is to convert the conditioned, deterioration-inherent signals into deterioration(-proportional) information by appropriate filter (e. g., mathematical model). In dependency on the desired quality of output information (accuracy, performance, kind of output data, etc.), different theoretic modeling techniques are available. Due to the multitude of these techniques, only the general idea of filter selection and parameterization is introduced. The practical realizations are shown in Sections 4.3 and 5.3. The filter result is assumed in the following as a deterioration(-proportional) information. In dependency on the availability of (analytic and/or heuristic) knowledge, physical failure models, and/or observed deterioration symptoms of the system (process), appropriate (several sequential) filters are selected. A comprehensive overview about available filters (models) is given beforehand in Chapter 2, especially in Sections 2.4 and 2.5.

To validate the assumptions about the sequence and type of filters as well as the acquired knowledge, baseline tests for comparable systems operated under comparable operations until failure are commonly performed. As operated under similar conditions, similar deterioration developments are expected. By taking only these information into account (immeasurable actual state-of-deterioration), the filter has to reveal the loading-deterioration connection, as depicted in Figure 3.5. If the real deterioration can additionally be measured at discrete points k in system usage, a correlation between the measurements and the filtering result reveals the accuracy of the combination and sequence of the chosen filters. This is idea is depicted in Figure 3.4. In dependency on the result, the filter have to be modified or exchanged to meet the measured deterioration level.

As some faults and/or state-of-deterioration only become observable during transient operation (e. g., special maneuvers), the baseline test have to be designed such that deterioration-specific information are provided by the deterioration-inherent signals. By performing the baseline tests at different states-of-deterioration, differences (proportional to the state-of-deterioration) are derived from the measured signals. These information are subsequently used to choose and adapt the filter.

In general, filter results with negative deterioration tendency are implausible for non-repairable systems as maintenance measures are not performed. Furthermore, neither self-healing effects nor faults due to sudden events (power shortage, etc.) are considered. The latter are commonly covered by redundancy countermeasures as described in Section 2.1. Hence, the filtering result is a monotonic increasing value over system usage as the deterioration is monotonic increasing.

Depending on the possibility to estimate the actual state-of-deterioration (at discrete instants of operation, etc.), one of the two following strategies is chosen.

Systems with Measurable State-of-Deterioration

For systems with an assessable state-of-deterioration D at discrete instants k of system usage, the assumed filter for continuous deterioration calculation is proved valid by the following scheme, depicted in Figure 3.4.

The estimated deterioration $\hat{D}$, calculated by a filter, is compared to the measured deterioration D. A measurable state-of-deterioration D can exemplary be the crack length of a tensile test specimen, the thickness of an oxidation layer, etc.

The deviation, calculated at instants k, between both is fed back to an algorithm, acting as a controller known from classical control theory. In the ideal case, the deviation is

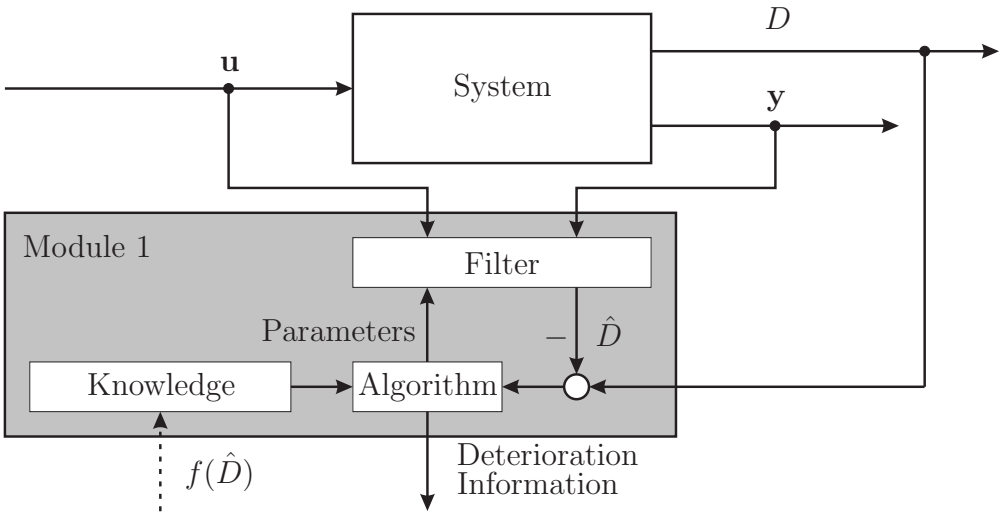

Figure 3.4: Determination of deterioration information for systems with directly measurable deterioration

equal to zero and hence, the filter (deterioration model) calculates the correct deterioration ($\hat{D} = D$)). For any other case, the filter has to be adjusted by the algorithm to meet the actual, measured deterioration D such that the deviation vanishes for all instants k. In the simplest case, a parameter estimation (e. g., maximum likelihood) is applied to adapt the filter parameters. Otherwise, sophisticated procedures are applied, e. g., artificial neural nets, Fuzzy approaches, decision trees, extended Kalman filters, etc. Additionally, further information (e. g., operational parameters) can be provided to the algorithm to derive a knowledge about the connection between loading and deterioration.

The deterioration measurement in combination with an adaption algorithm (knowledge) realizes a feedback and hence, closed-loop control of calculating the deterioration information. The deterioration information can either be derived from the filter or the algorithm. For reasons of simplification, the latter option is chosen for the graphical depiction, given in Figure 3.4.

Systems with Immeasurable State-of-Deterioration

In the case of an immeasurable state-of-deterioration D, neither an actual (intermediate) state-of-deterioration nor the progression itself for an individual system can be determined. Hence, the deterioration-proportional information are calculated feed-forward.

Again, either signal- or model-based filters are applied but with the challenging modification that the only measurable information about the state-of-deterioration is only obtained at systems' failure. Thus, the connection between the physical deterioration mechanism (causal for failure) and affected systems' output has to be investigated in order to ensure that the relevant quantities are measured correctly. Relevant information about typical deterioration-proportional signal contents can support the evaluation of the informational quality to proof the deterioration-proportionality of the derived information.

Commonly, the validity of the supposed causal chain is investigated by appropriate and sufficient test runs in detail. The evaluation of the test results is supported by module 2 in terms of a probabilistic-based conclusion about the variance and confidence about the

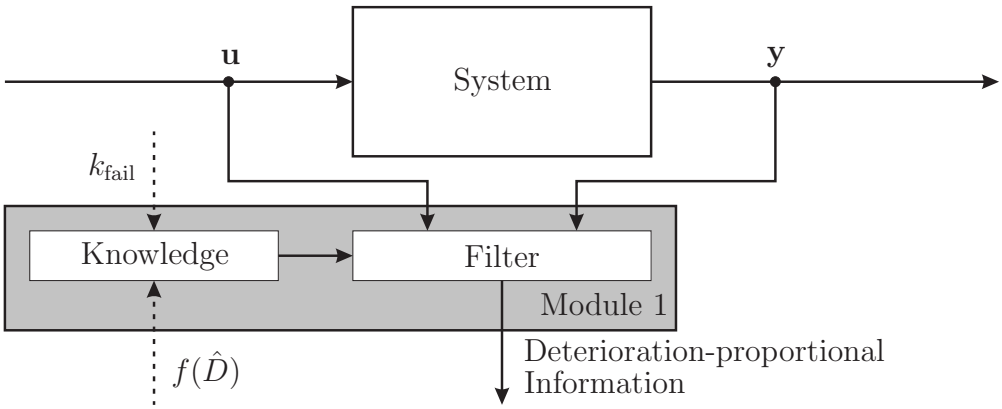

Figure 3.5: Determination of deterioration-proportional information for systems with immeasurable deterioration

derived deterioration-proportional information. If the validity is confirmed, the deterioration is extracted from the measured quantities. Otherwise, the filter has to be exchanged or modified in order to improve the information confidence.

A consistent, reproducible correlation between the quantitatively derived information and observed failures confirms the coherence between both. The result is that the deterioration-proportional information are calculated based on heuristic knowledge about the deteriorating physical effects on the system and thus, on the measured signal.

3.4 Module 2: Probabilistic-based Deterioration Model

Based on an adequate deterioration(-proportional) information, module 2 realizes the task of evaluating and ensuring the confidence of the proposed filter and determine the actual deterioration phase. If the calculated deterioration can be correlated to the real deterioration (measurable state-of-deterioration), module 2 plays a minor role since the evaluation of the proposed model is realized within module 1 by adapting the deterioration-specific parameters. Here, module 2 mainly serves as a confidence check of the chosen filter and adaption algorithm for local and global operational conditions.

For the estimation of a deterioration-proportional information, module 2 supports the assumptions about the proposed/assumed connection between measured signal and derived information to verify the chosen filter techniques and parameters. To compare the different progressions of the deterioration(-proportional) information with a sufficient degree of confidence, a sufficiently large data base (sample size of failed systems) has to be available. Since no correlation to the real deterioration is possible, the confidence check is realized by the comparison of particular, scattering maximum values of the deterioration-proportional information at failure of individual systems of one another.

The influence of the stochastical concurrent events under constant operation (leading to scattering instants of failure) have to be considered. Once a failure occurs, the individual maximum tolerable deterioration is exceeded and a value for the maximum tolerated deterioration is obtained. The unification of these varying values is necessary to compare the systems of one another. In the ideal case, many test with a large sample size of comparable

systems can be performed and their individual failures can be measured. These information about the distribution of deterioration-proportional information over system usage will be considered and fed back to module 1. Assuming identical phase-specific, damaging effects as well as identical accumulation, the accuracy of the calculation improves over the number of failed systems.

The scattering values for deterioration(-proportional) information at scattering instants of experimentally observed failures is considered within a probabilistic-based approach. The probability distribution function is assumed as Weibull, which is a widely spread approach [CFC06, GGQ, MZD03], etc. Furthermore, the Weibull analysis provides "reasonable accurate failure analysis and failure forecast with extremely small samples" [Abe05]. The discrete information about the calculated deterioration(-proportional) information at the instant of failure are the experimental basis for the estimation of an average deterioration progression.

From statistics it is known that a sufficiently large sample size is required to state the accuracy of the proposed distribution and its parameters. As fatigue tests, as these will be performed in the subsequent chapters, are time- and cost-intensive, the following considerations reveal only an initial estimate of the Weibull parameters α and β due to a multitude of uncertainties. Larger failure samples will detail and validate the first estimate. Nevertheless, the proposed parameters provide a base for the analysis of the propagation and influencing factors on the fault propagation. Hence, the updated parameters (from further examinations and observations) will slightly differ from the first approximation but will gradually stabilize and approach the true Weibull distribution [Abe05].

In [Wei51, GGQ], the estimation of the Weibull parameters from experiments is performed for the Weibull function, given in Equation (2.8). Following [MXJ04], the Maximum Likelihood Estimate (MLE) is used to reveal the parameters from experiment (complete data). The likelihood function is

$$L(\alpha, \beta) = \prod_{i=1}^{n} f(x_i; \alpha, \beta) \, , \tag{3.1}$$

with f as the probability density function (here: Weibull) at each considered data point x_i for n systems (failures) and the unknown parameters of the chosen distribution. The parameter estimation by MLE is performed numerically.

The approach assumes that the dynamics of the Weibull parameters are slow with respect to the deterioration. To prove the validity of the obtained parameters (goodness-of-fit test) typically methods are known in literature, e. g., the Chi-Square, Kolmogorov-Smirnoff, Anderson-Darling, and Nancy-Mann's test. As introduced above, the validation requires further failure samples and is hence, subject of comprehensive failure tests that are not discussed in this thesis.

The Weibull distribution mainly serves as an approach to describe the average deterioration $\overline{D}$ within the considered phase. Additionally, the confidence interval (expressed by the standard deviation) ensures the assumption and provides information about the applicability and accuracy of the proposed filter (module 1).

Once an estimate for the Weibull parameters is obtained, the applicability of the assumed distribution and numerically derived parameters is evaluated. Here, the standard deviation σ of the derived distribution is used as a measure of fit.

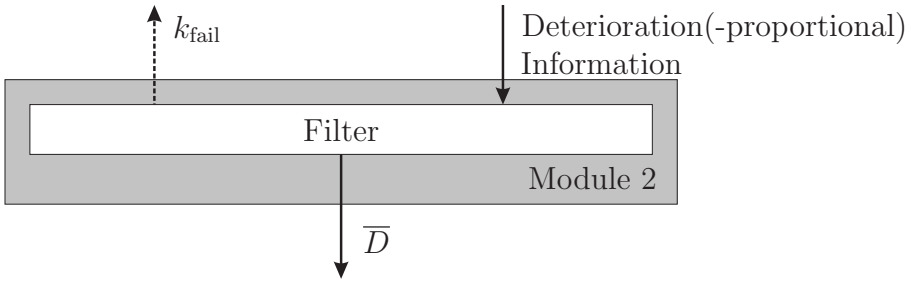

Figure 3.6: Module 2: Probabilistic-based evaluation of deterioration(-proportional) information

From Equation (2.4), the standard deviation

$$\sigma = \sqrt{\int_{-\infty}^{+\infty} \left(x - \widehat{f}(x)\right)^2 f(x)dx} \tag{3.2}$$

of the Weibull distribution is derived, describing the dispersion of the modal value $\widehat{f}(x)$ (see Equation (2.10)).

The desired result is a small deviation from the modal. A sufficiently fit is obtained, if all calculated, individual deterioration(-proportional) information vary less than σ from the modal deterioration $\overline{D}$. This information, in terms of $f(\hat{D})$, is fed back to module 1 in order to falsify or verify the assumed filter and parameters. If proved valid, module 1 has to be re-designed by an iterative, case- and application specific process to reach the best fit. Otherwise, $\overline{D}$ represents the reference value for further estimations, i. e., trajectory of the modal deterioration $\overline{D}$. This is especially important for comparing individual states-of-deterioration of different systems within the same deterioration phase with each other and thus, evaluating the initial deterioration of each system.

In this thesis, a significant difference between failures due to different operational parameters is expected. Hence, module 2 considers varying operational parameters by particular distributions. Each operational condition (in terms of parameters) reveal a distinct distribution. The general scheme of module 2 is given in Figure 3.6.

Finally, module 2 realizes the determination of the actual deterioration phase (run-in, permanent wear, or wear-out). This information is especially important for systems that suffer differently from certain maneuvers during different deterioration phases. The effect is that certain maneuvers must not be performed during a particular phase as the impact on deterioration is disproportional high than during other phases. As the amount, duration, relevance, etc. of each phase vary significantly from application to application, generic aspects of phase determination are given here. One indicator for a phase change can be a change in distribution parameters and can thus, be directly correlated to the parameters of the Weibull distribution. Beside that, the slope of deterioration can significantly change, e. g., from slow slope to high slope or vice versa. This effect is observed for the tribological system, discussed in Chapter 4.4.

The application of the proposed module is illustrated in the following by a numerical example. The deterioration is assumed to be depended on the chosen operational parameter

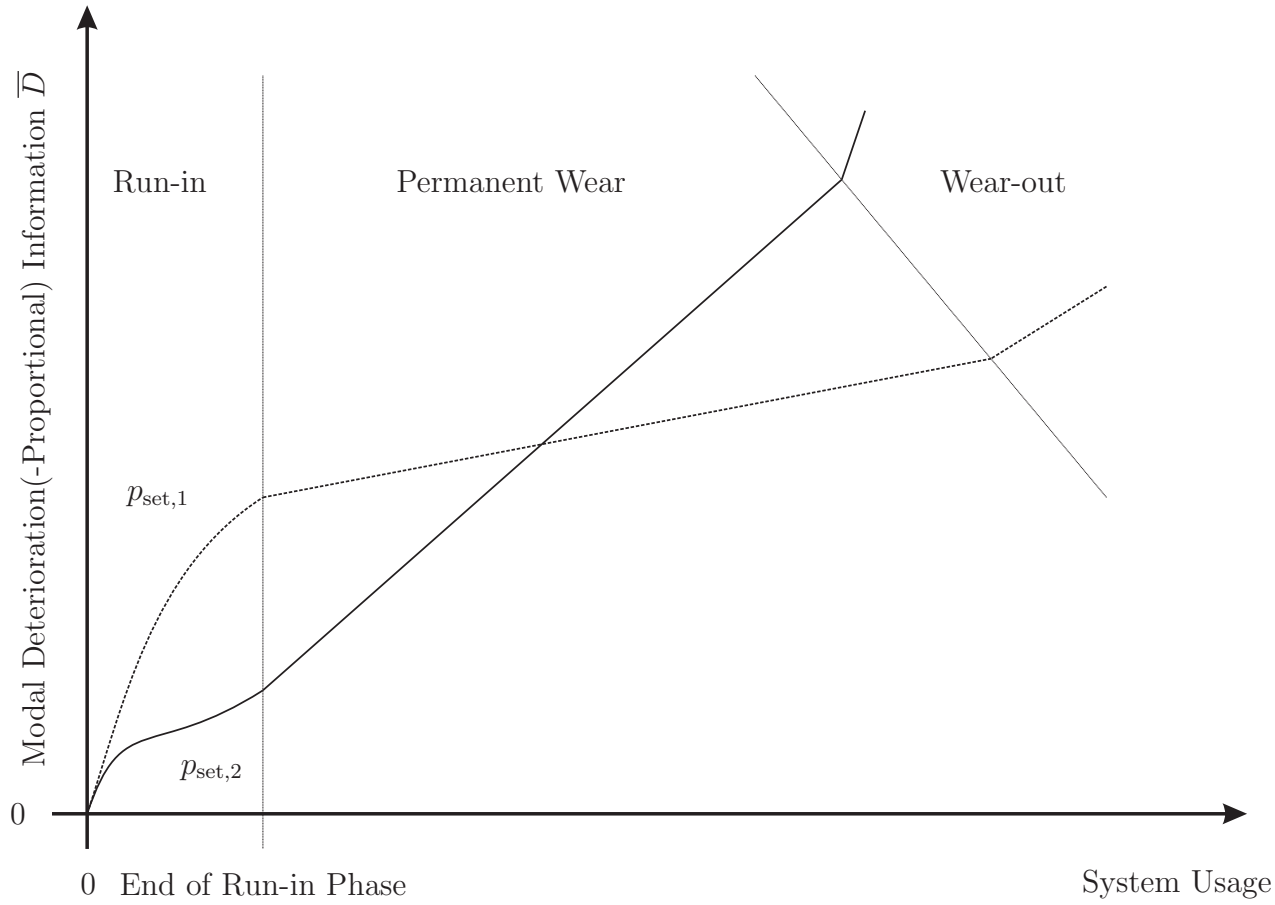

Figure 3.7: Simulated deterioration progression for comparable systems, operated under two different operational parameters

set p_{set}, and the individual behavior of the system. The parameter set consists of r individual operational parameters (u_1, u_2, etc.), which are independent among each other. Since the deterioration behavior changes, different deterioration progressions are possibly obtained for each constant operational parameter set and deterioration phase.

A mathematical model, representing the modal deterioration behavior $\overline{D}$, is simulated with one parameter set $p_{\text{set},1}$ until failure. The instance of failure is described by the calculated modal (average) deterioration(-proportional) information $\overline{D}_1$ over system usage until failure. The next deterioration test is performed with the identical model but different parameter set $p_{\text{set},2}$. Again, the damage trace $\overline{D}_2$ is calculated. Each set of parameters, which is kept constant over the test procedure, leads to a failure ($D_{1,2} = D_{\max}$) of the system after a certain system usage. The result is depicted in Figure 3.7.

The dotted line represents the deterioration progression due to $p_{\text{set},1}$, the continuous line depicts the deterioration due to $p_{\text{set},2}$.

According to the significant change in deterioration progression (change in deterioration slope), the above mentioned phases are introduced and the particular deterioration behaviors are classified accordingly. It is notable that the end of run-in phase is identical for both considered, different operational parameter sets but the transition from permanent wear

phase to wear-out phase is not.

The effect of the chosen set of operating parameters on the deterioration process thus depends on the particular phase. As depicted in Figure 3.7, $p_{\text{set},2}$ is less damaging during run-in phase than $p_{\text{set},1}$. The contrary is valid for phase 2. Derived from the simulation results, the operation should be modified at the transition points between the distinct phases in order to reduce the deterioration and hence, maximize the usable remaining life (in terms of system usage). The operating parameters are chosen phase-specific to maximize the possible system usage.

Furthermore, the maximum values for the instant of failure in system usage and the deterioration(-proportional) information vary significantly in dependency on the particular phase. This coincides with the demand of phase-specific, optimal operational parameters for reducing the deterioration. This fact is important for module 3, as this module modifies the operational parameters such that an optimal system usage is reachable.

Summing up, module 2 realizes the approximation of an average (modal) propagation $\overline{D}$ by a confidence interval of σ for each particular deterioration phase and thus, supports the plausibility of the filter, chosen in module 1. Furthermore, the impact of different operational parameters on the phase-specific deterioration is determined and support module 3 by determine the deterioration-optimal operation. The evaluation of the deterioration(-proportional) information is realized by a Weibull distribution and relevant statistical characteristics whose parameters α and β are derived from observation and an appropriate algorithm (MLE). With an increasing number of usage-failure relations, the observed behavior ((assumed) deterioration progression) can be described more detailed. In conjunction with sufficiently large failure samples, a validation of the proposed filter and its accuracy can be stated. Hence, a statistically ensured data base is developed that is subsequently used in module 3 to support the life time control algorithm.

3.5 Module 3: Deterioration Prognosis

The aim of life time control is the extension of a possible, deterioration-minimal usage of a system to its maximum life time along with the fulfillment of the primary function at the same time. The trivial solution (e. g., an immediate stop of the system/process at the occurrence of a fault) of avoiding deterioration is obviated by defining appropriate limits for the considered operational parameters. Hence, the task is to identify the deterioration-sensitive/-decisive operational parameters, possibly for each deterioration phase. The requirement and possible solutions of determining these operating conditions is discussed in this module.

In order to control the life time, the deterministic part of the deterioration process has to be manipulated, which mainly depends on the chosen sets of operational parameters at particular wear phases. The stochastic events that do not depend on the operational conditions, are covered by the probabilistic-based considerations in module 2. Therefore, the operational parameters, governing the deterioration process, have to be adjusted situation-specific. The analysis of scattering input parameters on the system performance is essential for dependability evaluation.

Once the adjustable parameters and limits are determined, the condition-based set of parameters has to be chosen, e. g., from a data base. The parameter sets need to encompass all applicable field conditions to ensure a sufficiently high confidence in reliability estimates

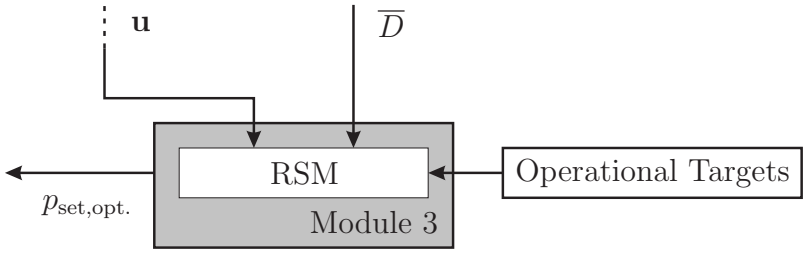

Figure 3.8: Module 3: RSM-based optimization of systems' life time

for field conditions. Thus, the proposed tests cover the relevant operating parameters and span the relevant parameter space. The set of control parameters is subsequently used to operate the system and control the process respectively. By providing upcoming events (e. g., trajectories or others) to the control algorithm, a predictive control can be realized, e. g., [Wol08]. The control error (in terms of derivation of calculated and observed output performance) is used to update the data base and improve the prediction result.

The tests performed to determine the failure probability in module 2 are used here to further analyze the effects of different operational parameters on the deterioration. Especially, when dealing with multiple operational parameters, the sensitivity of the deterioration on changed operation is hardly determinable by heuristics. Hence, a targeted, systematic approach is introduced by the Response Surface Model (RSM, see Section 2.6.2) in order to identify the most significant parameters and their connection amongst each other on the target value (here the usage). By determining an appropriate relationship (model) between both, operational parameters and deterioration, appropriate, phase-specific parameter trajectories can be calculated, leading to an optimized life time. The RSM can either be realized to reveal local or global optimization results. If the model's accuracy requires a refinement and/or does not converge to a local optimum, additionally tests are performed to improve the data base.

The general scheme of module 3 is depicted in Figure 3.8. The operational targets are defined externally of module 3. In analogy to the proposed realization of [Wol08], these targets comprise requirement for marginal reliability within the considered, future operation (time span). In analogy to the RSM methodology (see Section 2.6.2), the optimal operational parameters are determined by intersecting planes, formed by iso hyper planes (e. g., plane of constant velocity, etc.).

Once the chosen model fits the measured value sufficiently, first condition-based operational strategies can be derived. The system and its deterioration can be observed and the data base retrained with time. The deterioration predictions (based on different assumptions about the future usage) are calculated and appropriate measures are executed. The measure of effect is used to update the data base and increases or decreases the probability of an action (in terms of a set of parameters at a certain operational instance with a calculated goal).

As this is phase-specific, the proposed optimal operational parameters set varies in dependency on the actual deterioration. Since information about the deterioration are available, the proposed methods are applicable to cover systems with directly measurable deterioration and deterioration-proportional information.

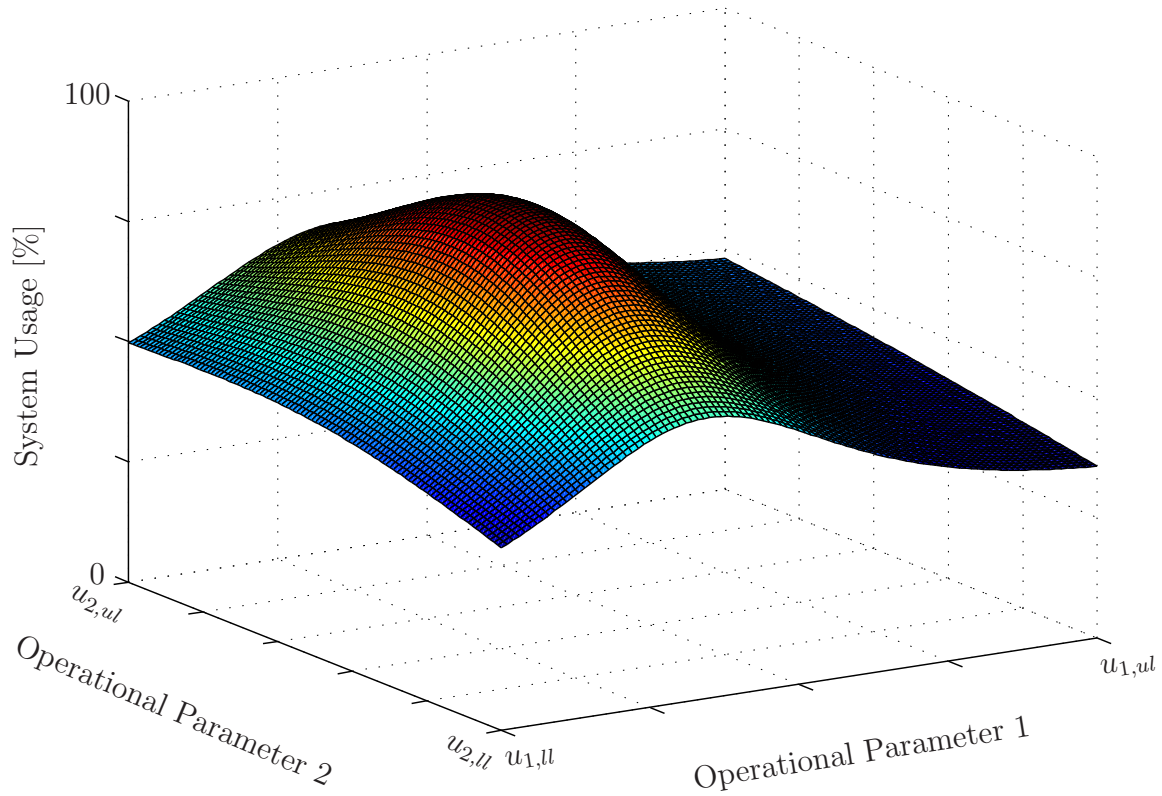

Figure 3.9: Simulation results for maximum system usage over two-dimensional operational parameter space

This module forms thus the missing link between classical structural health monitoring (SHM) approaches and structural health control (SRCE-concept) in order to realize the deterioration-depended control of the life time

The simulation example, introduced in module 2, is carried on in order to demonstrate the general idea.

The results are depicted in Figure 3.9. The upper and lower limits for each operating parameter must be determined and provided to the algorithm. Here, the individual limitations are denoted by $u_{r,ll}$ for the lower limit and $u_{r,ul}$ for the upper limit, respectively.

As shown, both parameters are varied within their specified limits. The resulting plane represents the maximum value $\overline{D}$ for system usage at point of failure. The information obtained by these (simulated) failure test is the optimal region for a constant parameter set. Referring to Figure 3.7, the constant set of operating parameters $p_{\text{set},2}$ leads to the maximum possible system usage. As depicted, the usage could be extended if the operation is changed when entering the permanent wear phase. During the run-in phase the different extend of damage can be determined detailed. Again, interpolating planes using the measured values as supporting points can help to point out the optimal set of operating condition for this phase. In the 2D space (only two independent parameters, $r = 2$), this is realized graphically. Once the system has more operational parameters $r > 3$, this method can

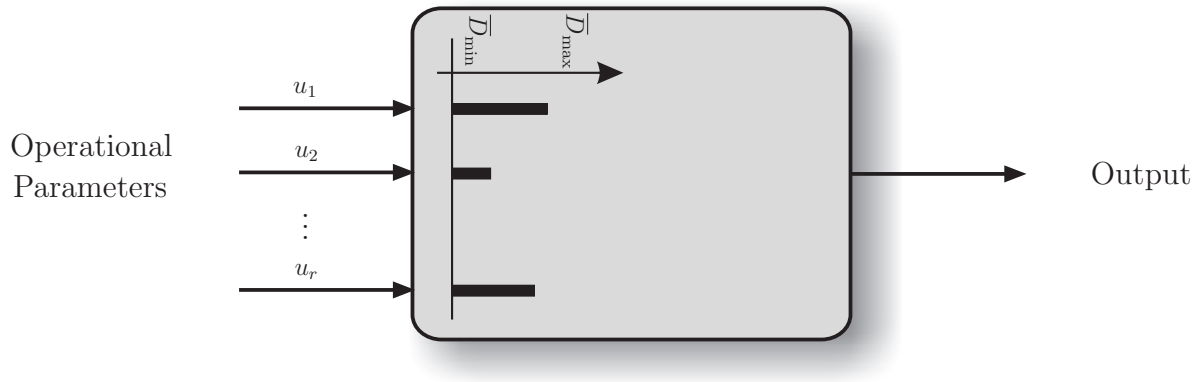

Figure 3.10: Exemplary connection between r operational parameters u and effected output

only be performed analytically. As the result, the gradient provides sufficient information to improve the operating conditions for other comparable systems.

In Figure 3.10 the sensitivity of individual input on the deterioration in dependency of the actual operational phase is depicted. It becomes obvious that this continuously updating data base forms the basis for situation-depended life time control.

Once a fundamental data base is derived from tests, individual systems can be equipped and supervised by this algorithm. One main advantage by the proposed method is that basic information about a life time extending way of operation can be derived from a relatively small database. Depending on the system, the number of manipulable operating parameters under individual limiting conditions, the connection between the input (set of operation parameters) and the longterm effect on the life time cannot be anticipated by the human operator. Different optimization goals (e. g., energy consumption, downtime per day, acceleration, etc.) can be considered in parallel. Hence, different optimal operating trajectories can proposed or directly executed by the control scheme.

3.6 Summary and Conclusions

In this chapter, the demand for compromising adaptively for safety and reliability is explained. Classical and novel approaches in the context of SHM are introduced and the missing parts of controlling the operational conditions phase- and operation-specific are worked out. Based on the Safety and Reliability Control Engineering concept and preliminary works on that, a novel method, extending the strategies known from literature, is introduced. The single modules of the extended SRCE-concept are introduced in detail. Especially the challenging aspect of concluding from deterioration-affected measurands to the actual state-of-deterioration is detailed. Furthermore, the adaptive probabilistic-based deterioration model realizes the continuously adaptive, time-variant, probabilistic correlation between deterioration-proportional information and the most probable deterioration. By this correlation, information about the RUL can be derived. As a direct consequence of the obtained deterioration estimations, appropriate strategies for modifying the operation of the systems (by limiting disproportionately high damaging situations, proposing alternative strategies, etc.), can be conclude. The chapter closes with a simulation example, depicting

the numerical applicability and potential of the proposed framework.

Finally, the progression of the deterioration(-proportional) information and the probabilistic evaluation have to be carried out for varying operation parameters. A similar idea has been investigated in [NF99]. There, the influence of variable operating conditions on the expected service life was evaluated by a multi-modal Weibull distribution. It is shown that similar results for the distribution parameters are obtained, whether constant or variable operation is observed.

4 Application to Tribological System

The modular concept from Chapter 3 is explained in detail by giving the example of a mechanical system, which suffers from wear effects induced by operating conditions, local material defects, etc. To gain the relevant information about the actual state-of-deterioration, the measured signals are filtered and correlated with meaningful baselines. Hence, a rough classification of relevant signals (signal contents, frequency range, etc.) can be stated. Furthermore, the connection between applied loading and resulting deterioration can be experimentally derived from observations and used in combination with a mathematical model to predict the remaining life time.

In order to reach these ambitious goals for an industrial machine, the process of deterioration is investigated in detail to determine the relevant physical failure mechanisms. Subsequently, a novel, specialized measurement chain is developed that is especially sensitive to the deterioration-relevant quantities. In conjunction with the material investigations and application-specific measurement concept, filters are designed in order to derive the deterioration-proportional information. The obtained results of different operation-to-failure tests are consolidated and evaluated by probabilistic considerations. In addition to the novel measurement chain and filters, optimized operational parameters are proposed for the first time, paving the way for an optimized, wear-reduced operation of the tribological system.

4.1 Motivation

In the following, the typical failure of a mechanical (tribological) system is considered. Generally speaking, tribology is a sciences dealing with surfaces that interact which each other due to relative movements [GfT]. It covers the complete field of friction and wear, including lubrication and interactions between boundary surfaces. In tribology, wear is defined as the continuing deterioration of a solid surface, caused by mechanical stress, e. g., contact and relative motion of a rigid counter body. It generally involves progressive loss of material. A tribological system contains all material components and their (variable) characteristics due to operation.

As an application example of a system suffering from wear, an industrial scrap bailing press is considered. This specific machine is mainly employed in the automotive industry, especially in car body plants. The scrap material (aluminum, steel, etc.), resulting from die cutting processes, is fed to the press and subsequently compacted into bales by hydraulic cylinders.

The linear compression movements of the hydraulic cylinders are guided by wear plates. The guidance is realized by a structural shape (corrugated washboard profile) of the wear plates. The tribological effects at the wear plate's surface are reduced by special materials (e. g., special blooming) in combination with automated lubrication systems. Anyhow, the main reason for failure is the occurrence of plate jams caused by an excessive surface wear-out. The current (preventive) maintenance strategies focus on an avoidance of wear-out failure by changing the wear plates in (constant) maintenance intervals. Hence, the on-line monitoring

of the wear plate's surfaces is necessary to optimize the system's reliability by condition based maintenance. The aim is to equip the machine with sensors in sheltered positions that provide deterioration-inherent signals to a wear monitoring and control system.

In order to develop a reasonable measurement chain and operational strategies, all relevant information about the considered system and its typical failure are evaluated. Therefor, wear plates from field failure are examined and typical effects are discussed in Section 4.1.1.

Based on this knowledge, a developed test rig, realizing the operational conditions, is briefly introduced in Section 4.1.2. Subsequently, the wear plates failures, produced by the test rig, are analyzed and the results are compared with the field failures. By showing that the wear plates fail due to identical deterioration mechanisms, the applicability of the test rig for failure examinations is proven.

Due to the complexity of the wear process (locally and timely distributed, stochastically occurring incremental deterioration), a signal-based approach for deterioration evaluation is chosen. As the physical failure mechanisms are investigated in detail, a direct correlation between abraded material (wear) and emitted acoustic emission (AE) is found to describe quantitatively and qualitatively the deterioration process. Therefore, adequate sensing technologies are introduced in Section 4.2 to sense these effects. Under the consideration of applicability and sensitivity to deterioration-indicating signals (tribological effects), an adequate measurement chain for acoustic emission detection is developed and applied.

As module 1 is developed in close conjunction with the AE measurement chain, appropriate filters are introduced in Section 4.3 that realize the extraction of deterioration-proportional information. The revealed information are correlated with classical process information to visualize abnormal behavior (stochastically occurring AE events). As the (progression of) deterioration is immeasurable, this correlation is especially important to identify and validate the assumed filter characteristics and chosen parameters. The proposed filter results reveal a relation between measured AE energy and observed instant of failure and is hence assumed to be appropriate to describe the incremental deterioration.

As expected, the operation reveal a stochastic life time distribution of comparable systems, operated under comparable operating conditions. Hence, module 2 (Section 4.4) details the idea to extract typical deterioration indicators over system usage to evaluate at an early stage an individual system with its individual deterioration behavior. It will be shown that the deterioration behavior is clearly divided into three distinct deterioration phases which are considered separately. Hence, module 2 evaluates the deterioration-proportional information of a supervised system during operation and correlates its individual behavior to history data. Based on this heuristic knowledge, the estimation of the most probable deterioration propagation is realized.

As proposed beforehand, the information about the RUL is an important quantity for maintenance strategies. The even more valuable information is, how to extend the current RUL by adapting the operation parameters adequately. The knowledge about the relation between the operational conditions (speed of cylinder movement, lubrication, etc.) and the instant of failure (correlating with the propagation of the deterioration-proportional information) is proposed to be the key information for adaptive, reliability-centered operation. It will be shown that the quality of the wear plates predetermines the maximum life time of the system. A targeted adaption of operational parameters is not sufficient to significantly influence the RUL. This will be illustrated based on the deterioration progression during run-in phase.

4.1.1 Field Failure

In [Bes05], a typical field failure of a wear plate is examined by hardness measurements, light optical microscope, Energy Dispersive X-ray (EDX), and Scanning Electron Microscope (SEM) analysis. Different probes from different positions in the wear plates were taken and analyzed by the above mentioned techniques. Three different wear mechanisms (terminology according to [CH10, BB10]) were identified: adhesive wear (cold-welding, scuffing), abrasive wear (scouring abrasion), and surface fatigue (crack growth). Those mechanisms are typical for systems under reciprocating slide wear, e. g., described in [FK01, FLK$^+$03].

Based on these examinations, [Bes05] proposes the following causal chain of wear: during the compression movement of the cylinder, bulk material from the wear plates is abraded of the surfaces. These hard and sharp debris (acicular martensite) gets strain-hardened and roughens the surfaces (scuffing, scouring abrasion, fretting). Subsequently, the wear debris (and other debris from crap material, e. g., thin pieces of metal and off cuts) galls again at different places. Insufficient lubrication with high (local) temperatures increases the wear-out rate even more. This procedure of break out and galling occurs alternately and concurrently. The washboard profile is deformed significantly and leads at some point to the failure, observed as a plate jam. In parallel to the conclusion of [Bes05], [FLK$^+$03] proclaims that wear under fretting load is the result of debris formation and ejection.

Hence, the failure results from extensive, stochastically occurring material changes, i. e., scouring abrasion, debris, and galling. The time instant of failure is thus depended on the abrasive debris (size, amount) and disadvantageous aggregation and ejection.

4.1.2 Test Rig

To examine the factors driving the material changes, a test rig is used and extended by additional sensors.

The relevant parts of the test rig are shown in Figure 4.1. The dimensions of all components are chosen in order to meet the field application and hence the operation conditions. The tribological system consists of two wear plates, the body locked into position, the counter body connected to the cylinder. An electro-mechanical valve, controlling the hydraulic cylinder, realizes the linear, reciprocating movement of the body. The horizontal movement is limited to a linear movement by the washboard profile of the wear plates. The vertical movement is prevented by an adjustable contact pressure, realized by a pneumatic cylinder and a lever arm (double T beam). An automated lubrication with field lubricant at fixed time intervals is also realized. Typical measurements from field application (normal force, acceleration, hydraulic pressure, temperature, etc.) are recorded by the real-time system (not depicted). The valve and hence the cylinder movement are controlled such that the relevant parameters (stroke velocity, ratio between operation and idle mode, etc.) are represented. In analogy to field operation, the counter body strokes over a distance of 1.6m within 40s and subsequently pauses for 70s (idle mode). This cycle of 110s is repeated steadily.

The test rig validation was performed by operating the test rig under application-relevant conditions. The failures produced by the test rig were examined and compared to the failures observed in field usage (see Section 4.1.1). According to [Bes07], the types of wear, the progress of damage, surface temperatures, thickness of accumulated material (by cold-welding, etc.) were identical, i. e., the test rig is applicable to reproduce application-relevant

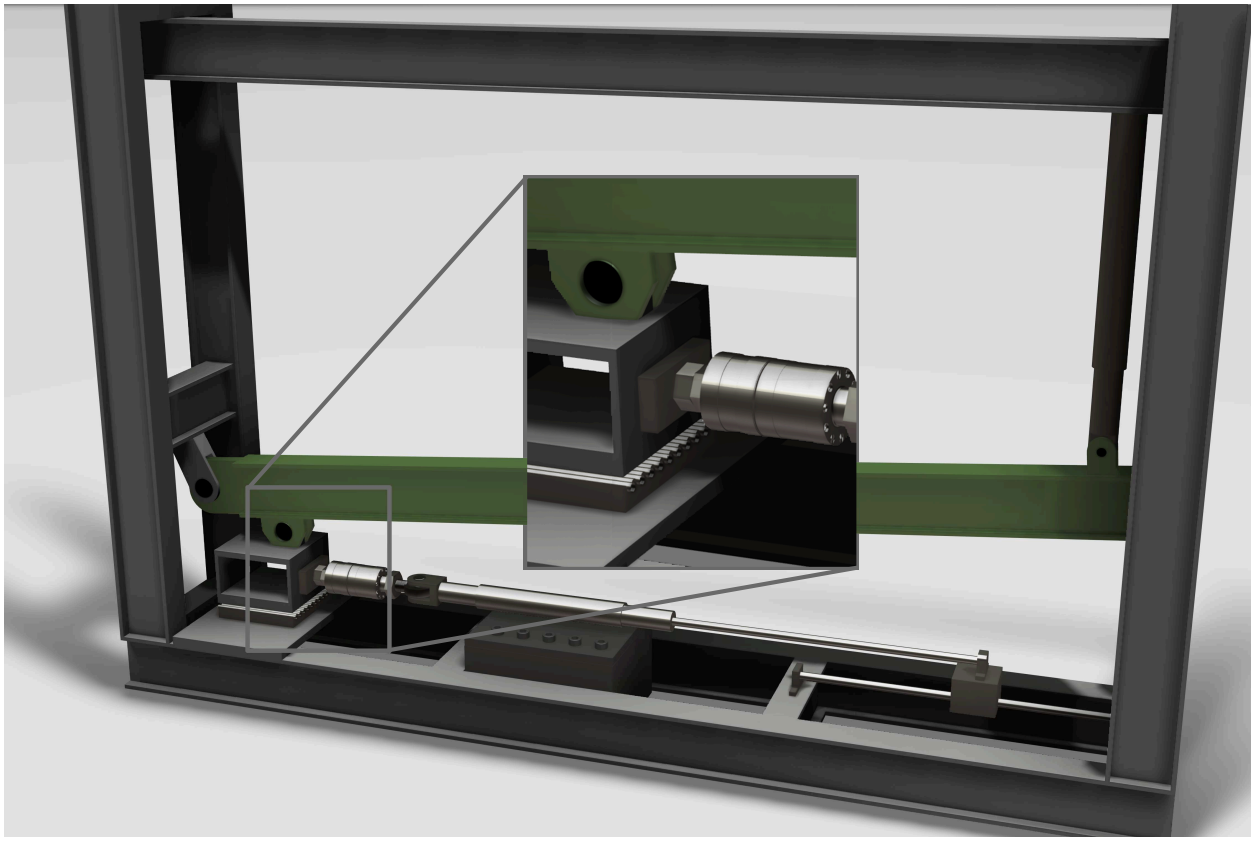

Figure 4.1: Test rig for wear examinations

conditions and hence field failure sufficiently accurate.

Various short- and long-term tests were performed to realize different damage progressions by varying the operational conditions. More specifically, the type of lubricant, the lubrication intervals, the hydraulic pressure (and hence the stroke velocity), the ratio between operation and idle mode, etc. were modified in a targeted manner. The worn out plates were analyzed and the results are discussed in detail, e. g., in [DS09, HDS10, RDS10, Rav11].

In Figure 4.2(a), the bulk material (acicular martensite) of a wear plate before operation is depicted. During operation and until fault, the material structure is changed by e. g., loading. A typical profile of a worn out plate is shown in Figure 4.2(b). Beside the bulk material (lower section of figure), different layers with deviating grain structures are present. Those layers consists of cold welded abraded bulk material and lubricant. The cavities (material defects) are starting points for micro and macro cracks that reduce the mechanical strength. When propagating through the material, the cold welded debris can abrade again. As discussed in [KRC$^+$10], martensite needles form microstructural barriers which prevent a crack propagation. In contrary to this assumption, martensite needles are assumed to provide a preferred crack propagation direction (along phase interfaces).

As stated and illustrated above, the test rig reproduces field failure. Hence, the test rig is used to obtain deterioration-relevant information for fatigue life time examinations in terms of baselines. Furthermore, specially designed experiments are used to examine the deterioration behavior under various operation conditions.

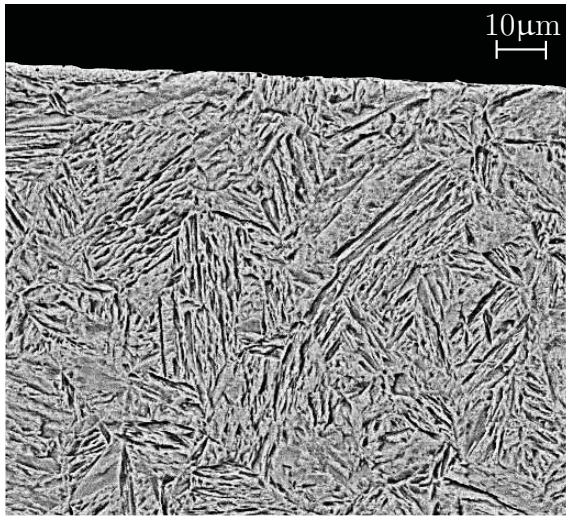

(a) Bulk material of unused wear plate

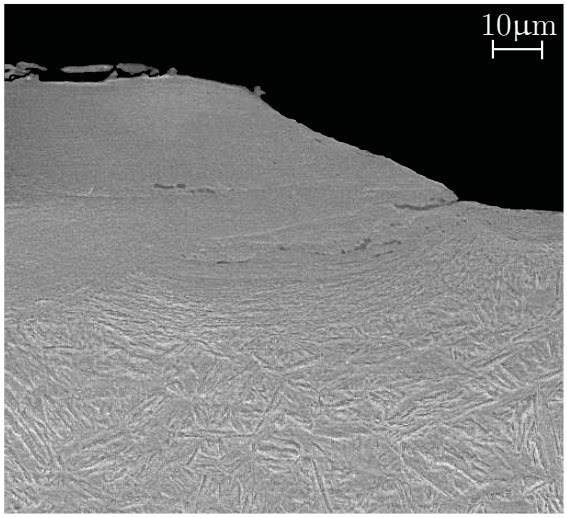

(b) Worn out plate; cold-welding, micro cracks, and bulk material

Figure 4.2: SEM results for wear plates

As the primer effect leading to failure is known and reproducible by the test rig, henceforth appropriate measurement techniques have to be evaluated to reveal unambiguous information about deterioration.

4.1.3 Acoustic Emission due to Material Change

As described in Section 4.1.2, the failure appears as a result of excessive material changes (scuffing, cold-welding). Especially abrasion is identified as the primary cause of deterioration and hence, failure. During the various examinations of worn out plates, the position of abrasion and subsequent cold-welding was stochastically distributed over the plate surface. Therefore, the deterioration is a highly stochastically process which depends on the operational conditions and initial plate damage and has to be supervised continuously by appropriate techniques.

A multiplicity of research has been done in literature on the effect of abrasion in metallic material and its detection. Especially the detection of acoustic emissions turned out to be promising in the context of structural health monitoring. In general, acoustic emission is defined as "the class of phenomena whereby transient elastic waves are generated by the rapid release of energy from localizes sources within a material", [AST90, DIN EN 1330].

In [Hol82] is stated that the "formation and propagation of micro cracks are associated with the release of energy." This energy (shock wave) propagates through the material and moves to its surface. In [Poh03], micro-structural deformations of material are detected by measuring the emitted acoustic emission during deformation. These emissions offer a great potential for non-destructive analysis of deterioration and supervision.

In [BMS90], acoustic emission analysis is used to differentiate between different wear mechanisms occurring in dry and lubricated sliding metallic contacts. The test conditions indicate a direct empirical relationship between the AE signal and the wear volume removed (abrasion). Further research show that "the time-dependent nature of the acoustic signal is able

to detect the presence of wear-reducing additives and the predominant wear process occurring" [BM91]. Hence, the correct (wear-depended) lubricant is essential for wear-minimal operation. It is stated that "acoustic emission signals increase with alumina particle concentration added to the lubricant." Hence, the acoustic emission also depends on the type (quantity) of (wear) debris.

The evaluation of AE events are a "possibility for continuously monitoring wear and for basic studies of the wear process", as these signal arise from fundamental wear processes [HK91]. Again, a dependency of acoustic emission activity and wear rate is measured in sliding metallic contacts. It is shown by experiments that "changes in acoustic emission count rates correspond to changing wear rate."

In [LYY93], material change is described as the "deformation processes in solids, such as dislocation movements, crack propagation [...] (that) produce stress waves at ultrasonic frequencies [...]." Experimental test with metallic specimens in relative sliding motion are performed and "clear indications that AE is intimately related to the fundamental material and surface actions in the wear zone" are found. The measured acoustic emissions (predominant frequencies) are finally assigned to the severity of deformations and wear conditions.

As stated by [MvKM05], "acoustic emission is a non-destructive method that is sensitive to mechanical waves created in many materials by sudden displacements due to microscopic stress release." Acoustic emission is not limited to deformation processes in metals but is also wildly used in general structural health monitoring domains, e. g., carbon fiber components in aeronautics, etc.

A crack, as a common appearance of a defect, is considered in [BFG06] as a typical source of AE. Such burst signals are attributed to plastic deformations in metallic materials. Subsequently, SHM-related examinations are discussed for composite materials with the goal of residual life time prediction.

Finally, in [BBHF07] the applicability of AE measurements for deterioration estimation is discussed. It is stated that a change in measurement of AE on the same structure at different times is related with a change in material. These changes "yields indications of defect accumulation or growth when keeping all other test parameters (e. g., emitter efficiency, receiver sensitivity, and coupling) constant." In conclusion, acoustic emission signals, especially in ultrasonic frequency range, contain deterioration-equivalent information.

4.2 Acoustic Emission Measurement

The goal is to identify a relation between the obtained stochastically, transient occurring emissions (due to material changes) and the deterioration to reveal a unique connection between both. Therefore, the three elements (see Figure fig:GenMeasChain) of the novel, problem-specific measurement chain are introduced in the following to realize the in-situ measurements. Furthermore, these measurements are integrated into the test rig control to enable correlations to existing process information, e. g., chamber pressures of the cylinder, position and acceleration of the piston, body temperature, compressive force, etc.

4.2.1 Transducer

The measurement of material changes by acoustic emission detection is a promising but also a challenging task. The stress waves at ultrasonic frequencies, generated by material

changes, propagate through the structure and meet the (plate) surface. To measure these potentially very small and short-time surface displacements without any coloration or unwanted side effects, a no-contact measurement (e. g., laser interferometer) would be best. Due to low robustness of these systems, surface-bonded transducers with high sensitivity and wide bandwidth have eo be chosen. According to [Shu02], a transducer with piezoelectric properties is best suited for this purpose.

The direct piezoelectric effect relates the (rapidly changing) mechanical load (surface displacement due to shock wave) to a changing voltage on the insulated electrodes of the piezoelectric element. The piezoelectric voltage should be measured reactionless to avoid any shifting effects like attenuation, amplification, phase shift, etc. The physical effects of piezoelectric materials are described in detail, e. g., in [Fra10, MvKM05, TEKP10, JBS+04].

Derived from thermodynamics, the energy conversion (piezoelectric effect) is analytically described by

$$D_3 \;=\; d_{33}T + \epsilon_{33}^{T}E \tag{4.1}$$

as a linearly coupling of two different effects, namely electricity and mechanics [Ike90]. The equation (4.1) describes the relation between the mechanical stress T, the electric field E , and the electrical flux density D.

The constants d, and ϵ describe the piezoelectric constant, and the dielectric permittivity, respectively. The superscript T denotes that the parameter is obtained at constant (zero) stress T and is hanec a consant. For frequency-dependent investigations, the permittivity is used instead. The subscript 3 denote the direction of the stress axis, the index 33 that the polarization axis is parallel to the stress axis.

According to [Ike90], the electric current I is calculated from equation (4.1) by integrating the electric field

$$I \;=\; j\omega \int\limits_{x_1,x_2} D \,\mathrm{d}x_1 \,\mathrm{d}x_2 \;, \tag{4.2}$$

with x_1 and x_2 both perpendicular to the stress axis S and equal to the diameter $d_{\oslash}$ of the chosen ceramic.

The formula for the current I, induced by the direct piezoelectric effect, yields

$$I \;=\; j\omega \left[d_{33}F + \epsilon_{33}^{T} d_{\oslash} U \right] \;, \tag{4.3}$$

with I as the electric current, F as the applied force, and U as the voltage.

All values are varying with the frequency ω of the input F. Hence, the frequency-dependency of the permittivity ϵ is considered by replacing ϵ by the admittance Y of the piezoelectric element.

Additionally, [Ike90] proposes a constant ϕ to summarize the material constants, coupling condition, etc. By operating the transducer in open circuit condition ($I = 0$), the transfer behavior of a piezoelectric material as a sensor is

$$U \;=\; -Z_{\phi} v \;, \tag{4.4}$$

with Z as the impedance, v as the velocity of surface movement, and Z_{ϕ} as the governing factor of the dynamics. It is important to notice that any movement (and hence velocity v), perpendicular to the direction of plate movement, generates a voltage U.

Material type	PIC 255
Curie-Temperature	$T_c = 350°\text{C}$
Piezoelectric charge constant	$d_{33} = 400e{-}12$ C/N
Frequency constant of thickness oscillation	$N_t = 2000\text{Hzm}$
Geometry	Diameter $d_\oslash = 10\text{mm}$ Thickness $TH = 0.55\text{mm}$

Table 4.1: Data of piezoelectric material PIC255 [PI11]

Amongst a variety of piezoelectric materials, a non-resonant broadband, lead-zirconium-titanate (PZT) ceramic in disc shape with metal silver electrodes and wrapped contacts is chosen. The important geometric dimensions and directional material property for thickness oscillations of plates are given in Table 4.1.

The serial resonance frequency for the chosen PIC 255 material is

$$f_s = \frac{N_t}{TH} = 3.6\text{MHz} \; . \tag{4.5}$$

In the frequency range less than 3.6MHz, this unbonded ceramic provides an electrical impedance response Z as shown in Figure 4.3. The expected capacitative behavior is observed. The frequency response measurement was performed on a Network Analyzer according to [DIN 50321-1] and validated with OEM measurements.

To guarantee a minimum attenuation of the emitted acoustic signals, the transducer has to be attached as close as possible to the wear zone. Therefore, the transducer is bonded to the backside of the moving wear plate. The requirements for the attachment are: good mechanical coupling, low (frequency-depended) attenuation of couplant, reproducibility, and electrical insulation.

The couplant between the ceramic surface and the wear plate is required to reduce the acoustic impedance mismatch (reflection coefficient) and guarantee an electric insulation. The latter is realized by a polyvinyl chloride (PVC) layer between the ceramic and the metal surface (surface resistivity of PVC $> 10^{13}\Omega$). The layer needs to be very thin (here: approx. 20µm, see Figure 4.5) to avoid an acoustical insulation and hence signal attenuation. The same holds true for the glue layers. To attach both, the insulating layer to the metal and the ceramic to the insulating layer, a cyanoacrylate glue is used; the adherents are free of grease, dust, and adhesives. The glue cures at room temperature to avoid artificially aging of the material as described in [BBHF07]. The aging of the piezoelectric material, as it mainly refers to reduction in remnant polarization due to service loads, environmental exposure, etc., is not relevant for the considered short-term experiments and hence neglected [BBHF07]. Only during soldering of the contacts, the effect of aging is considered by keeping the soldering temperature below $\frac{T_C}{2}$. To reduce reflections of the acoustic emissions on the surface, the nominal surface roughness is reduced by grinding with sandpaper P1200 (grain size according to [DIN 6344]).

The schematic application of the ceramic, insulating layers and wear plate is depicted in Figure 4.4.

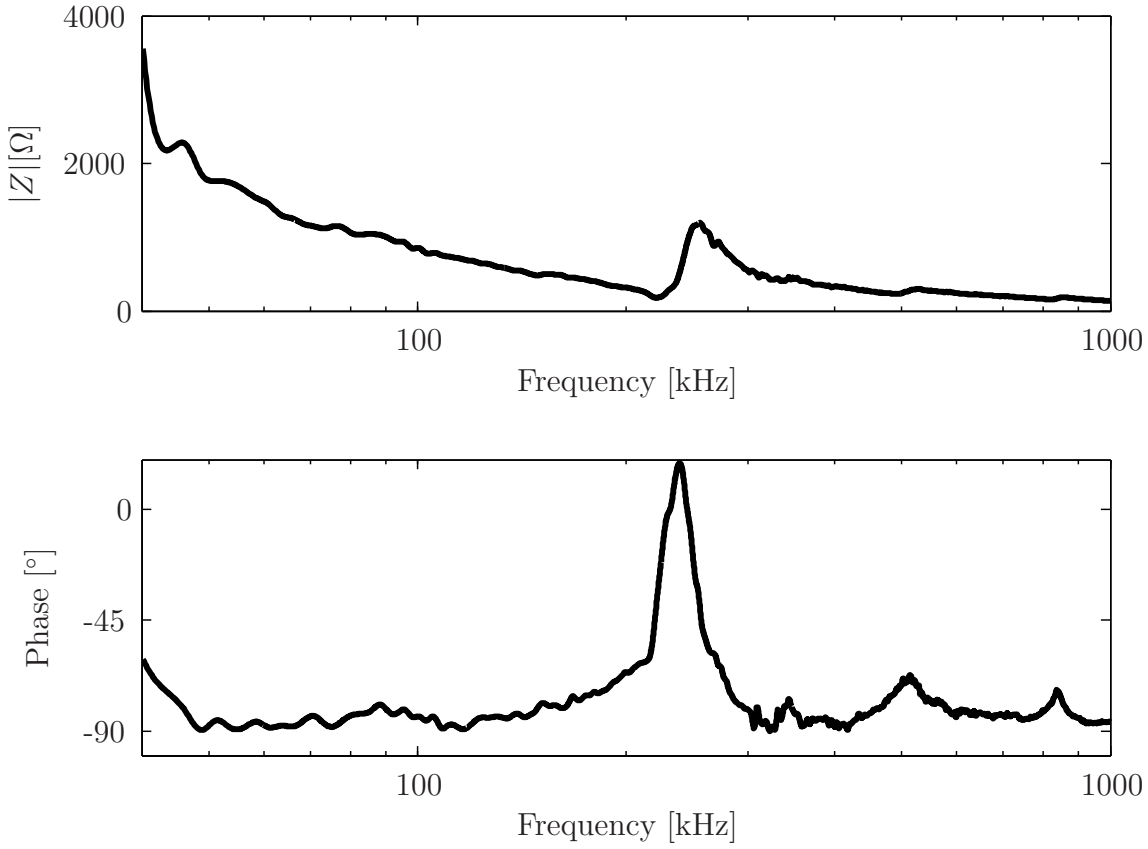

Figure 4.3: Measured impedance curve of bonded PIC 255 ceramic

In Figure 4.5, a SEM image of the piezo ceramic is given. The insulating layer (glue and non-conducting foil) meters approx. 20µm.

Finally, the mechanical impedance response Z_ϕ according to Equation (4.4) of a bonded ceramic (as described above) was compared to an unbonded one, depicted in Figure 4.3. As expected, only quantitative changes are observed in the absolute values of $|Z_\phi|$ which only is attributed to ϕ. Hence, Z represents the (electrical) transfer behavior of the considered piezoelectric material. The qualitative behavior is constant for comparable transducers and only varied quantitatively by ϕ in the amplitude. To compensate for the effects of ϕ, an estimation about the amplification behavior over frequency is derived from measurement. By exciting a structure (thin flexible plate) with transducer, bonded to the structure as described above, with a known velocity v and measuring the resulting voltage, all necessary information are obtained. Considering the inverse transfer behavior of the measurement chain (see below), a good estimate about Z_ϕ was derived and considered in Z_{comp} in Figure 4.8.

In summary, it is obvious that the impedance plays a major role in the measurement chain. To further improve the measurement results, an impedance converter is designed to meet the required characteristics (sensitivity and flatness of transfer behavior in mentioned frequency range, robustness in rough environment, shock resistant, etc.). This is detailed in

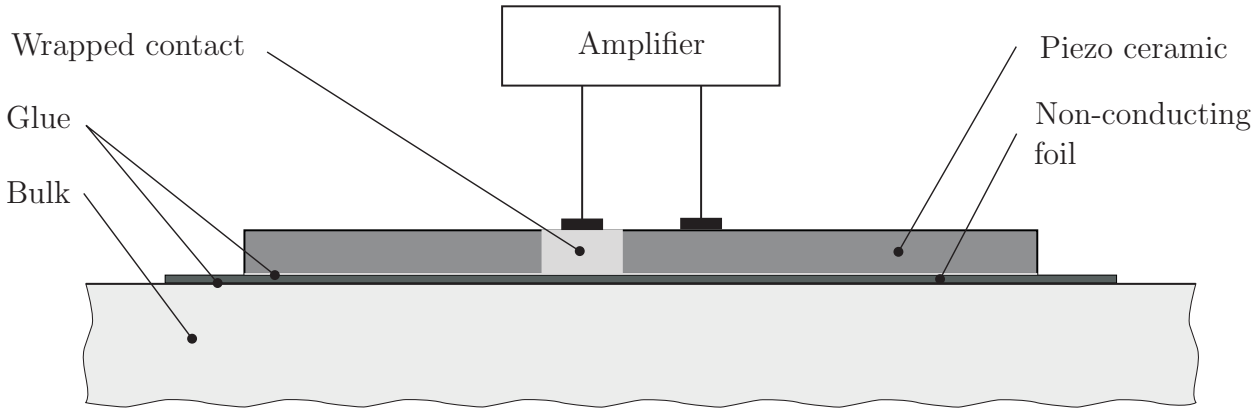

Figure 4.4: Application of transducer

the following Section.

4.2.2 Instrumentation Amplifier

A piezoelectric material is an active material with high impedance that produce an electrical response (voltage at electrodes) when mechanically excited due to electric displacement of charge. As obvious from Table 4.1, the electric charge generated by surface displacements (e. g., force) is of low power. As discussed in Section 4.2.3, the digitizing of an analogue signal bases on a capacitor, which is electrically charged by the charge to be measured. This process drains the charge from the electrodes and hence, adversely affect the measurement itself. Additionally, the prerequisite from above (open circuit, $I = 0$) is not fulfilled. Accordingly, the direct digitizing of the generated voltage by an AD-Converter is not possible.

Beside the challenge of measuring low power signals, attention is devoted to the noise reduction. The sensitivity of the analysis depends on the quality of signal, which is primary limited by ambient background noise. The major sources of noise are electromechanical radiations and fields. For the experimental setup as well as subsequent field usage, electrical machines or devices in direct environment are relevant, which produce varying electromagnetic fields (e. g., drives, pumps, valve, etc.). Hence, an additional challenge in measuring low power signals (charge in terms of voltage drop over electrodes) with avoidance/reduction of background noise has to be solved.

An instrumentation amplifier with high input impedance and low output impedance is developed to couple the transducer with the A/D-Converter and hence, to maximize the transfered power. As detailed in [TSG08], this amplifier is very sensitive to noise, especially due to capacitive interspersions. One countermeasure is to connect the shielding of the measuring line with the ground of the electrical circuit. Additionally, special double shielded, twisted pair HF cables are used for all cabling. Cable motions (as expected by wear plate movements) can produce erroneous sensor readings; hence, the cable length are chosen equally and as short as possible. The PE wire (physical earth; ground) of the measurement equipment is the same for all; ground loops (potential differences between transducer, amplifier, and host PC) are avoided by not connecting the measurement shielding with the test rig.The amplifier is housed to additionally reduce the influence of electromagnetic in-

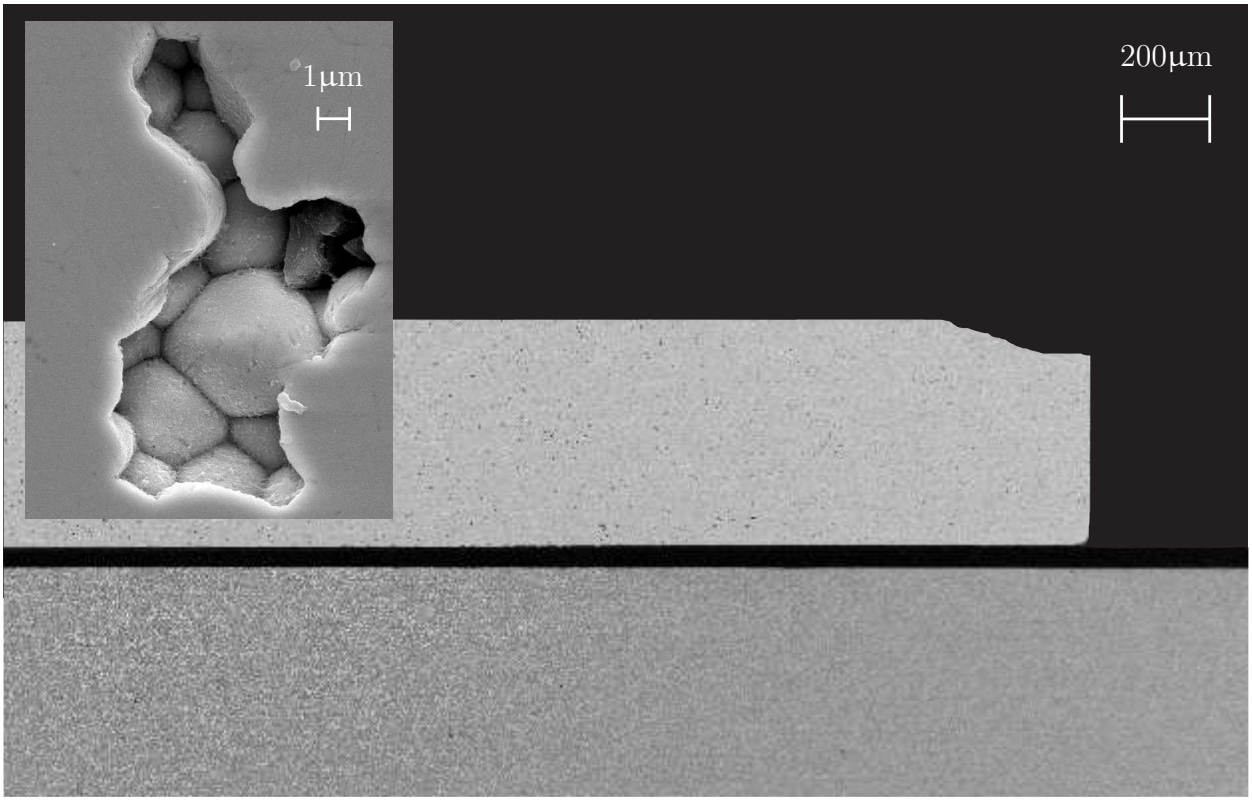

Figure 4.5: SEM image of applied transducer; detail: zirconium titanate structure

terspersions from valves, etc. Finally, the amplifier is located as close as possible to the transducer [MvKM05].

The amplifier itself is independently powered by batteries and hence, no ripple voltages are induced by the power supply. Additionally, no ground loop is induced by an external power supply in the enclosed housing. Finally, the output of the amplifier is electrically resilient and can drive the downstream A/D-Converter (see Section 4.2.3).

In Table 4.2, the input characteristics of the subsequent A/D-Converter are given. For the design of the output characteristic of the instrumentation amplifier the valid measuring range is important. In preliminary tests, piezoelectric voltage up to ±3V were recorded. Hence, a balanced potential divider is necessary to avoid damage to the AD-Converter.

The electrical connection diagram of the amplifier with integrated balanced potential divider circuit is depicted in Figure 4.6.

The balanced potential divider is designed such that the ratio can be varied by DIP switches from 1:1 to 4:1 conversion. Accordingly, the output of the amplifier can be adjusted to special applications to match the maximum input ratings of the resilient A/D-Converter.

The impedance of the measurement chain (connecting cable with impedance converter with balanced potential divider at voltage division 2:1) without the transducer is shown in Figure 4.7.

This characteristic is assumed be time invariant and hence considered during signal analysis as a constant transfer behavior.

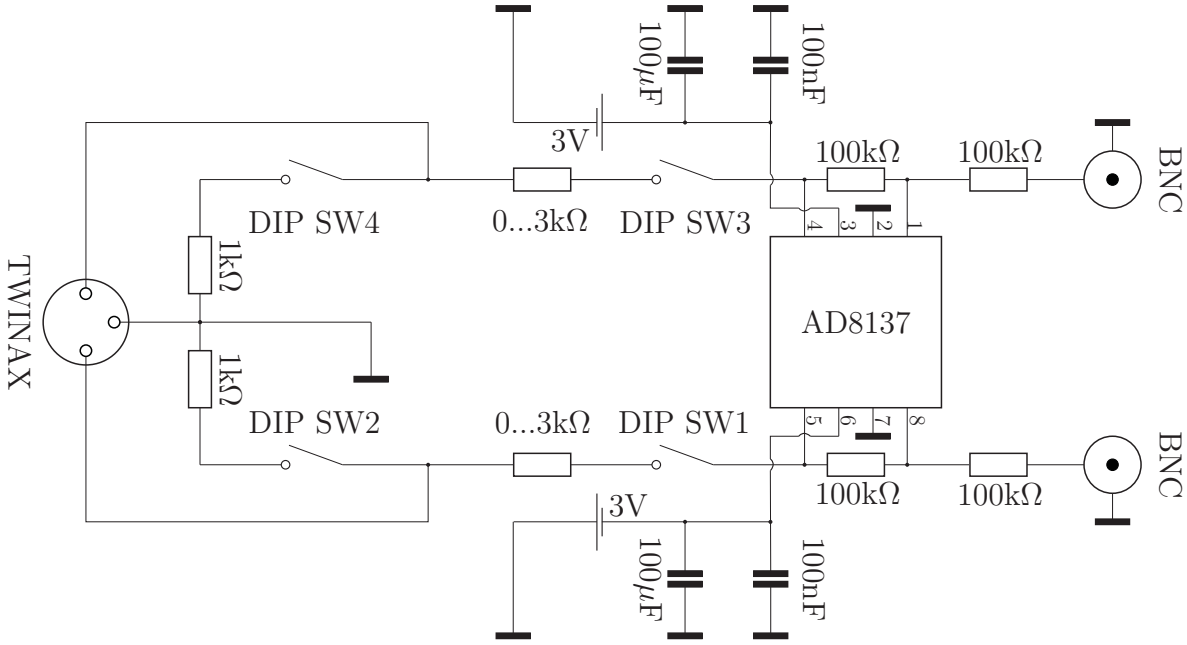

Figure 4.6: Electrical circuit of impedance converter and balanced potential divider

The success of these countermeasures to noise was evaluated by various test scenarios. The comparison between measurements without and with the above mentioned actions is performed by frequency investigations.

4.2.3 A/D-Converter

The last step in the measurement chain is the digitizing of the analogue signal. In general, an A/D-Converter (ADC) quantized an analogue signal into a time and value-discrete series values. The resolution in time is called the sample rate and denotes the equidistant recorded number of data points per second. The conversion is realized by charging a capacitor by the input charge for one time step (sample-and-hold element) and passing it to an high-impedance ADC. Subsequently, this charge is measured over a certain time and represented in a digital manner. The reference of the measured value is normally the supply voltage of the ADC. Here, a differential measurement is used to improve the common mode rejection. Hence, the difference between both measurement lines is digitizes.

In general, the electrical specification (in terms of bandwidth, electrical compatibility, response time, etc.) have to be adapted to the output of the amplifier, the input of the CPU, and the desired resolution for further examinations (filters, etc.).

The relevant data of the hardware being used is summarized in Table 4.2.

Beside the high-speed A/D-Converter, a Field Programmable Gate Array (FPGA) is available to directly perform mathematical operations in real time. The advantage is a flexible, low-cost hardware that can easily be adapted to different applications.

Summing up Section 4.2, the deterioration-proportional signals are identified as acoustic emissions. These physical signals are adequately transformed into electrical signals by a transducer using the direct piezoelectric effect. The generally neglected but very important

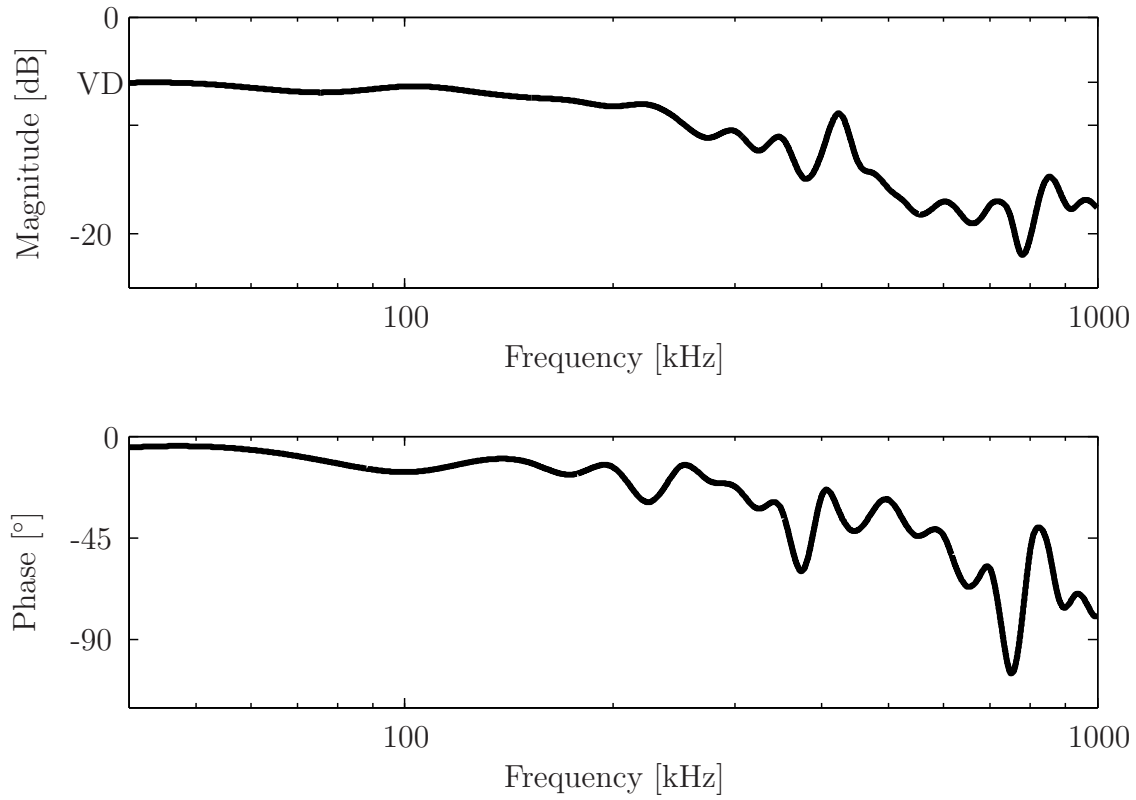

Figure 4.7: Dynamic behavior of measurement chain without piezoelectric ceramic in frequency domain

impedance considerations are discussed in detail to provide a reliable measurement basis for subsequent analysis steps. One central part of the novel development was the impedance matching by adequate couplands (non-conducting foil and glue) and application-designed amplifier (instrumentation amplifier). Beside these central challenges, the problem of noise reduction (shielding, etc.) are discussed and adequately solved. To provide the sensible information to signal analysis algorithms etc., the electrical signals are digitizes by a high-speed A/D-Converter, which can perform basic standard algorithms (e. g., Fourier Transform) by a downstream FPGA.

4.3 Module 1: AE-based Wear Estimation

As introduced in Section 3.3, the filter is understood as a method that modifies a signal to extract deterioration-proportional information, e. g., in terms of wear-specific frequency contents, phenomena, energies, etc. For this application, the direct deterioration measurement can not be performed (neither with sensors, nor by visual inspections). Hence, the essential information about the (actual) state-of-deterioration have to be extracted by adequate filters from the (loading and) deterioration-inherent signals. The choice, sequence, and parameters

FPGA-based ultrasonic measurement hardware	
FPGA	Xilinx Spartan3A DSP, 1.8M gate
ADCs	8 simultaneously sampling 16-bit, 25 Mega Samples Per Second (MSPS)
DACs	44 bit
Max. input rating	±2V
Cont. data rate	180MB/ sec
Software	VHDL, MATLAB®/SIMULINK®, Hardware Co-Sim

Table 4.2: Relevant data of signal acquisition and processing hardware

of (each) filter are refined in a heuristic process and introduced in the following.

At first, the digitized acoustic emission signals are adjusted by the inverse transfer function of the measurement chain (Section 3.3). This signal conditioning is derived from separately measured transfer behaviors (according to Figures 4.3 and 4.7) and is shown in Figure 4.8. As the result, the falsifying effects due to the individual transfer behaviors of the transducer, adhesive layers, electrical insulation, and auxiliary elements (cable, etc.) are reduced and an appropriate estimate about the real acoustic emission signal is obtained.

The adjusted acoustic emission signal is subsequently investigated for its frequency content to identify relevant events, ranges, patterns, etc. Here, the focus is set on the plausibility check of the proposed measurement chain with subsequent filtering steps. Therefore, a method is used that easily visualizes the results.

Due to the capability of the FPGA, the computationally efficient Radix-4 FFT algorithm in decimation-in-time, introduced by [CT65], is used. To preserve the time information within this filtering step, the single FFT results are used for the Short Time Fourier Transform (STFT) filter. As a result from the cut-off frequency from Equation (4.5), and the sample rate of the ADC, a STFT with a non-overlapping data windows, each with $N = 2^{16}$ measurements (data points) at a sample rate of 10 Mega Samples Per Second (MSPS), resulting in 152 dft's per second, with 152Hz as the lower and 5MHz as the upper frequency is used.

As shown in Equation (4.4) the output voltage U is induced by any surface velocities v. To reduce the disturbing effect of non-relevant structural movements and hence mechanical excitations of the piezoelectric ceramic, an additional filtering step is applied to narrow the wear-relevant frequency range to 40kHz to 1MHz. This filter can be modified to bandpass filter special frequency ranges.

The comparison between AE and filtered signal is depicted in Figure 4.9. For reasons of consistency and comparability, the signal analysis is performed at the same position, identical duration, and direction of movement of the cylinder. Hence, the point in AE measurement is kept identically, so the AE are taken at identical movements and positions. Accordingly, changes in the AE signals indicate a change in the process and surface condition respectively. The severity of the change can be indicated by typical transient frequencies, amplitudes, etc. Therefore, the same sections in time are compared in the following in detail to extract the characteristic information from the signal. The four highlighted details of Figure 4.9 are examined for their transients events. On the left side of Figure 4.9, the wear plate during the run-in phase is depicted. The surface is not deteriorated yet. As a result, the wear plate

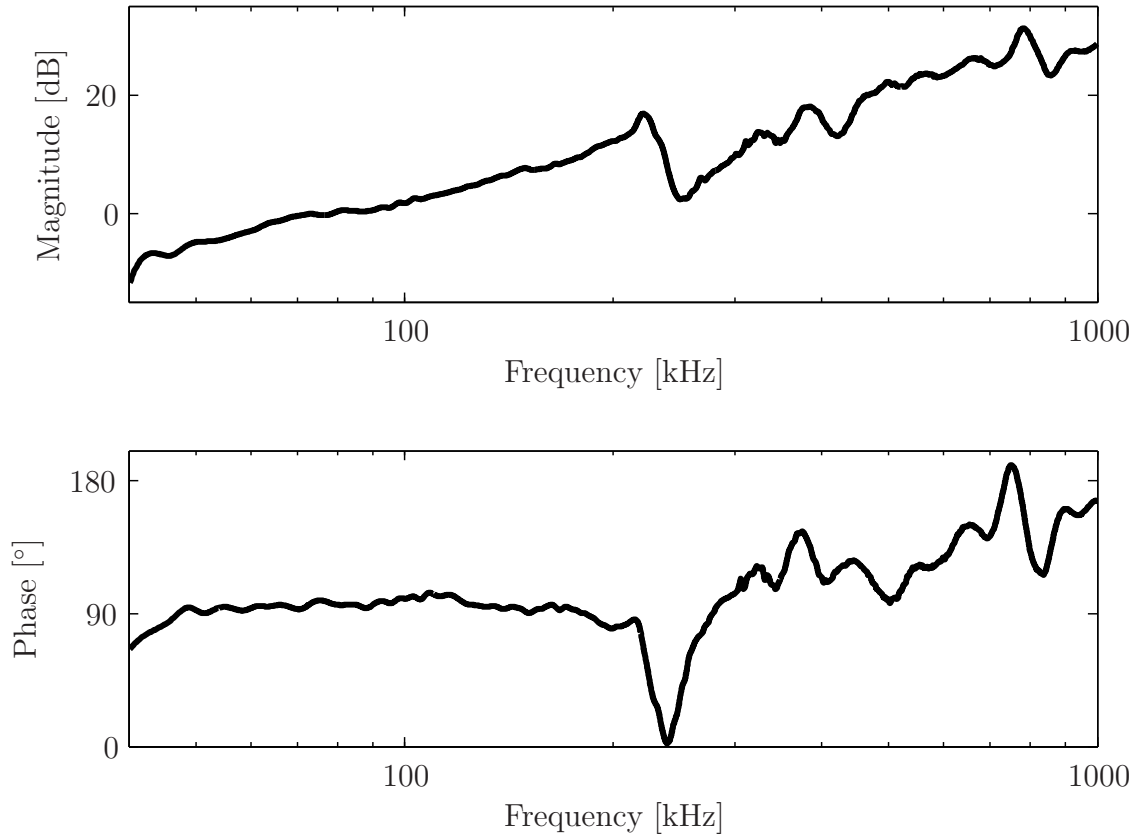

Figure 4.8: Compensation function of measurement chain (potential divider at voltage division 2:1)

is smoothly moved by the cylinder (steady movement of position signal). After a certain time of operation the surfaces deteriorate.

On the right side of Figure 4.9, the wear plate is shown after being operated. The AE activities increased and therefore the wear increased. Each signal, transformed by the STFT reveals information about this change. The deterioration-inherent information (frequency content, duration, position of occurrence) of short time transient events can be seen in the STFT spectrum. A transient event is analyzed for its containing frequencies, amplitudes, and energies and is represented as a vertical contour line (comparable with the waterfall diagram). Frequencies indicated by the blue color (-120 dB) are not found in the signal and truncated to -120 dB, whereas red colored frequencies (-80 dB) are dominant in the analyzed signal.

As expected, the STFT information of the highlighted details in run-in phase are nearly identical. Furthermore no transient occurrences are detected. Hence, no detectable wear occurred in this early operation stage. In comparison to that, the highlighted details on the right side of the figure show high AE activities, varying from the normal behavior.

In summary, the observed phenomenon of an increasing wear rate over system usage

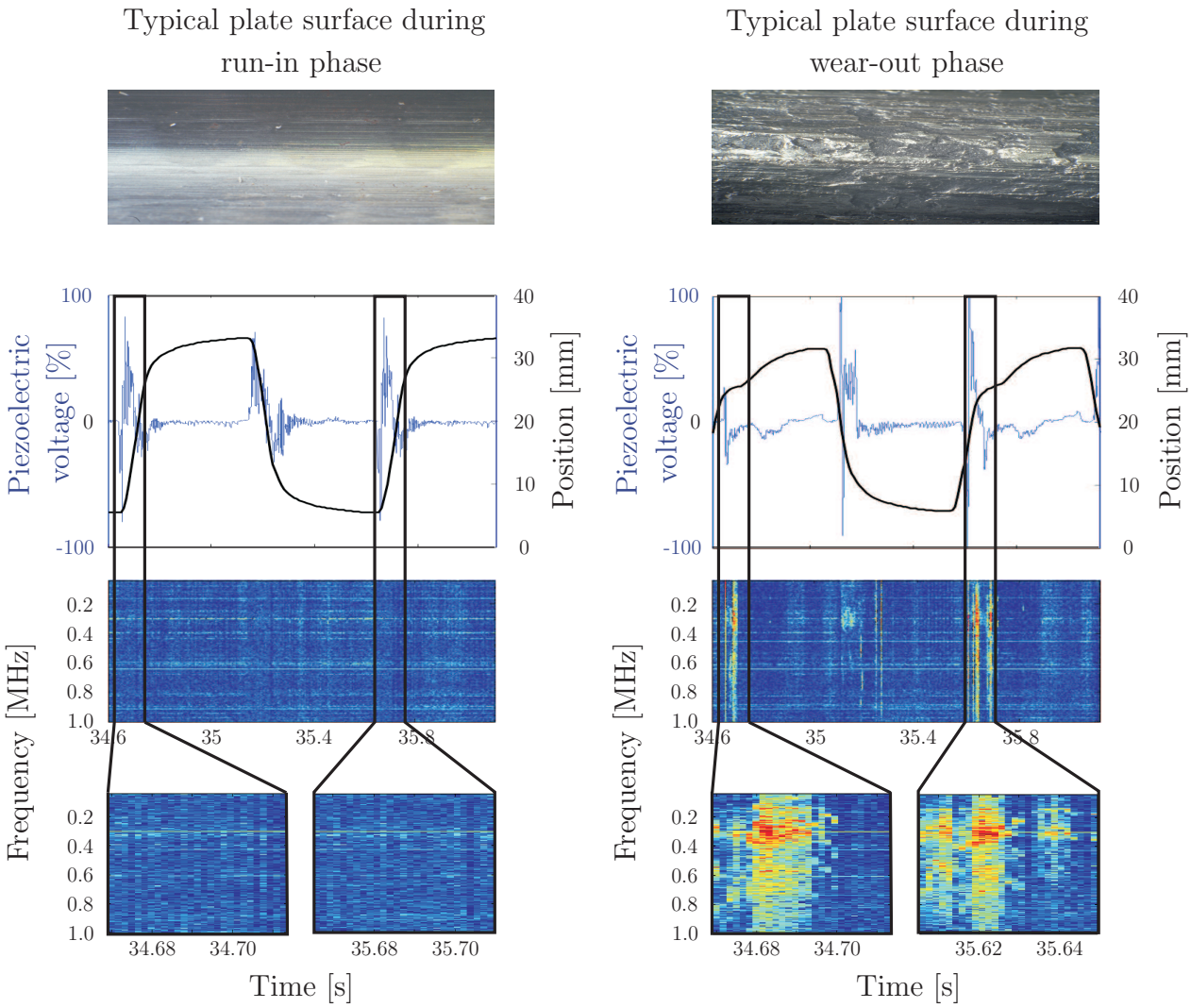

Figure 4.9: Superposition of cylinder position and acoustic emission signals with examination results in time and frequency; comparison of wear plate during run-in and wear-out phase

is also indicated by the adapted combination of measurement chain and subsequent filter techniques. The depiction of STFT results is helpful to see wear-relevant events in time (qualitative information); for the automation, quantitative information are needed to process these information with a PC. Hence, further filtering steps have to be applied. The correlation with standard process information (position, velocity, etc.) supports the directed acquisition of information.

Since the examinations, depicted in Figure 4.9, focused successfully on the plausibility check of the suggested strategy, the focus is widened such that the whole movement is measured. This reveals a detailed insight into the wear process (increasing wear rates) by measuring continuously the emitted transient AE events.

In [FLK+03], a linear correlation between dissipated energy (derived from Archard model [Arc53]) and worn out material (volume) is discussed. Applied to a hard coated material un-

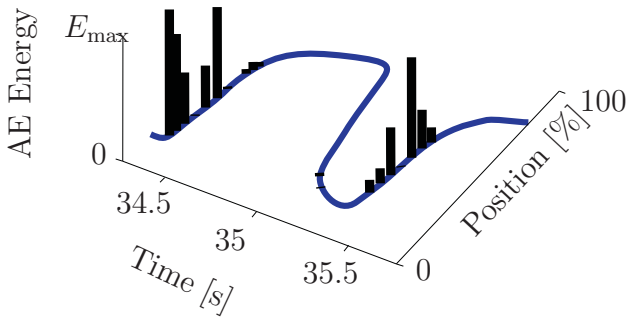

Figure 4.10: AE Energy over position and time

der oscillating sliding contact, a quantification of wear and hence surface life time is derived. In [BBHF07], "the acoustic emission signal energy was found to be particularly sensitive to damage increase. [...] A clear trend of increasing acoustic emission signal energy was observed with consecutive damage stages [...]." Further examples for successful deterioration estimation by AE energy is found in literature. It is commonly conducted that a high AE emission (and hence energy) indicates a significant effect on the life time of the considered system.

The acoustic energy is derived as

$$E(\omega) = |X(\omega)|^2 \ , \tag{4.6}$$

with $X(\omega)$ as the Fourier transform of the AE signal y in time domain.

The correlation of the AE energy (of each STFT time interval) with standard process information (here: cylinder position) is depicted in Figure 4.10.

This representation is useful to visually detect wear zones and abnormalities. Furthermore, stochastically occurring events (due to wear) can be distinguished from nominal, process-induced energy events (due to normal excitations of the process itself). By adapting the filter adequately, the portion of non-wear events can be reduced to minimum and only wear-related information are depicted and further investigated.

Based on this promising result for AE energy, the accumulation over system usage is finally realized. The last filtering step is thus the accumulation of deterioration-proportional information. Based on the observed behavior, a summation of deterioration-equivalent AE energies is used as the damage accumulation hypothesis to obtain the deterioration-proportional information.

According to Section 3.3, the purpose of this module is to acquire knowledge about the chosen measurement chain and filter techniques in correlation with the observed deterioration and failure behavior. The conclusion drawn from this observation are essential to evaluate the accuracy and applicability of the above introduced modules. The determination of the deterioration-proportional information with immeasurable deterioration is detailed in Figure 4.11.

As the major challenges of determination of deterioration-inherent information are solved, the proposed measurement chain in conjunction with the proposed filter bank of module 1 is validated by test runs. Three test runs are performed, each with a new pair of wear plates. The test procedure is designed such that the plate pairs are operated until failure. The loading is kept constant for all three test runs. After individual failure of each pair,

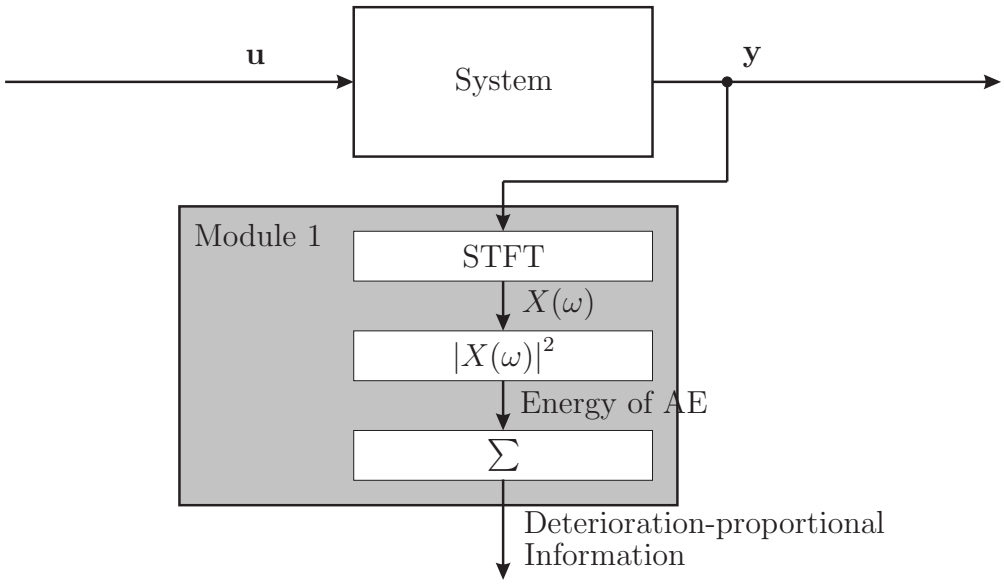

Figure 4.11: Module 1: Schematic overview of filter bank

the results are consolidated in order to identify similar informational contents in all three results. As this task is detailed and proved valid in Section 4.4, here the final results are presented.

In order to illustrate the need of the proposed filtering steps, the results of the last two steps are illustrated in the following (indicated by dotted lines in Figure 4.11).

The result of the individual AE energy emissions (gray bars) and accumulated energy (colored line; deterioration-proportional information) during run-in phase are depicted in Figures 4.12, 4.13, and 4.14. All test runs were carried out at constant operational conditions, as described in Section 4.1.2.

The end of the run-in phase is clearly indicated by a reduction of AE events and coincides with a system usage of approximately one hour (33 cycles) of operation for all tested specimen. Based in this observation, run-in phase is considered to correlate with a constant value of cycles.

In Figure 4.15, the progression of the deterioration-proportional information (accumulated AE energy) for the considered three test specimen is depicted, which appears to scatter over a range of approximately 0.18 at the end of run-in phase. As the value of the deterioration-proportional information is used as an indicator for the deterioration level, the absolute value is less important than the relation to other observations (tendencies, etc.). This means for the observed three test specimens that system 3 (red line) reveals a disproportionately high deterioration (above average) during run-in phase. The impact of this observation on the RUL will be discussed in following.

It is important to notice that the operation of the system (operational and environmental conditions) are not varied for the whole test until failure.

In Figure 4.16, the subsequent progression of the deterioration-proportional information are depicted.

Although the operation has not been modified, the observed deterioration (in terms of AE activities) has changed in comparison with the progression and gradients of the activities,

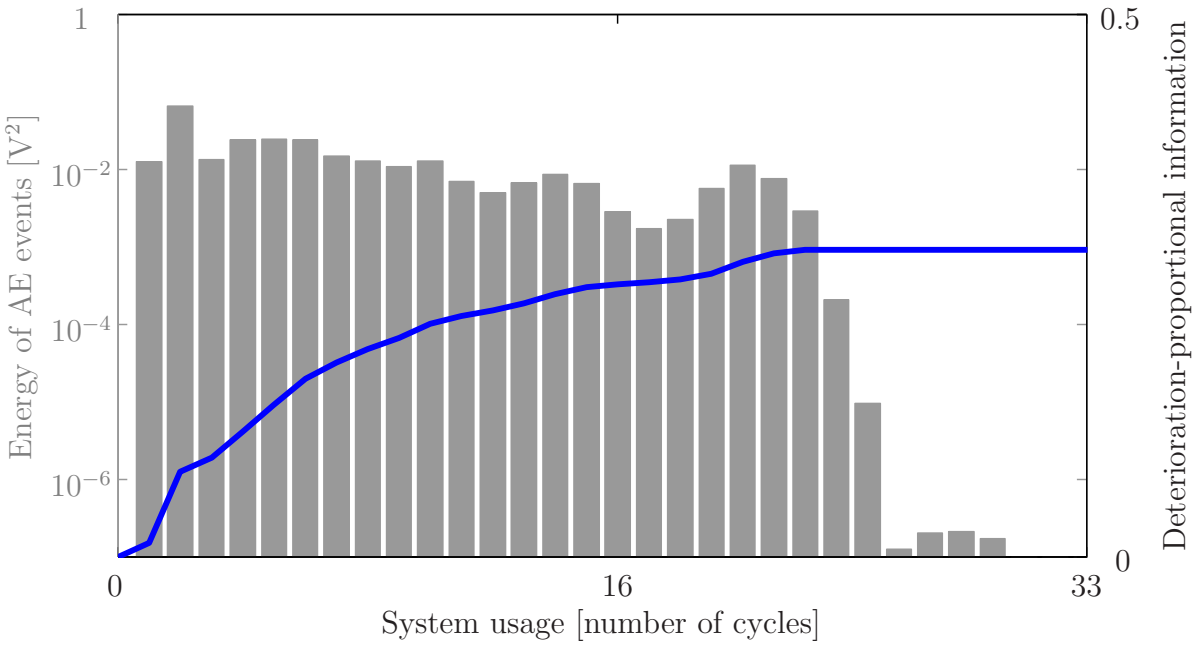

Figure 4.12: Acoustic emission energy events (gray bars) and derived progression of deterioration-proportional information over system usage for specimen 1 during run-in phase

observed during the first cycles (run-in phase). Therefore, the deterioration behavior of the systems itself is considered to be changed and denoted by permanent wear phase.

Again, system 3 shows a distinct deterioration behavior, as only few but high AE events (and hence, measured AE energies) determine the curve progression and hence, indicate severe wear events. The end of permanent wear phase is reached much earlier than for systems 1 and 2. These systems deteriorate over a long period of cycles before entering the wear-out phase.

The last phase of system usage is again ruled by several cycles with noticeable AE events, ending up with the termination of movement. The exact definition of the transition from permanent wear phase to wear-out phase is not as unambiguous as from run-in phase to permanent wear phase. Here, the last adjacent AE events are associated to wear-out phase after ending up with failure. The individual deterioration progression due to a changed deterioration behavior during the last phase of system usage are depicted in Figure 4.17.

Again, the stochastic aspect of material wear is observed in the scattering instant of failure, denoted by varying maximum system usages.

Once, a sufficiently large number of observations for each particular phase is available, a quantitative statement can be stated about the correlation between the index and the real deterioration.

Based on the observed behavior, the hypotheses of a correlation between the deterioration and the observed instant of failure is stated. The analysis result is assumed to be appropriate to describe the incremental deterioration. Hence, the summation of AE energies is a quantity, equivalent to the extent of deterioration.

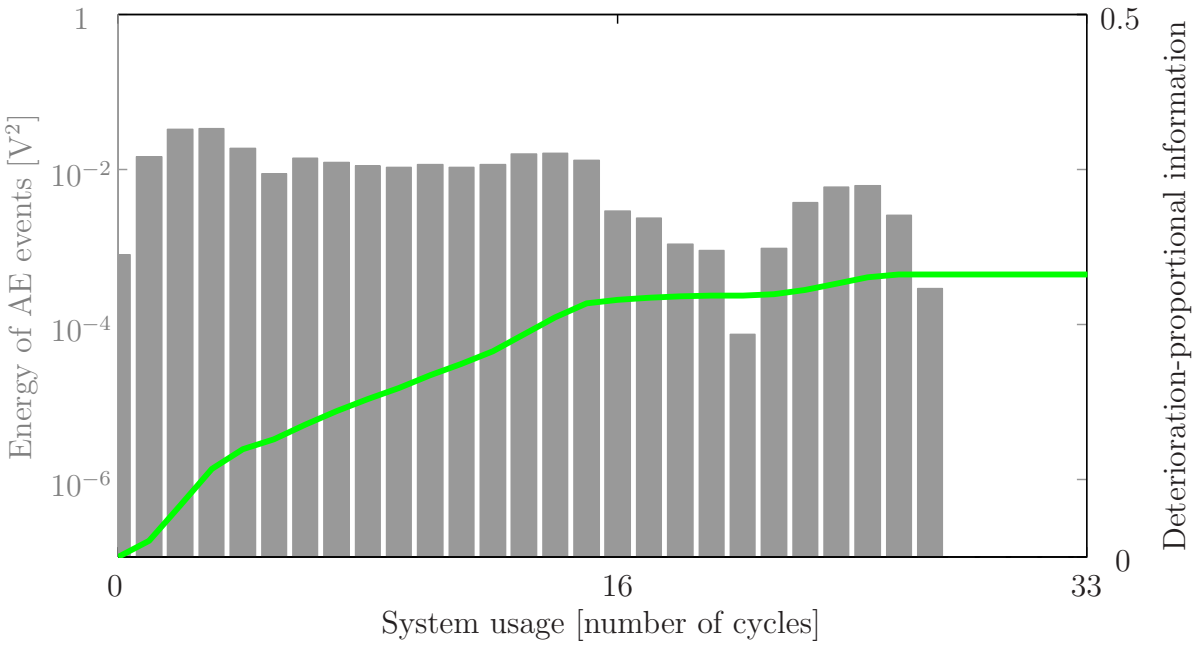

Figure 4.13: Acoustic emission energy events (gray bars) and derived progression of deterioration-proportional information over system usage for specimen 2 during run-in phase

In summary, qualitative information are derived from these baseline test. The determination of the current wear phase is important for the estimation of the impact of observed AE events on the state-of-deterioration of the system. Especially the run-in phase is recognized to essentially influence the RUL by (above average) premature deterioration. This aspect is important for module 2 to evaluate the probable premature damage due to phase I and to derive appropriate countermeasures in terms of prolonging the RUL by appropriate operational conditions.

According to Section 3.3, the off-line phase for module 1 is completed as a deterioration-proportional information is derived and validated in terms of the accumulated AE energy. As observed, the information scatter over system usage as the three systems fail at different, individual instants of system usages with scattering maximum deterioration-proportional information. Hence, the subsequent module 2 gathers the information and derives an appropriate measure for average, phase-specific deterioration estimation.

4.4 Module 2: Average Deterioration Estimation

The purpose of module 2 is the determination of an average propagation of the deterioration-proportional information by evaluating the past and actual, individual propagation. Based on the experimentally derived knowledge from module 1, the different, phase-specific deterioration progressions (derived under constant operating conditions) are examined. Therefore, each phase is considered and evaluated separately.

As introduced in Section 3.4, the unification of the varying deterioration-proportional

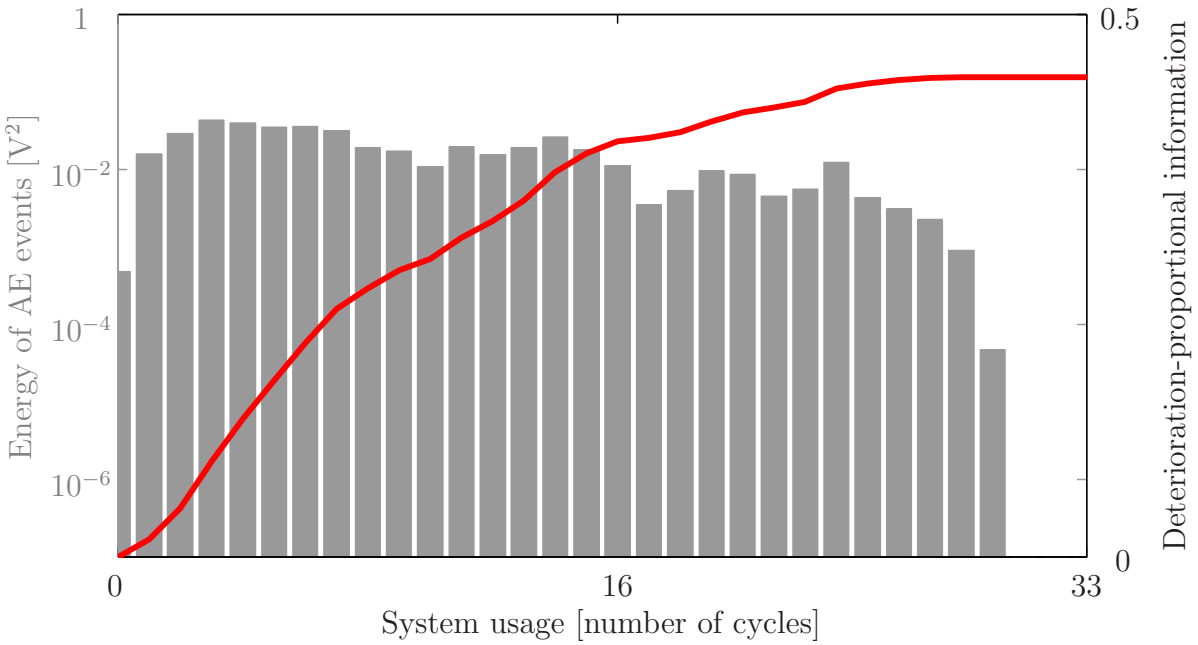

Figure 4.14: Acoustic emission energy events (gray bars) and derived progression of deterioration-proportional information over system usage for specimen 3 during run-in phase

information is necessary. Therefore, the different deterioration-proportional information, calculated by module 1 for the considered systems, is unified in terms of the system usage until failure. This is depicted in Figure 4.18.

The drawn distinct lines in Figure 4.18, separating the phases from each other, are assumptions, based on measurements. As more systems are operated and more information are gained, these separating lines will be adapted and refined. Especially the clear separation of permanent wear phase to wear-out phase is supposed to be a rough estimate of the real transition. Nevertheless, this criterion serves as a starting hypotheses and will continuously modified according to subsequent observations. The importance of the transition for maintenance strategies between the permanent wear phase and wear-out phase is obvious, as the system, once entered wear-out phase, is close to fail. The even more important information (RUL, etc.) are gathered during the clearly determinable run-in phase.

Following Section 3.4, the Weibull distribution is considered to describe wear deterioration processes adequately. The result of an adapted Weibull distribution to the experimentally derived deterioration progressions is shown in Figure 4.19 for run-in phase. The dashed line represents the median of the two parameter Weibull distribution. The parameters are derived by the MLE algorithm.

By comparing the actual deterioration-proportional information of a system to the median value (dashed line) of the Weibull distribution, an information is derived if the actual considered system has been deteriorated disproportionately small or high during run-in phase. In conjunction with further investigations of permanent wear phase and wear-out phase, an estimate about the probable RUL can be stated.

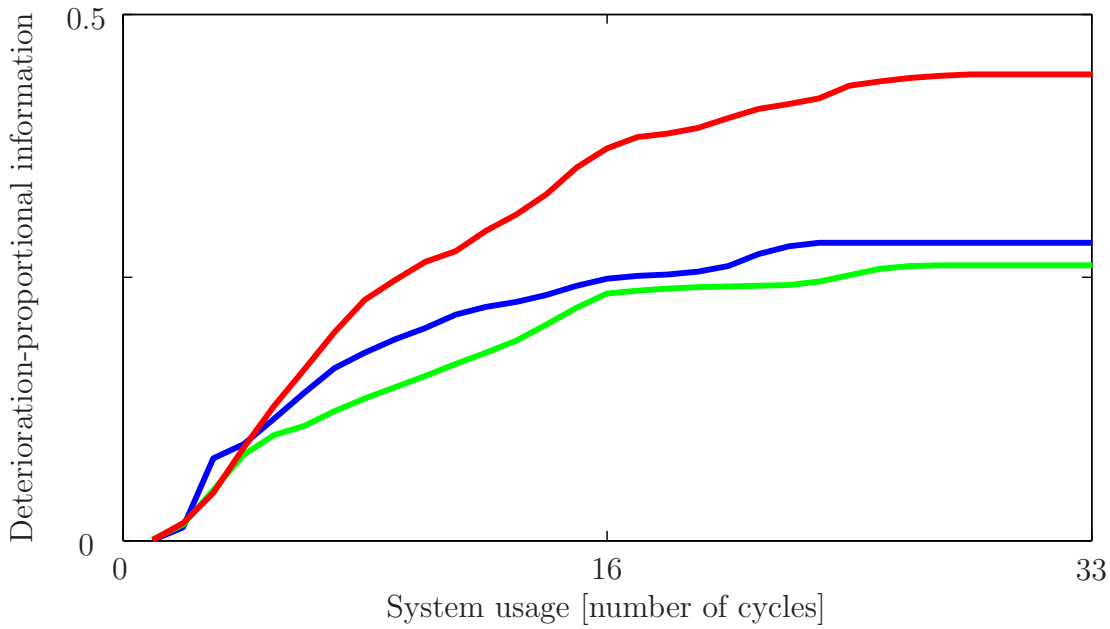

Figure 4.15: Progression of deterioration-proportional information over system usage for all three specimen during run-in phase

In comparison to run-in phase, a moderate slope is obtained during this phase which is an indicator for constant wear. Stochastically and severe wear events (in terms of observed AE energy) is only observed for the this system (red line) after approximately 40% of operation in permanent wear phase.

Further studies have to investigate the individual propagations in each phase in more detail. The phase-specific distribution are modified in terms of their parameters. The most critical phase is the run-in phase. Hence, the tests will mainly focus on this phase as it determines the remaining life time.

4.5 Module 3: Wear Prognosis

As the parameter space $\boldsymbol{\xi}$ is limited, no extensive tests were carried out to evaluate the influence of varying operational parameters on the deterioration (progression) and instant of failure. As this investigation is relevant for further developments, future work should concentrate on selectively changing the operational parameters like material, etc.

The deterioration-influencing factors are identified as the type and frequency of lubrication. As the system operates in a tight industrial network, the arbitrary modification of other operational parameters (pressure, velocity of cylinder, etc.) would lead to a decelerated process and hence to unwanted effects for the preceding and following process steps. Therefore, the focus is set upon the estimation of deterioration and hence, giving deterioration-based information about the probable remaining useful life. This information can subsequently be used to initiate appropriate maintenance strategies and to use the components up to their most probable end of life time.

4.6 Summary and Discussion

The failure due to wear of the central functional element of an industrial machine is investigated. According to a detailed material analysis, three main tribological mechanisms which lead to failure were identified. For investigation purposes, a test rig, which reproduces the main wear-out effects, was presented. Based on the literature, acoustic emissions were identified to be the most promising effect for indicating the deterioration progression.

Therefore, a novel measuring chain based on the direct piezoelectric effect was developed and operated. The main challenges of and solutions for measuring piezoelectricity are discussed. In particular, the frequency-dependent amplification from source to the digital correspondent was considered within the first filter. Subsequent models used baseline information about typical acoustic emission events to identify relevant signals. This process was supported by adequate visualization, which indicated the regions and the severeness of stochastically occurring wear. For the most typical material and lubrication combination, several comparable wear-out tests were performed. A high correlation between the point of failure and the measured damage-equivalent signal was shown.

In short, the deterioration under normal operation can be estimated within sufficient probabilistic limits on the basis of the novel measurement chain and an adequate, FPGA compatible filter.

In the future, different operating parameters can be chosen to support the strategy described above. In particular, the database has to be enlarged to cover a larger range of conditions than the one tested above. To improve the measurement even more, a housed piezoelectric ceramic reduces the effort of calibration and impedance measurement. Furthermore, the effort of gluing several thin layers of identical thickness and material properties without inducing a mechanical strain (deformation) due to mounting can be reduced. The integration of the proposed admittance in the electric circuit of the impedance converter improves the signal-to-noise ratio, and hence signal quality. The admittance of the subsequent measurement line can be integrated in the FPGA to obtain an even high correlation between calculated signal energy and surface displacement. The investigation of individual failure modes (different material changing effects) and correlation with characteristic frequency ranges, amplitude patterns, etc. can be improved.

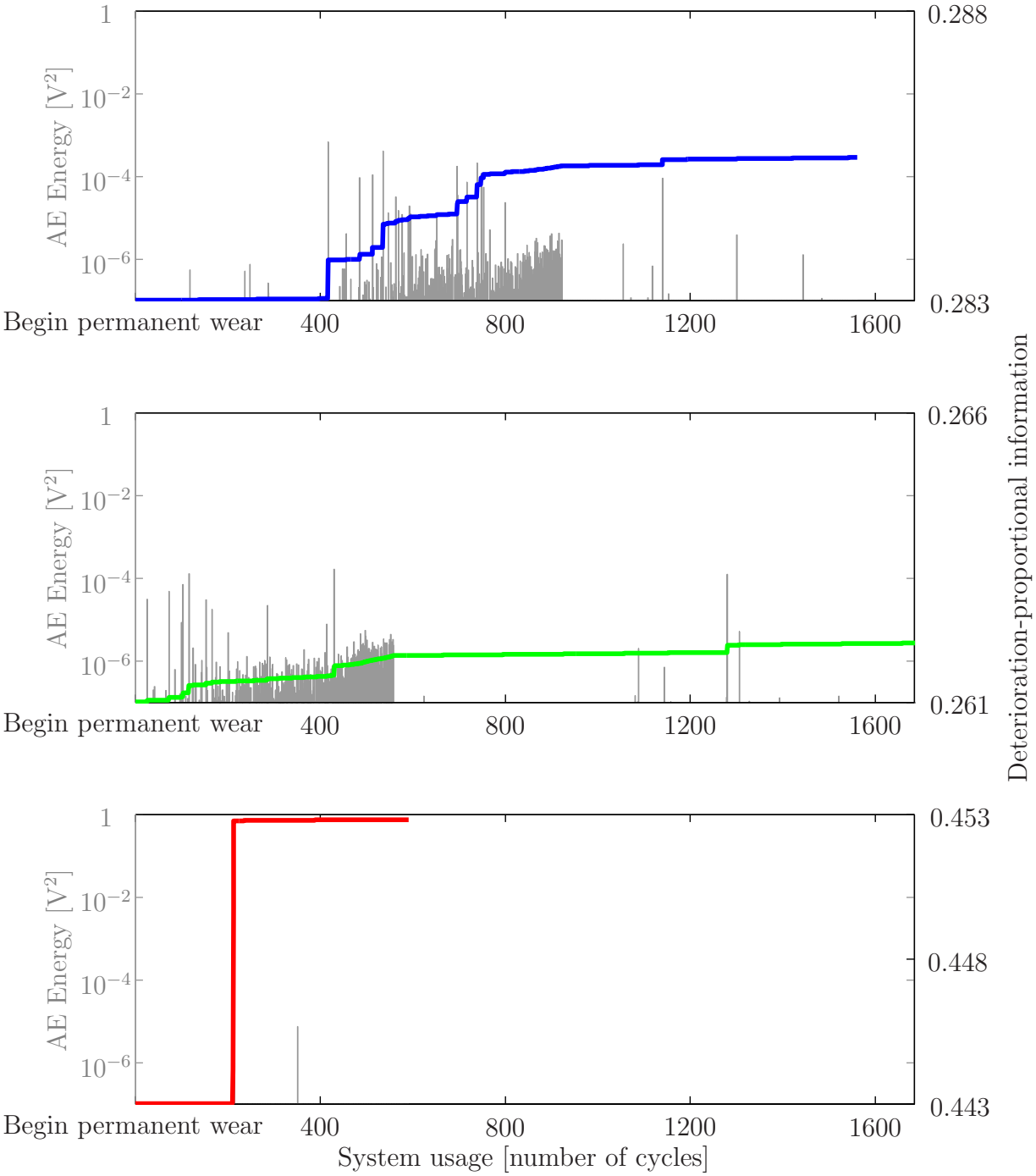

Figure 4.16: AE power and derived progression of deterioration-proportional information over system usage for all three specimen, during permanent wear phase

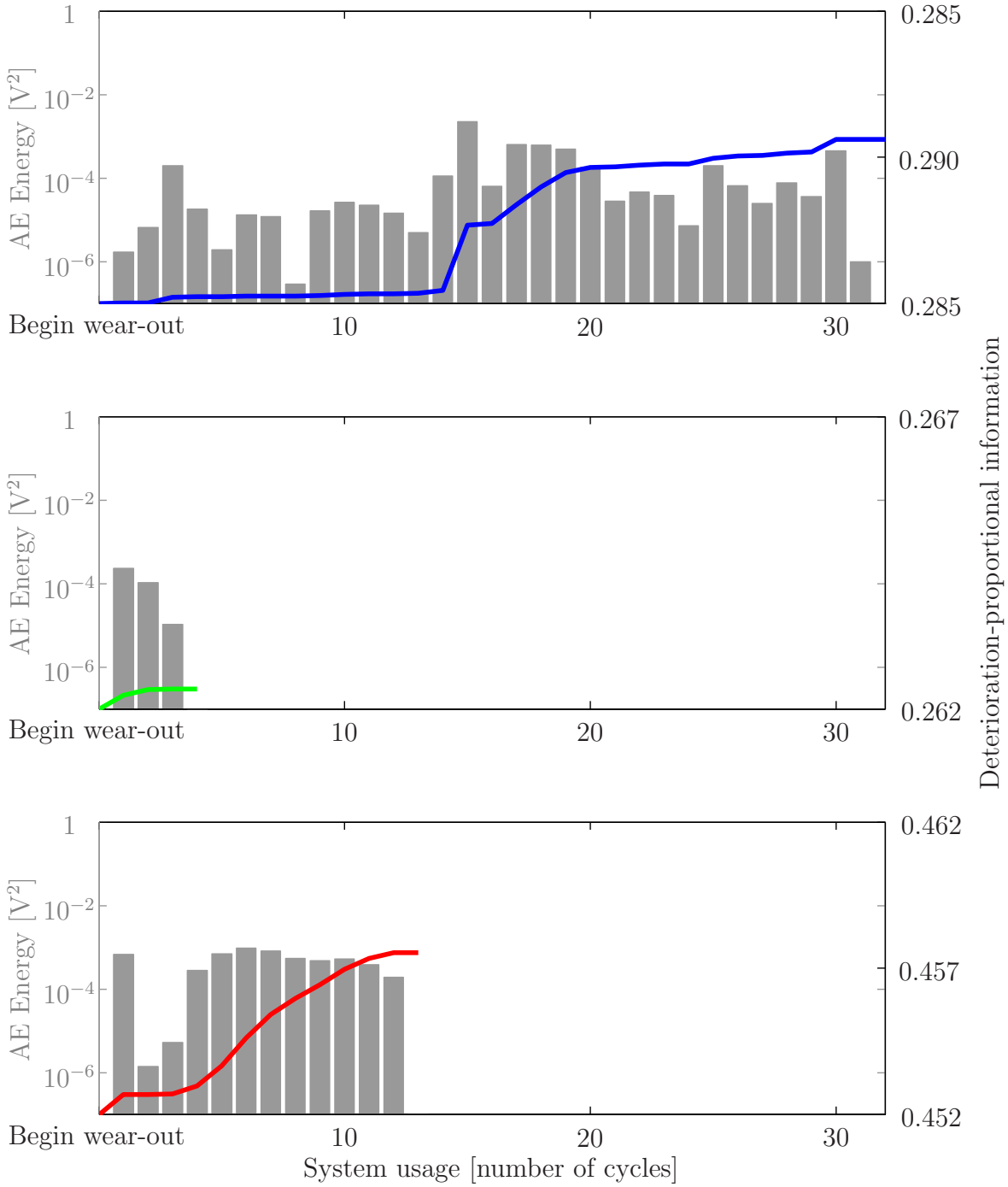

Figure 4.17: AE power and derived progression of deterioration-proportional information over system usage for all three specimen, during wear-out phase

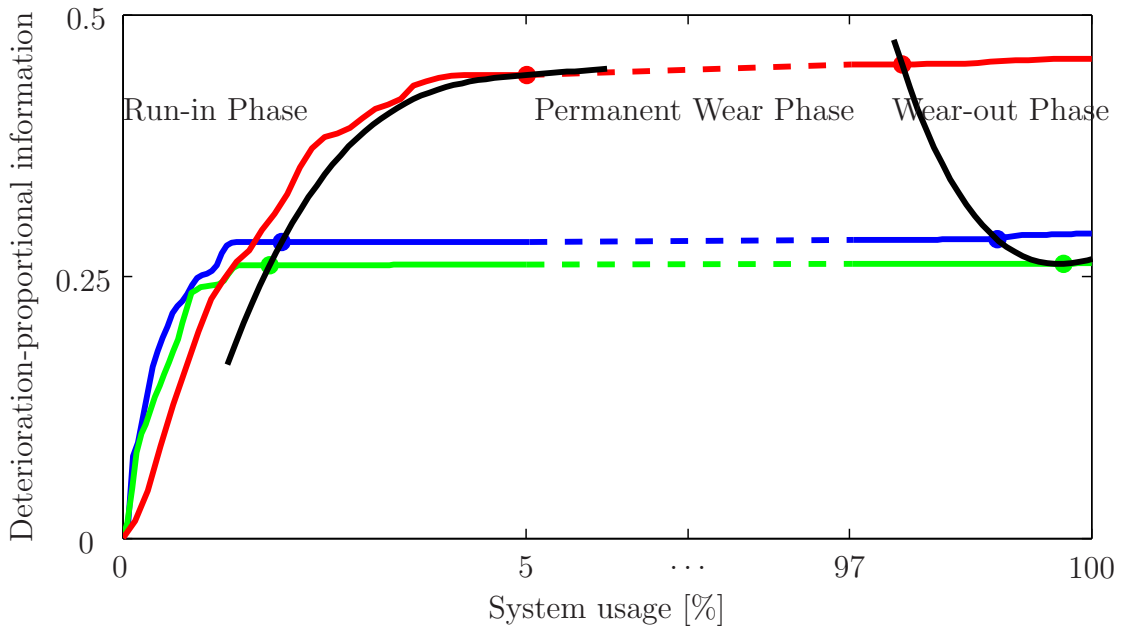

Figure 4.18: Normalized progression of deterioration-proportional information over normalized system usage with focus on different wear phases

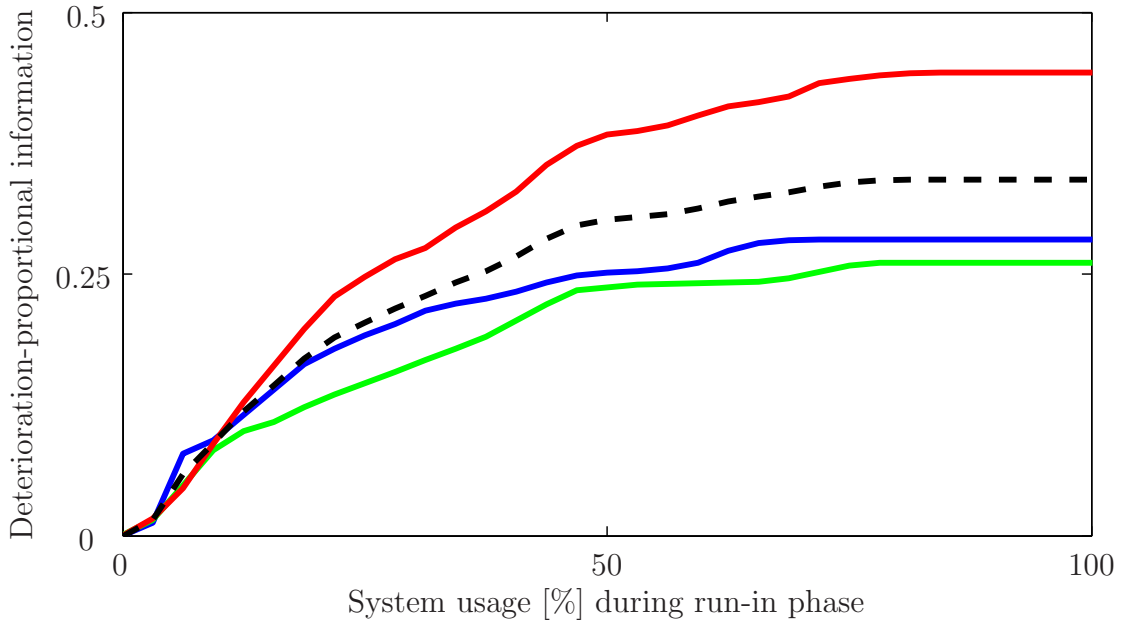

Figure 4.19: Run-in phase: Progression of deterioration-proportional information

5 Application to Electro-Chemical System

Today, ecological awareness and the attitude towards environmentally harmful technologies are a central issue. Against the background of off-shore oil production (drilling platforms) and oil transportation and the dire environmental consequences of accidents, finding solutions for clean, sustainable energy production is becoming more and more important. Apart from the long-term environmental consequences of such disasters (Exxon Valdez, Gulf of Alaska in 1989; Deep Water Horizon, Gulf of Mexico in 2010), carbon dioxide production, which mainly results from fossil fuel combustion (energy production and road transportation) [RMC+07], contributes to the greenhouse effect. Reducing the main source of these greenhouse gases makes a huge contribution to environmental protection.

Fossil fuel is mainly used for liquid fuel production, e. g., gasoline, fuel oil, and so on. Hence, fuel combustion should be reduced to a minimum. Furthermore, as fossil fuel resources diminish and an oil crisis is looming, gasoline prices are rising. Increasing pollution from gasoline-powered vehicles is causing major concern about economic and environmental consequences. Advanced electric road transportation technologies and sustainable electricity production can help to reduce the environmental problems.

These aspects inspired the automotive industry to develop novel power train concepts by integrating a power source and electrical components. Different energy sources (e. g., fuel cells [Jon09], lithium ion accumulators [VNW+05, SCW+09, KBSM09], nickel metal hydride accumulators [SCGR05, CSGR06, BSM+07], lead-acid accumulators [SSB+07], etc.) and different topologies for energy flow control were considered [Özb10]. The advantages and disadvantages of those concepts are discussed in [Rai09, HH09], for example. In general, all concepts share the idea of supporting or even substituting the common combustion engine by an electric motor.

As a consequence, electricity is the primary source for the novel drive propulsion system. Besides electricity generation, its storage is obviously becoming increasingly important, as the energy storage system decisively determines the overall availability, price, and reliability of the vehicle. In order to find a compromise between these competing demands and to realize a widely accepted, highly reliable solution, the life time change due to various loadings (operating conditions), individual usage, and at various instants of usage (state-of-X) have to be evaluated first. Subsequently, smart power management solutions can help to support the deterioration-optimal usage of an individual storage system.

5.1 Motivation

In general, batteries are classified into two types: primary (or disposable) batteries are irreversibly discharged. Secondary (or rechargeable) batteries (also called accumulators) can handle both, negative (discharging) and positive (charging) currents. For the intended application of serving as a reusable energy storage systems for novel portable applications, accumulators are considered in the following.

Beside the challenge of developing novel low-cost, high-reliable, and safe accumulators that can serve as a real alternative to fossil energy sources, the deterioration behavior of actual accumulators is of interest. As [MFSF09] states, "managing the degradation is particularly challenging because the associated mechanisms (resistive film growth) [...] are currently impractical as neither a direct access nor a control of the deterioration effects in the cell are available." Since the usage and thus, the degradation of an accumulator, is highly individual, the arising question of how the accumulators deteriorate under varying, non-conform, and unpredictable charge-discharge cycles has to be answered in order to create confidence in this novel technology. Therefore, the extended SRCE-concept again plays a major role to help realizing this ambitious goal of operating the individually aged accumulators such that a maximum usage can be realized.

Since the application-specific terminology is used in the sequel, basic definitions of accumulators are detailed, followed by the description of typical aging processes and effects. Based on the clearly defined task, the SRCE methodology is applied. In Section 5.2 the developed test rig is introduced and the central aspects are illustrated. In contrast to the preceding chapter, module 1 realizes a model-based fault detection. Again, the focus is set to the estimation of a deterioration measure. In combination with the measurement chain, appropriate tests are designed that reveal relevant deterioration information (physical parameters) and are applicable during field usage. As the validation phase of module 1 reveals a relatively deterministic aging behavior, module 2 plays only a minor role. This might change, if significantly more tests are performed and a scattering quality of the accumulators is observed. In Section 5.5, the results of the Design of Experiment (DoE) and Response Surface Method (RSM) reveal a remarkable insight into the deterioration behavior of the considered accumulator. Especially with the support of module 1, the deterioration prediction archives very good results.

5.1.1 Accumulator Characteristics

Within the domain of accumulator aging phenomenas, the following life time related terms and definitions are used in literature.

Nominal and Actual Capacity
The capacity of an accumulator is a measure for the amount of stored energy that can be withdrawn from the accumulator and is commonly denoted by C and given in Ampere Hours. The capacity, determined by measurement under specific test conditions, is depended on many operational parameters, amongst others discharge current I_{D} and cell temperature T [DAS06]. Furthermore, the capacity depends on the state-of-deterioration and is thus commonly used as an indicator of deterioration. The nominal capacity C_{n} denotes the capacity at the beginning of the usage (non-aged state). The actual capacity C_{a} is determined at subsequent instants of usage after aging under identical test conditions as used for the determination of the nominal capacity.

State of Charge (SoC)
The state of charge is a quantity that describes the amount of energy, remaining in the accumulator and is commonly given as a percentage of the accumulator's nominal capacity C_{n}. As the remaining amount of energy cannot directly be measured, the SoC is approximated by various methods, e. g., Open Circuit Voltage (OCV) measurement, ampere counting dur-

ing charging/discharging, etc. For ampere counting, a higher capacity is determined when discharging at a low rate than at a high discharge rate. On the other hand, a too low rate will stimulate self-discharge effects and reduce the efficiency and determined capacity. The ratio between remaining and nominal (or actual) capacity does not represent the state of charge accurately.

Depth of Discharge (DoD)
The depth of discharge denotes the amount of energy that is withdrawn from the accumulator. The DoD describes the complementary characteristic of the SoC and is stated as a percent of the nominal capacity C_n.

State of Health (SoH)
The state of health is defined in various ways in order to provide an information about the degree of deterioration. In general, the state of health is correlated with the actual capacity C_a in comparison with the nominal capacity C_n. According to [JW06], the End of Life (EoL, SoH = 0%) time of an accumulator is reached, if the actual capacity C_a is equal than 80% of the nominal capacity C_n.

Calendar Life
The calender life describes the maximum storage time until the accumulator becomes unusable (usually considered as a capacity fade of 20%). The storage time is a function of ambient temperature, SoC, etc.

Cycle Life
The number of complete charge-discharge cycles until the failure criterion is fulfilled (80% of nominal capacity) is described by the cycle life of an accumulator. Many manufactures state the cycle life time of an accumulator in dependency of full cycles (number of consecutive charge-discharge cycles) under optimal operational conditions (C-rates, ambient temperature, rest periods, etc.).

Impedance
The behavior of an accumulator as a function of frequency is investigated by the impedance measurement. A stimulus (current with varying frequency and alternating direction) is applied to the accumulator and the reaction (voltage) is measured in terms of amplitude and phase shift. As the deterioration process has an (non-linear, state-depended) influence on the frequency behavior of an accumulator, the Electrochemical Impedance Spectroscopy (EIS) is an appropriate measure to detect faults [Bar05]. In [SG09], "the features extracted from EIS are used to estimate the internal parameters [...] The values of these parameters [capacitance, resistance, Warburg impedance, electrolyte resistance, etc.] change with various aging and fault processes." The impedance curve of an lithium-based accumulator mainly consists of an inductive branch at high frequencies, followed by semicircles at medium and low frequencies [LMWK01]. The intersection of the impedance curve with the imaginary axis represents the ohmic resistance of the cell. The physical property is later used as a deterioration measure.

Power
The power of an accumulator is described by the product of current and voltage. For accumulators, the voltage is defined by the cell chemistry (material of anode, cathode, etc);

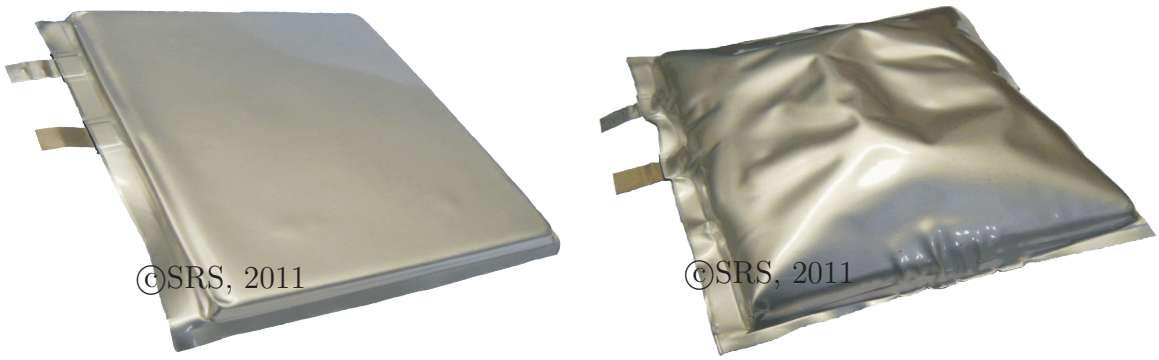

(a) Normal shape of accumulator (b) Accumulator after overcharging

Figure 5.1: Accumulator failure due to overcharging

hence, the ability to provide current makes the difference. Conversely, this means that a rising resistance leads to a reduced power. Therefore, peak power tests are common for rough deterioration estimation.

Discharge and Charge Rates (C-rate)
It is common practice to characterize the discharge and charge rate as a ratio of the nominal capacity C_n. The C-rate is given in Ampere. As the field usage of accumulators is usually higher than 1C, the C-rate is an important factor for life time investigations. In [Vez10], the life time of a lithium ion accumulator is reduced by 40% compared to the 1C-rate, if a 4C-rate is applied.

Temperature
High temperatures facilitate the irreversible reaction between electrode and electrolyte. Referring to the data sheet of the considered accumulators [Gro11], the cells are optimal operated during charging within the range of 0°C to 40°C, and for discharging within −20°C to 60°C.

Over(dis)charge
The different, specific chemical potentials of the used materials within an accumulator are the cause of the cell voltage. A detailed insight into this chemistry aspect of accumulator is given in [JW06]. By discharging the accumulator, the chemically stored energy is transformed into electrical energy and positively charged ions (cations). Within the specified operational conditions, the electrical energy is provided by the chemically stored energy. By proceeding with the discharging or charging process, the cell chemistry will sustainable be damaged.

The overdischarging scenario assumes a discharging process that is continued beyond the limits of the specified voltage range. Once all the charge has been drained from the accumulator, the electrodes get completely reversed and hydrogen gas builds up, often causing the accumulator to vent.

On the other hand, an overcharge leads to an exothermic reaction within the cell as the electrically provided energy cannot be stored chemically any more and is thus, transformed directly into thermal energy (heating). As the electrolyte starts to vaporize, the pressure within the cell continually increases. If the overcharging persists, the gas pressure will increase enough to burst the cell. In Figure 5.1, the failure due to overcharging is depicted.

Cell Specifications	Range	
End of Charge Voltage	U_{EoC}	$4.2\mathrm{V} \pm 0.03\mathrm{V}$
End of Discharge Voltage	U_{EoD}	2.7V
Max. Conti. Charge Current	$I_{\mathrm{C,max}}$	20A
Max. Conti. Discharge Current	$I_{\mathrm{D,max}}$	30A
Max. Discharge Rate (30 sec)		50Ah
Nominal Capacity	C_{n}	10Ah
Nominal Voltage	U_{n}	3.7V
Operation Temperature	T	$-10°\mathrm{C} \ldots + 55°\mathrm{C}$

Table 5.1: Technical data of KOKAM lithium polymer cell

The aspect of over(dis)charging becomes evident, if a stack of cells is considered. Due to capacity imbalances, individual cells may fall beneath or rise above the specified operational conditions and can thus, be destroyed. For this reason, charge equalizing circuits (cell balancer) takeover the function of avoiding high voltage gradients and hence, preventing an over(dis)charged cell within a stack.

5.1.2 Lithium-Based Accumulators

In the following, the actually most promising storage technology for accumulators based on lithium is considered. Anyhow, the proposed SRCE-concept is not restricted to this lithium-based accumulators but can again be enlarged to other accumulator technologies. The accumulator investigated in this thesis is a 10Ah Superior Lithium Polymer Battery (SLPB, Model 98106100) by KOKAM in pouch bag. The technical data of the cell are given in Table 5.1.

During charging, the electrical energy is provided to the terminals of the cell. The electrons and lithium ions then move from the cathode through the electrolyte and separator to the anode. There, the anode (graphite) intercalates the electrons and ions. Beside the intercalation process, the energy is also converted (by side effects) into internal energy losses and thus, lost in terms of chemical energy. In the opposite case of discharging the accumulator, the electrons move through the external load from the anode and are attracted to the cathode. For further explanations about electrodes, electrolytes, additives, and interfaces for various cathode and anode materials, typically used for lithium-based accumulators [Oza09] provides a detailed overview.

The ideal process of energy conversion in terms of the chemical reaction of a lithium cell with a lithium cobalt oxide cathode is given in the chemical equations

$$\text{Anode} \qquad \mathrm{LiC_6} \underset{charge}{\overset{discharge}{\rightleftharpoons}} \mathrm{Li_{1-x}C_6 + xLi^+ + xe^-} \quad \text{and}$$

$$\text{Cathode} \qquad \mathrm{Li_yCoO_2 + xLi^+ + xe^-} \underset{charge}{\overset{discharge}{\rightleftharpoons}} \mathrm{Li_{y+x}CoO_2}\ .$$

In anticipation of the succeeding section, the aging behavior depends “sensitively on individual cell chemistry and cell design as well as performance data and will vary from battery

manufacturer to battery manufacturer", [WM04]. Thus, the general aging aspects, valid for the majority of lithium-based accumulators, are discussed in the sequel in order to remain the global applicability of the subsequently presented results.

5.1.3 Basic Principles of Accumulator Aging

Depending on many factors and particular technologies, accumulators can be recharged many times until the recharge ability decreases significantly [BCS+01, Ram03]. Two major effects contribute to this aging process: degradation due to storage and due to operation. The primer aspect is not considered here, as the deterioration due to storage contributes comparatively little to the overall deterioration. Additionally, the effect of aging due to storage can be reduced by keeping the cells close to room temperature, reduced humidity and at average state of charge [RLB+01].

For aging due to operation, two main basic aging effects are encountered when dealing with lithium-based accumulator: power and/or capacity fade [Pic07]. If only the former degradation effect is present, the accumulator is capable of supplying all the stored energy, but reveals the lack of capability of providing a high current. For the latter degradation effect, a high current can still be withdrawn from the accumulator after aging but cannot deliver all the stored amount of energy.

The reasons for this aging effects are manifold but all base on different (non-linear, stochastic) electro-chemical processes, taking place in parallel. "In general, the situation reported in the literature is difficult to analyze as each lithium-ion cell system has its own chemistry and many aging effects are influenced by the nature of the cell components (e. g., active material and electrode design, electrolyte composition, impurities, etc.)", [VNW+05].

In Figure 5.2, a graphical overview about the main deteriorating effects is given, depicting the major aging effects as mentioned in [MFSF09, BMFF11, RHG+04, VNW+05].

At the anode side, three different deterioration effects are depicted. All effects are a result of the chemical reaction taking place at the interface between the electrode (here: graphite) and electrolyte, particularly during charging. At the beginning of cycling, a protective layer builds up that covers the electrode (formation phase). The layer is a decomposition product of the reductive reaction of the electrolyte (gray circles), taking place during charging. If the layer realizes a protective function, the layer is denoted as the Solid Electrolyte Interface (SEI) Film (light yellow). During this phase, a slightly increasing capacity is measured. The film is permeable for lithium ions (red circles; intercalation and deintercalation), but nearly impermeable for electrolyte components. Hence, this layer realizes a desired function in order to reduce further reduction of the anode. On the other side, the amount of mobile lithium is reduced as chemically bonded to the SEI Film and hence, the performance of the accumulator is reduced. The film has a time and spatially varying thickness. According to [VNW+05, ACL+01, SLWW02, LMWK01, ZHD+00, ZW08], the film growth contributes to a capacity and power fade and an increased impedance. If the protective function cannot be realized due to inhomogeneous current and potential distributions within the cell, lithium ions and electrolyte intercalate into the graphite and cause an irreversible damage to the structure (graphite exfoliation, cracking). Already intercalated lithium ions may be trapped and thus, lost. Finally, the lithium can corrode the interface of the electrolyte and the electrode, form a metal plating, and permanent capacity loss (wear-out phase). The metallic lithium forms dendrites that grow until penetrating the separator and contacting the cathode;

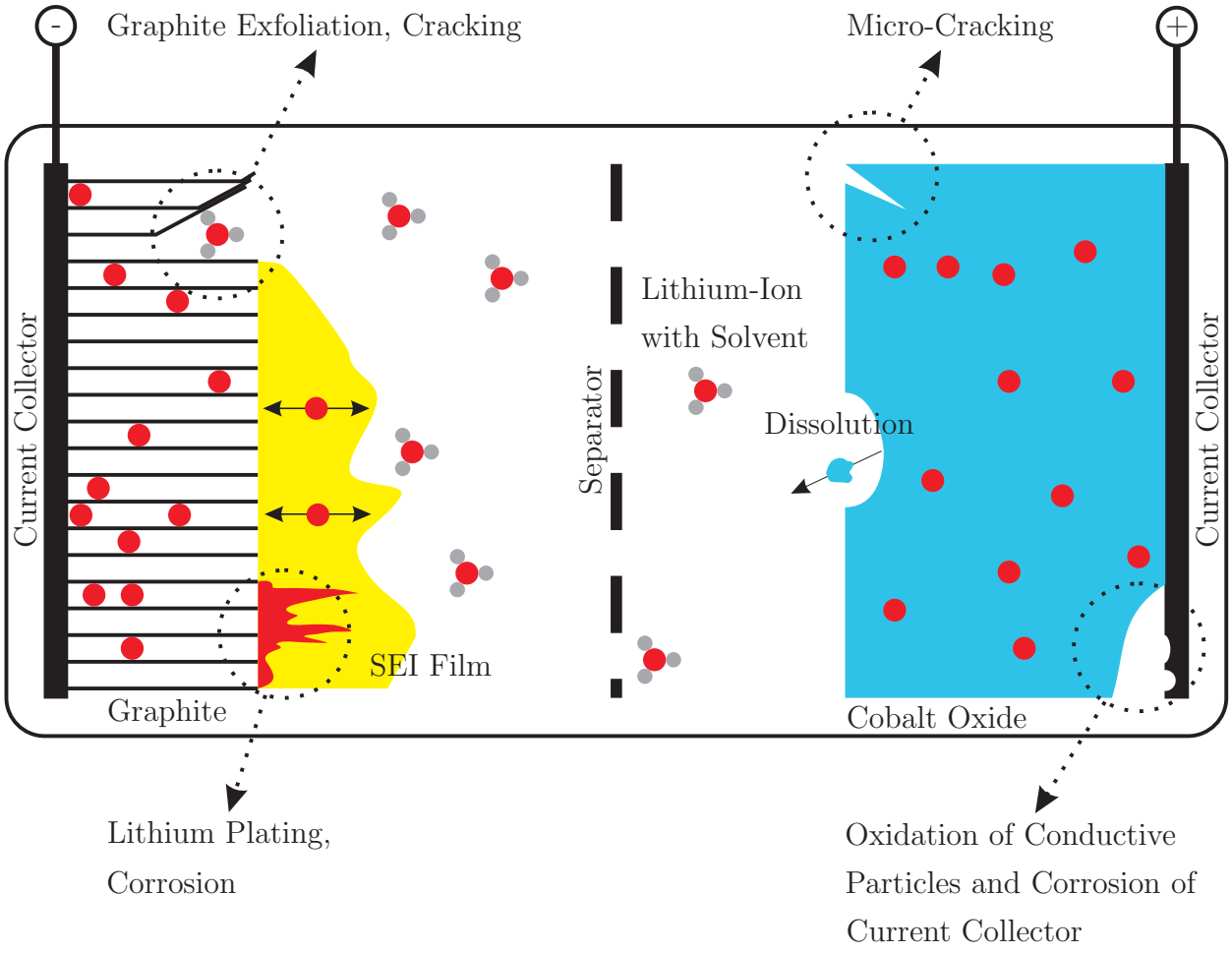

Figure 5.2: Overview on main aging mechanism within a lithium-based accumulator

a short-circuit of the cell is realized and an explosion is likely to occur.

On the right side of Figure 5.2, the deteriorating effects of the cathode are depicted. As the cathode material significantly determines the deterioration behavior, only globally valid statements about general effects are discussed in the sequel. In analogy to the anode, the cathode material is stressed by the intercalation and deintercalation of lithium during charging and discharging. As lithium ions are inserted into the active material (light blue) during discharging, the lithium may induce mechanical stress and strains to the oxide particles [VNW+05]. A direct consequence is a structural change and thus, the (micro) crack formation. Encouraged by inhomogeneous chemical reactions, persisting micro cracks and a distorted crystal lattice, the bulk material can dissolute into the electrolyte. As this processes can also take place at the conductive interface between the active material and the current collector, the contact loss also contributes to a reduced capacity and power performance.

In summary, the majority of research work accounts the changes at the interface between the anode (graphite electrode) and the electrolyte for being mainly responsible for the aging [VNW+05, BBB+05]. As manifold drivers of deterioration occur in parallel "and cannot be discussed independently from each other" [WM04], the overall deterioration is evaluated

from (directly measurable) physical properties. Here, the internal resistance at specific frequencies is measured and is considered as the major measurable indicator of a decreasing accumulator performance. This idea is supported by various research work in literature, e. g., in [RBM+10] where the health-governing cell degradation indicator is identified as the "increase of the internal resistance of the battery cells over the whole life time of the battery." The resistance is identified "with the special identification signals of terminal voltage and current." Subsequently, the variation of the resistance is used to state a degradation index.

5.2 Measurement Chain

The purpose of the test bench is to conduct reliable aging experiments on lithium accumulators. The test benches will be operated automatic and unattended since the tests will take large amounts of time. This in turn requires the test benches to be safe.

After a short introduction into the test rig and its specifications, typical measurements are discussed. The implicit measurement of deterioration (change of internal resistance, actual capacity, etc.) is introduced and illustrated with experimental examples. By repetitively charging and discharging the accumulator with specifically designed aging cycles, small but permanent damages are stimulated that cause the accumulator to never regain its original performance.

5.2.1 Test Rig

A novel test rig is developed such that arbitrary charge and discharge profiles can be applied to the accumulator (KOKAM cell, technical data see Table 5.1) and special tests for parameter estimations (see module 1) can be performed. In Figure 5.3, a schematic representation of the developed test rig for accumulator aging is depicted.

The central component is the accumulator. Since the genuine aging of an accumulator without disturbing effects due to additional balancing are investigated, a single cell is used. The surface temperature of the cell is measured by a NiCrNi temperature element (temperature range from $-30°\mathrm{C} \ldots +100°\mathrm{C}$) and linearly transformed into a voltage ($0\mathrm{V} \ldots +10\mathrm{V}$). The cell voltage is measured at the terminal clamps of the cell. A buffer amplifier is used to transform the input voltage (maximum range: $-5\mathrm{V} \ldots +5\mathrm{V}$) into an adequate output voltage ($10\mathrm{V} \ldots +10\mathrm{V}$).

In order to automate the test procedure, an electric switching between charging and discharging is realized by an electronic power switch (semiconductor, solid-state relays). In dependency on the operation, the electrical circuit is closed with the power source (for charging the accumulator), the electronic load (for discharging purpose) or left open (for idle mode). In the case of an power shortage of the processes control unit and hence, lost of control, the switch automatically opens and disconnects all devices from each other (fail safe).

Charging is accomplished using a DC power supply. The power source is capable for currents up to 20A and 65V. The nominal values and actual values for current and voltage are externally controllable and measurable.

An electronic load is used to withdraw current from the accumulator. The device can realize a discharge current between 10mA to 50A within a voltage range of 2.5V to 80V. In

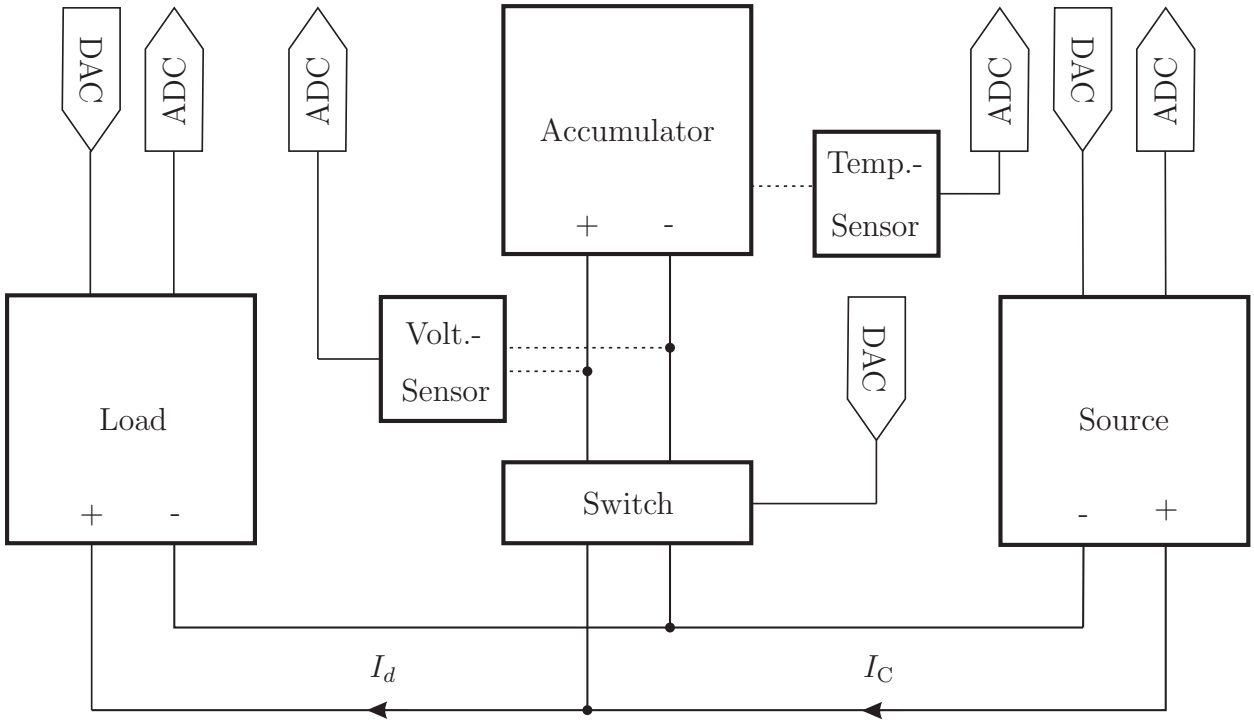

Figure 5.3: Test rig for accumulator testing

analogy to the power source, the relevant process signals are controllable and measurable from an external source. Beside the specifications for current and voltage, the reaction speed of the load is important in order to realize the required measurements (step response). This particular device is able to realize a step demand within less than 100µs.

The process signals are connected either by analog-digital converts (ADC) or digital-analog converters (DAC) to a real-time process control system (dSPACE, not depicted) in order to control remotely the load and power supply. Arbitrary current profiles and charge controllers can be realized in MATLAB®/SIMULINK® and are then applied to the accumulator through the power supply and electronic load. The data acquisition and control is accomplished using MATLAB®/SIMULINK® software such that the measured input signals are processed to realize particular test sequences, e. g., discharge and charge trajectories and supervision purposes, e. g., cell temperature. Furthermore, all relevant process signals are recorded in order to analyze the data for deterioration content, extract relevant parameters for subsequent models, etc. Additionally, life time models can be implemented to on-line supervise the actual (incremental) deterioration due to applied loading.

5.2.2 Aging Cycles

The purpose of the aging cycle, consisting of charging and discharging, is to specifically stimulate the aging effects and causing an incremental deterioration at each cycle. In anticipation of modules 1 and 3, the framework of the used aging cycles is briefly introduced here. The justification for the particularly chosen parameters (for charging, discharging, etc.) is given in Chapter 5.5.

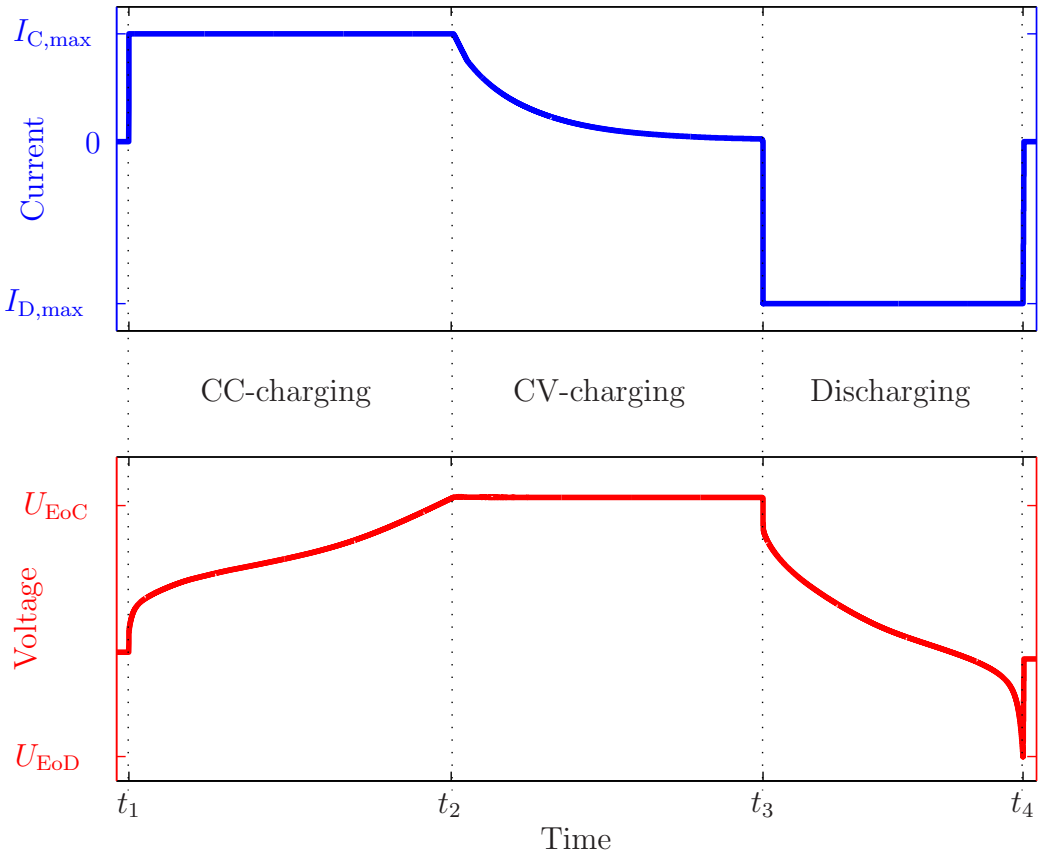

Figure 5.4: Standard aging cycle

The standard scheme of a current profile with resulting voltage curve is given in Figure 5.4. This standard cycle is varied such that different purposes are fulfilled.

First, the standard charging procedure for lithium-based accumulators is described by this standard representation. A constant current is applied until the accumulator voltage U reaches $U_{\mathrm{EoC}} = 4.2\mathrm{V}$. Then, the voltage is kept constant until the current drops to $I_{\mathrm{C}} \leq 50\mathrm{mA}$. This procedure is denoted as the CC-CV (constant current-constant voltage) charging procedure. Referring to [Gro11], the optimal key data for the charging profile are given as 10A and $U_{\mathrm{EoC}} = 4.15\mathrm{V}$.

Secondly, the parameters, defining the key data of charging (I_{C}, U_{EoC}, and U_{EoD}) can be varied in order to optimize the usability and/or availability of the accumulator by enhancing the recharging time, etc.

The discharging profile in field usage is individual and hardly predictable. Therefore, test parameters with maximum performance are chosen in order to test for maximum loading capacity. The discharging procedure is defined such that the accumulator is discharged at a constant C-rate. As the terminal voltage U reaches the end of discharge voltage $U_{\mathrm{EoD}} = 2.7\mathrm{V}$, the discharging is stopped. Due to the limited rate of diffusion of ions through the electrolyte, the efficiency of an accumulator varies at different discharge rates. Again, [Gro11] proposes

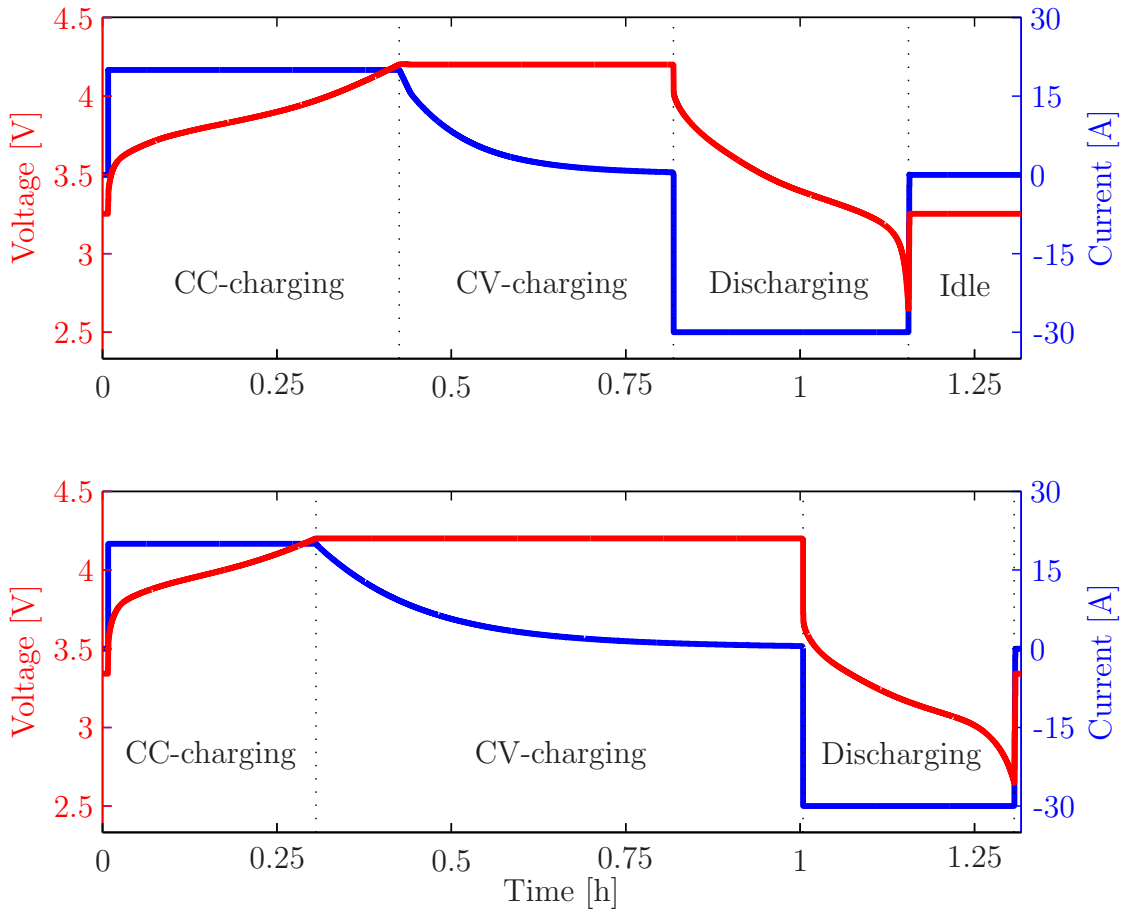

Figure 5.5: Charging and discharging behavior of an accumulator;
Upper plot in non-aged state, lower plot in aged state

optimal key data for the discharging that remain below the maximum ratings. The discharge is performed with $I_{\mathrm{D}} = 10\mathrm{A}$ and $U_{\mathrm{EoD}} = 3\mathrm{V}$.

As these parameters determine the operation, the variation of the charging and discharging parameters are considered to considerably influence the life time.

In Figure 5.5, the result of the application of the aging profile is depicted. The CC-CV charging is exemplarily shown at a C-rate of 1.5C; the subsequent discharging is performed at 3C. In the upper plot, the behavior of the accumulator at the non-aged state is illustrated where the lower plot depicts the result at the aged state (identical cell). The shape and duration of each charging and discharging phase varies in dependency on the SoH. By varying the particular operational parameters of the aging profile, the accumulator will individually deteriorate and provide an insight into the deterioration progression. The deterioration-depended behavior during charging and discharging is quantified in the sequel by appropriate test procedures.

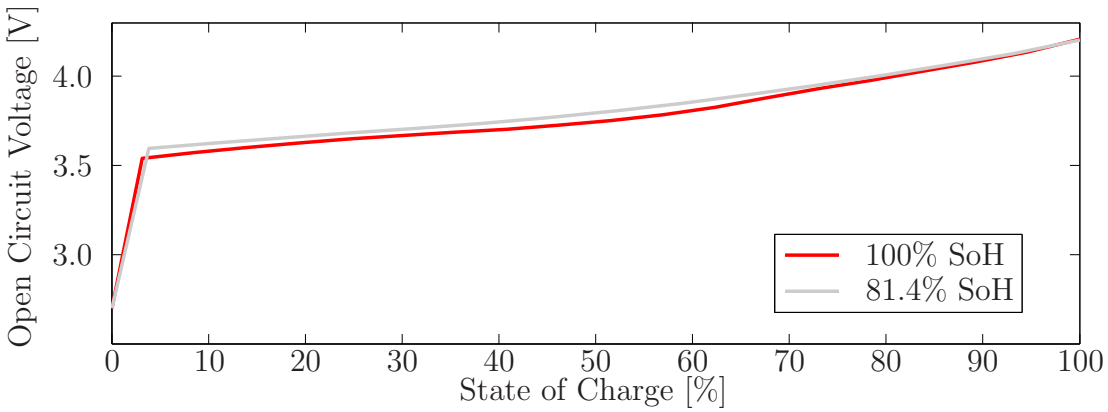

Figure 5.6: Measurement of SoC-OCV curve; red line denoting non-aged cell, the gray line aged cell

5.2.3 Measurement of Deterioration

In order to assess the individual aging of the accumulator due to the above introduced aging profile, deterioration measurements (in terms of determination of relevant electrical parameters, e. g., internal resistance, actual capacity, etc.) are performed for each cell before starting the aging cycles. For the validation of the later introduced model, these test are conducted periodically. By comparing the results (measurement and calculation results) along with the accumulators life time, the aging gets evident. By performing these measurements after known operational trajectories (in terms of operational parameters, number of successive aging cycles) the incremental deterioration due to the applied loading can be determined at various (discrete) initial states of deterioration.

The aim is to provide deterioration-relevant information to the subsequent module in order to investigate the impact of the aging cycles on the accumulator performances. All tested accumulators are selected from one batch. After the initial measurement, the aging cycles are performed several times. Then, all of the below described measurement cycles are performed, before starting again with the aging cycles.

SoC-OCV Measurement

As Figure 5.4 indicates, the terminal voltage rises with increasing charge. This suggests that the voltage can be correlated to the State of Charge. Since the State of Charge is in turn connected to the State of Health, a typical SoH indicator is derived from the connection between the Open Circuit Voltage (OCV) and the State of Charge (SoC). To measure the OCV, a measurement cycle is developed and applied as followed:

1. Discharge 5% of charge with $I_{\mathrm{D}} = 30\mathrm{A}$ for 60s.
2. Idle mode (20 minutes)

The accumulator is assumed to be fully charged and rested for a sufficient period of time in order to cool down and let chemical processes taking place. The scheme is repeated until the accumulator is fully depleted (U_{EoD} reached; theoretically 20 times). For the proposed test scheme, the SoC-OCV curve is measured every 5% of SoC. The corresponding voltage is measured after the idle mode. A typical result, consisting of 20 measurements, is depicted in

Figure 5.6. The equally spaced measurement points are connected by an interpolating line; the red curve denotes an non-aged accumulator whereas the blue curve shows the result for an aged accumulator (SoH approx. 80%).

The slope of the curve is commonly denoted by the factor k. It is obvious that the correlation between OCV and SoC is possible but not very sensitive to the deterioration as both curves only slightly differ (in terms of k) from each other.

Capacity Measurement

As the overall degradation is of interest, the ampere counting method is an indicator to estimate the actual capacity C_a. Although the measurement is time consuming and "leads little possibility for on-the-fly on-board vehicle assessment, [...] it is the best way to assess battery life" [Pic07]. To avoid energy loss due to thermal dissipation (energy dissipating effects like heating due to chemical reactions [DAS06]), the discharging and charging is conducted at very slow rates (e. g., I_D = C/20-rate). Additionally, the accumulator has to rest in between the charging and discharging period; in literature, time periods up to 24 hours are described as sufficient. Following these recommendation, the complete measurement cycle lasts for approximately 50 hours. By comparing the obtained value with previous measurement result (e. g., with nominal capacity C_n), the fade of capacity becomes obvious.

In this thesis, the main interest is dedicated to the gradient (change) of deterioration due to operation. The counted ampere hours are neither completely stored into chemical energy during charging, nor is the drained energy completely converted to electrical energy but also comprises thermal energy. Thus, an average capacity is determined by ampere counting of both, charging and discharging currents.

Measurement of Electrical Parameters

In contrast to the application example, discussed in Chapter 4, here, physical properties, indicating the degree of deterioration, are implicit measurable by specially designed test procedures under standardized conditions. The methods for acquiring the relevant electrical parameters are based in the research work of [WZX09].

The basic idea constitutes that the impedance changes characteristically with a decreasing SoH. Thus, the internal resistance of the cell is measured in order to investigate the result for deterioration content. In conjunction with the equivalent circuit (model), depicted in Figure 5.8, three deterioration-depended parameters have to be evaluated: the ohmic resistance R_o, the polarization capacity C_p, and the polarization resistance R_p.

For the determination of the primer resistance, a peak current measurement is applied in order to measure the voltage response of the accumulator to a discharge current step. In Figure 5.5 the effect of a peak current measurement is shown. The voltage drop of the aged accumulator (lower plot) differs significantly from the nominal behavior (upper plot). In Figure 5.7, the voltage drop is depicted (characteristic points U_0 and U_1).

The result is the ohmic resistance R_o, measured as the voltage drop at the current step

$$R_\mathrm{o} = \frac{U_1 - U_0}{I_\mathrm{D}} \; . \tag{5.1}$$

After the voltage drop due to the ohmic resistance, the capacitive properties become dominant. After stopping the discharging, the voltage raises again rapidly to U_3 and propagates asymptotically to the final (open circuit) voltage U_4.

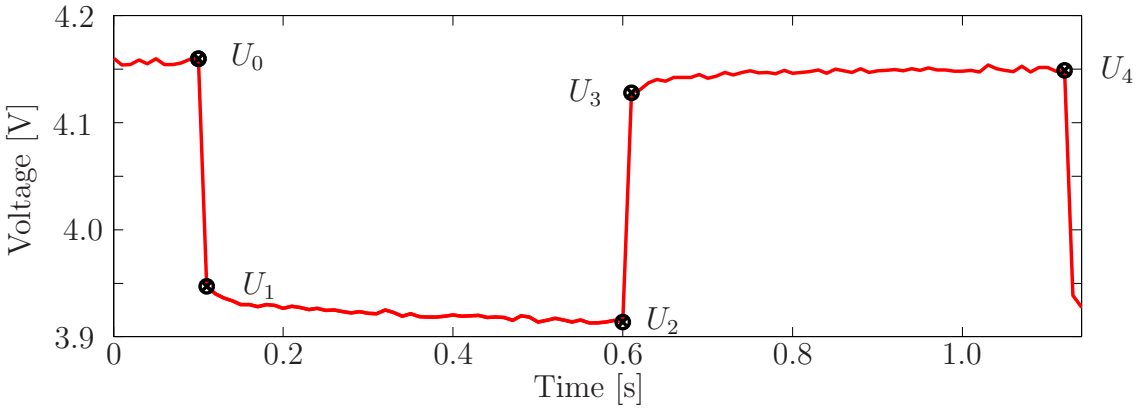

Figure 5.7: Voltage drop as the reaction on a discharging current step

According to [CV05], the polarization resistance is determined by this measurement as

$$R_\mathrm{p} = \frac{U_2 - U_1}{I_\mathrm{D}} \,, \tag{5.2}$$

and the capacity is

$$C_\mathrm{p} = \frac{\tau}{R_\mathrm{p}} \,. \tag{5.3}$$

According to [VPB07], the polarization time constant τ is derived by

$$\tau = -\Delta t \ln\left(1 - \frac{U_4 - U_3}{U_0 - U_3}\right) \,, \tag{5.4}$$

with Δt indicating the discharging time (here: 0.5s).

Measurement of Temperature
The temperature gradient also reveals a characteristic behavior along with an increasing aging as the temperature rises more rapidly when the accumulator is aged. This symptom is reducible to the common entity, the varied internal resistance. Hence, the measurement of the internal resistance (as the cause of the temperature increase, varying voltage drop, etc.) is assumed to be a major indicator of deterioration.

5.3 Module 1: SoH Estimation

Referring back to the intended application (electrical storage and source for automotive application), the charge and discharge profiles are the major life time determining factors. In contrast to manufacturer information, an accumulator in field usage will fail earlier due to individual, non-optimal charge and discharge trajectories than specified. Hence, a model, approximating the actual state of health (SoH), needs to consider (amongst other factors) the past loading and their specific (incremental) effects on the life time. The task of module 1 is thus to provide a sufficiently precise and accurate filter that is based on available measurements of deterioration-effected physical parameters.

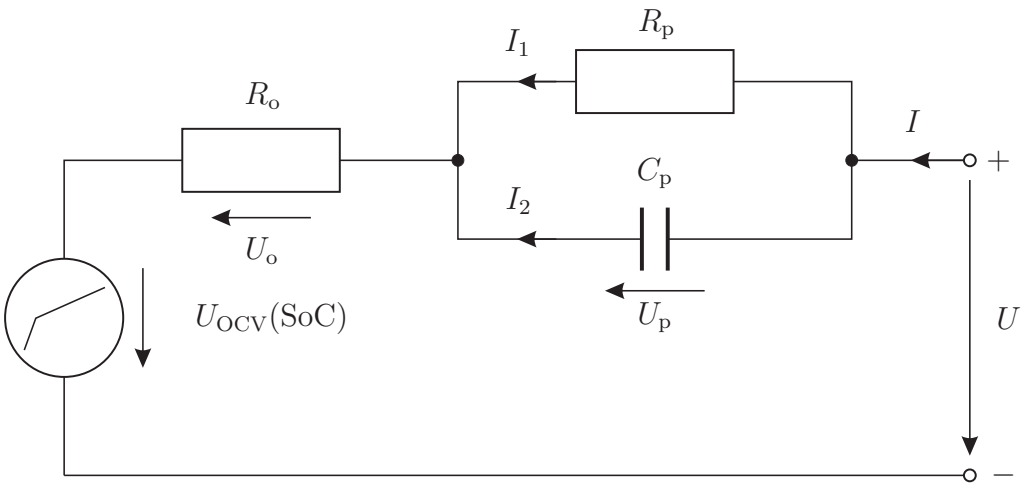

Figure 5.8: Equivalent circuit diagram with lumped parameters of an accumulator [WZX09]

Several models for estimating the deterioration behavior of an accumulator are discussed in literature.

In [BCL+05, SW08], an adapted model is proposed to accumulate an incremental damage. By introducing experimentally determined factors, the deterioration behavior is approximated. The main drawback of the proposed model is that it static and thus, not capable of considering aging effects.

In [SG08, SG09, SGPC09], a Bayesian approach is discussed. The Bayesian models are used in order to state the probability "as the degree of belief that a proposition is true." As the Bayesian PDF adapts to the change in data, this technique is also denoted as self-correcting. This ability to adapt to novel situation (e. g., changed data base) is used to construct an adaptive battery health monitoring approach. The deterioration prediction is supported by the particle filter approach that estimates "the evolution in time of the system under analysis." The particle filter "is a technique for implementing a recursive Bayesian filter using Monte Carlo (MC) simulations [...]." In summary, the method considers a non-exact, non-linear, and non-stationary model with non-Gaussian noise. The shown results are promising, but the method is time-consuming and requires intensive experimental investigations of accumulator behavior.

The applied model, detailed in the following, is a simplified Randles-circuit [Ran47], introduced by [Kim10], as it reveals the main information for deterioration estimation. The main advantage of this model is that physical properties (e. g., ohmic restistance) are measured only once (at beginning of life time) and subsequently intentionally kept constant in order to deduct the erroneous system behavior due to the deviation in calculated and measured output quantity performance. Thus, the model focuses on the detection of a varied impedance due to deterioration. Although, the (physical, chemical) sources of an increasing impedance are manifold, only the effect is considered in the sequel. Therefore, a model of the accumulator is chosen that considers the relevant electrical effects at a macroscopic level in order to reduce the modeling and numerical efforts.

The main components of the model, depicted in Figure 5.8, are the non-linear voltage source $U_\mathrm{OCV}(\mathrm{SoC})$, an ohmic resistance R_o, and a RC model, constituted by the polarization

$$a_1 = \frac{1}{R_\mathrm{p} C_\mathrm{p}} , \qquad a_{11} = k a_1 , \qquad a_2 = \frac{1}{R_\mathrm{o} C_\mathrm{n}} , \qquad a_{22} = k a_2 ,$$

$$b_1 = \frac{1}{C_\mathrm{n}} \frac{1}{C_\mathrm{p}} \frac{R_\mathrm{o}}{R_\mathrm{p} C_\mathrm{p}} , \text{ and} \qquad b_2 = \frac{1}{C_\mathrm{p}} .$$

resistance R_p and the polarization capacitance C_p. The terminal voltage is denoted by U.

The differential equations, describing the dynamical behavior of the accumulator model are given as

$$\dot{U} = -\frac{1}{R_\mathrm{p} C_\mathrm{p}} U + k \frac{1}{R_\mathrm{p} C_\mathrm{p}} SoC + \left(\frac{1}{C_\mathrm{n}} + \frac{1}{C_\mathrm{p}} + \frac{R_\mathrm{o}}{R_\mathrm{p} C_\mathrm{p}} \right) I , \tag{5.5}$$

$$\dot{SoC} = \frac{1}{R_\mathrm{o} C_\mathrm{n}} U - k \frac{1}{R_\mathrm{o} C_\mathrm{n}} SoC - \frac{1}{R_\mathrm{o} C_\mathrm{n}} U_\mathrm{p} , \text{and} \tag{5.6}$$

$$\dot{U}_\mathrm{p} = -\frac{1}{R_\mathrm{p} C_\mathrm{p}} U_\mathrm{p} + \frac{1}{C_\mathrm{p}} I , \tag{5.7}$$

with the parameter SoC denoting the state of charge that varies between 0 and 1, representing fully discharged and fully charged, respectively.

The characteristic behavior of the assumed non-linear voltage source is determined by the SoC-OCV measurement in terms of the factor k, describing the slope of OCV over SoC. In [Kim10], the parameter k is expressed as a function of SoH. For the considered KOKAM cell, k is considered as a constant.

According to Equation (2.23) and (2.24), the differential equations are transformed into state space representation

$$\begin{bmatrix} \dot{U} \\ SoC \\ U_p \end{bmatrix} = \begin{bmatrix} -a_1 & a_{11} & 0 \\ a_2 & -a_{22} & -a_2 \\ 0 & 0 & -a_1 \end{bmatrix} \begin{bmatrix} U \\ SoC \\ U_\mathrm{p} \end{bmatrix} + \begin{bmatrix} b_1 \\ 0 \\ b_2 \end{bmatrix} I , \tag{5.8}$$

$$y = \begin{bmatrix} 1 & 0 & 0 \end{bmatrix} \begin{bmatrix} U \\ SoC \\ U_\mathrm{p} \end{bmatrix} , \tag{5.9}$$

with the variables

As introduced in Section 2.4.1, model-based methods for fault detection are chosen, if the nominal behavior of the system can sufficiently be stated by a mathematical model. Since the electrical parameters, stated in Equations (5.5) to (5.7), are measurable, the derived model is used to realize a model-based fault detection. In this particular case, a law-driven model (state observer) for fault detection is chosen. The advantage is that the modeling errors (simplified, inaccurate linearized model) and noise (internal and external sources) are reduced by an appropriately chosen observer gain matrix $\mathbf{L}$.

As mentioned, the observability criterion has to be fulfilled in order to design an observer. As the matrix

$$\mathrm{rank}\,(\mathbf{Q}_\mathrm{o}) = \mathrm{rank} \begin{bmatrix} 1 & 0 & 0 \\ -a_1 & a_{11} & 0 \\ a_1^2 + a_{11} a_2 & a_2 a_{11} + a_{22}^2 & a_2 a_{22} + a_1 a_2 \end{bmatrix} = 3 . \tag{5.10}$$

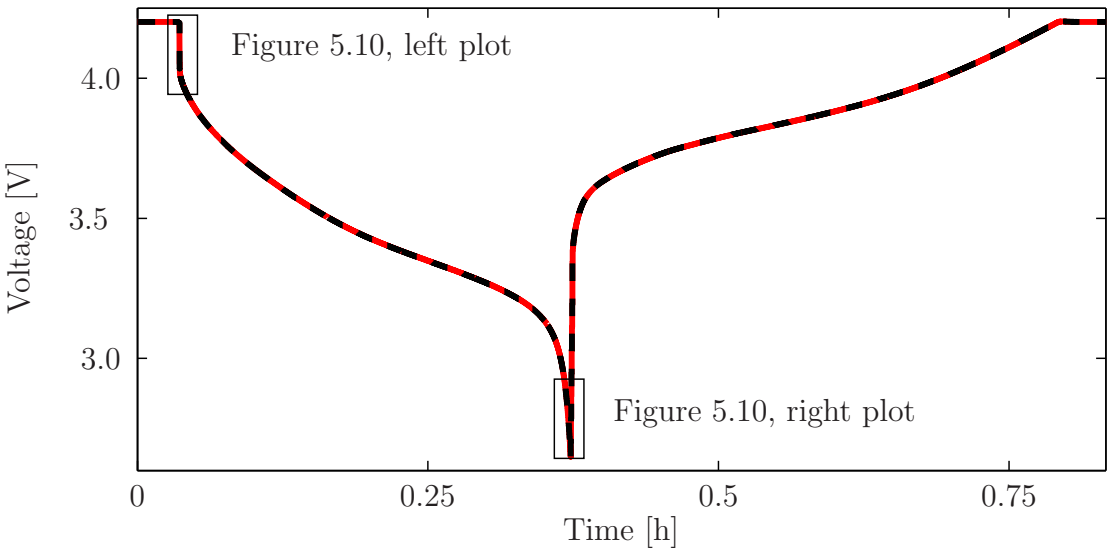

Figure 5.9: Comparison of measured (continuous red curve) and observed (dotted black curve) voltages for non-aged accumulator

always fulfills the rank criterion, the system is fully observable. After determining the dominating eigenmotion of the process model, the observer gain matrix $\mathbf{L}$ is designed accordingly to the pole placement method [Lun08].

The error dynamics (residual r, constituted by the comparison of the measured and observed terminal voltages) are considered as an indicator for deterioration progression.

For validation purpose, the results for a non-aged accumulator with observer are shown in Figure 5.9. The solid, red colored line describes the measured terminal voltage, where the dotted, black line depicts the observer result.

The numerically relevant dynamics are detailed in Figure 5.10, namely switching from charging to discharging (Figure 5.10, left plot) and vice versa (Figure 5.10, right plot).

For the non-aged accumulator, the residual r is depicted in Figure 5.13. The two peaks at the switching point from charging to discharging reveal two relevant information. First, the negative peak reveals the step height of the voltage drop and thus, an information about the actual ohmic resistance. Ideally, the voltage drop is small and so the negative drop is. The subsequent counter peak reveals the speed of the observer in order to vanish the residual. This second peak is ideally equal to zero which, in theory, can be obtained by speeding up the eigenvalues (moving further to the left) of the observed system. In reality, the overshoot of the negative peak increases simultaneously to faster eigenvalues. Thus, this measure is counterproductive for the first peak.

The results for the same but aged accumulator are shown in Figures 5.11 and 5.12. As detailed above, the voltage drop at switching from charging to discharging is more pronounced than for the non-aged state. Thus, the calculated voltage progression diverges from the real progression which results in a significantly different error progression (residual) which in turn reveals information about the state-of-deterioration.

The idea is to use the strengths of an observer, based on directly measurable, deterio-

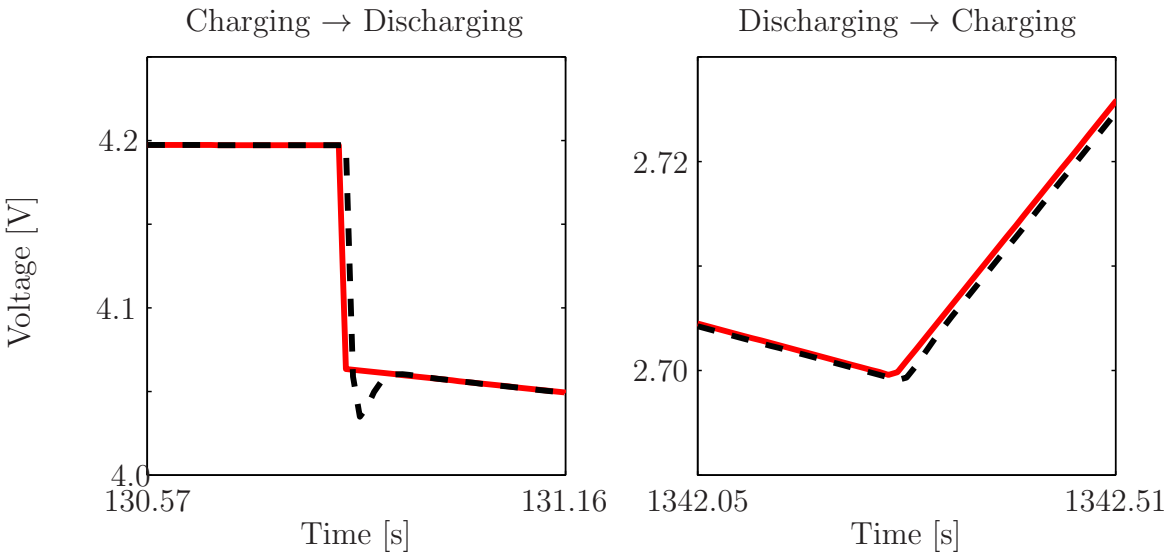

Figure 5.10: Details of relevant dynamics for non-aged accumulator

ration-effected physical properties, in combination with a subsequent signal-based decision making. This method is practicable as it can be applied during operation of the accumulator without connecting any additional measurement devices.

The second couple of peaks at the switching from discharging to charging reveals the same information but the other way round: first, a positive peak is obtained, as the real voltage suddenly raises. This is subsequently compensated by the observer, again in dependency on the designed eigenmotions. The same holds true for the above mentioned challenge of overshoot. Therefore, a balance between speed and damping is found by placing the eigenvalues two times faster than the dominating eigenvalues of $\mathbf{A}$.

In Figure 5.14, the correlation between two, independently from each other derived information about the state-of-deterioration are depicted. The blue curve denotes the progression of the actual capacity C_a (measured by ampere counting method after each 30 consecutive aging cycles), approximated by linear interpolation between the discrete values. After slightly increasing at the first intervals (formation phase), a constant capacity loss (negative, constant gradient) is observed. At approximately 250 cycles, the wear-out phase is entered and the degradation increases disproportionately. The actual capacity drops below the critical capacity of 8Ah (= 0% SoH).

Independent of the capacity measurement, similar deterioration information are obtained by the model-based fault detection. The depicted residual progression is obtained by stringing together the first peak due to varying ohmic resistance (Figure 5.13) of each aging cycle. The envelope of this peaks is depicted as the bold black curve and constantly increases until the same characteristic point of 250 cycles. Short before that point, the curve characteristic changes from a linear to a exponential shape. As the end of life is reached (SoH = 0%), the absolue value of the residual is approxemately 0.32V.

In the simplest case, the actual state-of-deterioration is obtained by performing the proposed peak current measurements at fully charged condition and observing the residual. As

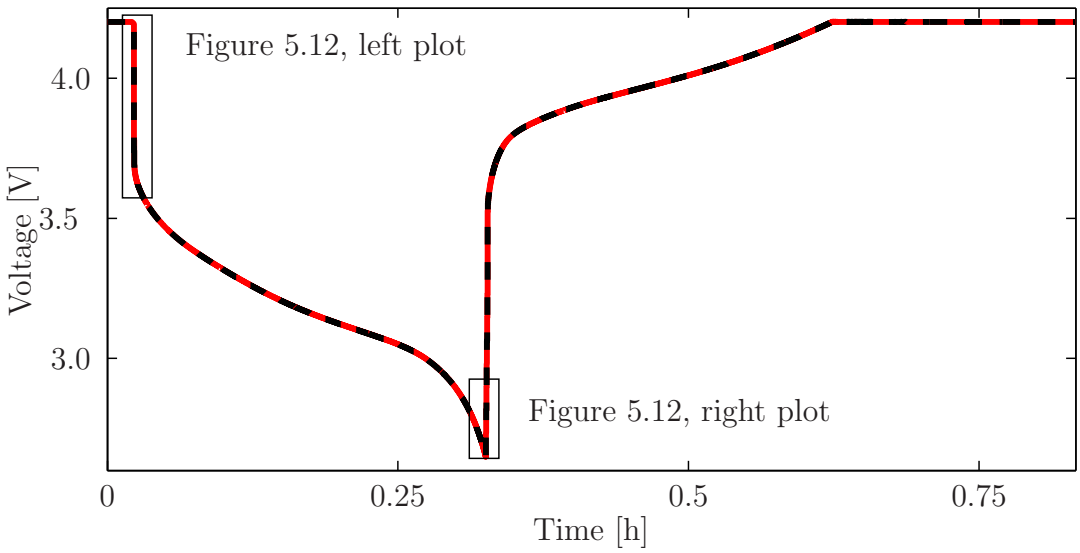

Figure 5.11: Comparison of measured (continuous red curve) and observed (dotted black curve) voltages for aged accumulator

demonstrated, the residual behaves inversely proportional to the SoH (defined as the ration between actual and nominal capacity) and is thus, applicable for deterioration investigations.

In summary, the proposed mathematical model, describing continuously the deterioration-depended behavior of the considered accumulator, in combination with an appropriately designed model-based fault detection method (observer) is capable of describing the voltage curve due to a charging and discharging current. Furthermore, the obtained residual reveals information about the chosen eigenvalues of the observer (dynamic, overshoot) as well as the state-of-deterioration (voltage drop due to changed, ohmic resistance) of the accumulator. The relevant physical parameters can easily be measured by standard sensors and specially designed test cycles in order to validate the method. Since only the nominal capacity C_{n} is relevant for the observer-based on-line fault detection, the time-consuming measurement of the actual capacity C_{a}, as described in Section 5.2.3, is obsolete. Nevertheless, this information will additionally be provided in the subsequent modules in order to validate this assumption.

5.4 Module 2: Confidence Check

As stated in Section 3.4, module 2 plays a minor role for this particular system as the deterioration (capacity fade) is measurable. Hence, module 2 is less important in this context and only serves as a plausibility check whether or not the measured and observed deterioration progressions coincide.

The distribution of the initially measured ohmic resistance (and hence feature) is depicted in Figure 5.15.

Although the tested cells originate from the same batch, differences in the physical parameters are measured. The test specimen are chosen such that the scattering is relatively small.

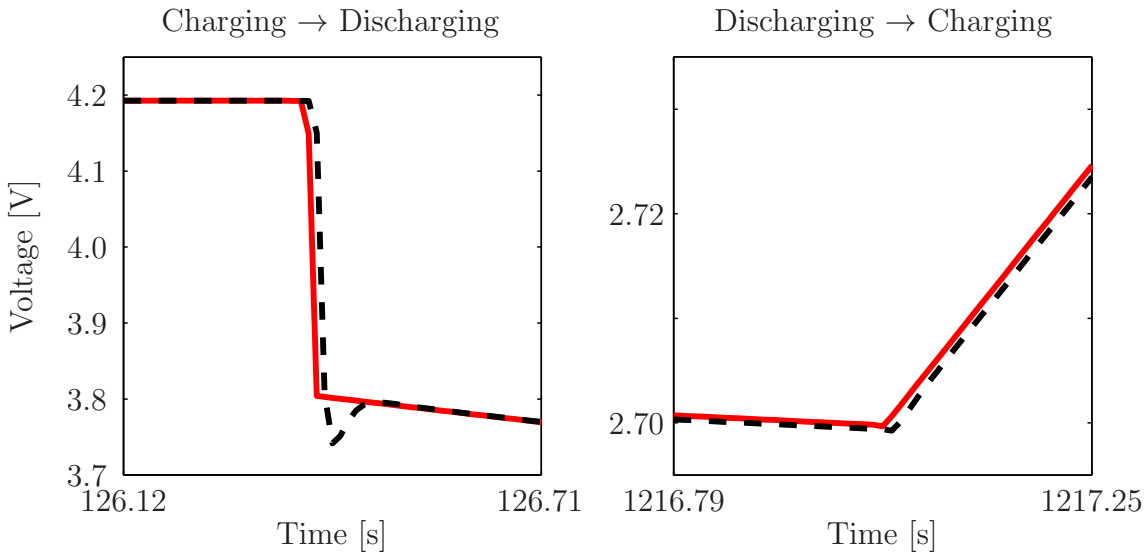

Figure 5.12: Details of relevant dynamics for aged accumulator

In the sequel, the individual initial properties are considered during the result discussion in Sections 5.5.2 and 5.5.3.

5.5 Module 3: SoH Progression

The purpose of module 3 is to evaluate the qualitative effect of manifold operational parameters on the deterioration by experimentally investigate the deterioration behavior of the considered system by appropriate tests.

In order to reduce the test amount to a minimum, the test matrix for the relevant operation region is stated first. Subsequently, the proposed test are performed and the results, obtained by measurement and numerical approximation are discussed.

5.5.1 Design of Experiment

For this particular system, the variety of independent operational parameters and their effect on the deterioration is the major challenge to solve. Since the operation of an accumulator (discharge current, discharge time, partial state of charge cycling, ambient and/or cell temperature, etc.) varies within a wide range, only the constant and externally controllable operational parameters are varied in the following, namely: end of discharge voltage U_{EoD}, end of charge voltage U_{EoC}, and charge current I_{C}. These relevant operational parameters are investigated and modified in a targeted manner. All other parameters remain unchanged and constant.

A geometric interpretation of the sub-space, spanned by the investigated relevant operational parameters, is depicted in Figure 5.16. As the accumulator shows a non-linear deterioration character, the deterioration progression cannot be determined by measuring the deterioration with operational parameters at boundary values solely. Instead, the subspace is again divided into meaningful partial sub-spaces. The subdivision is realized based

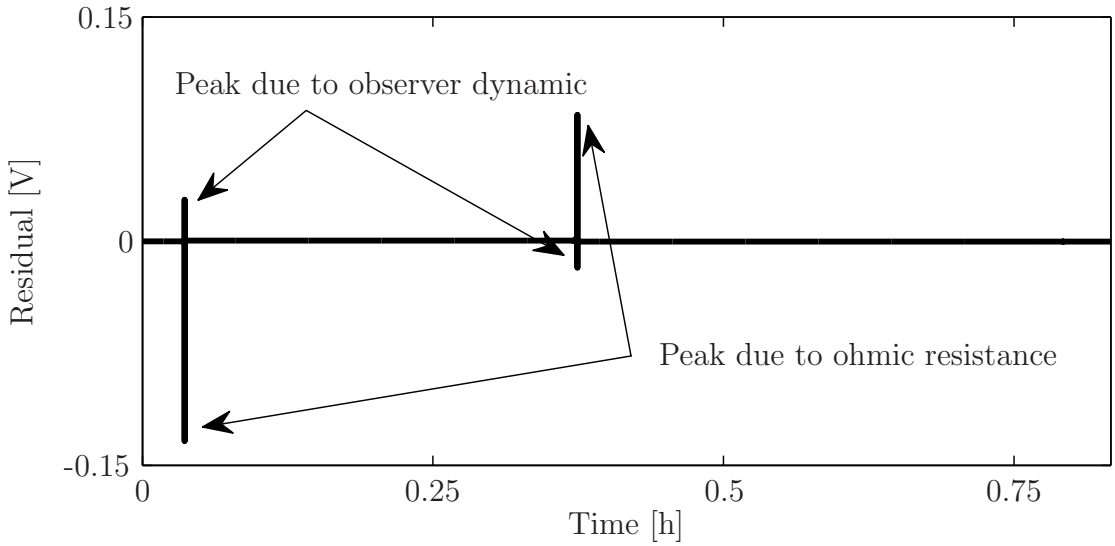

Figure 5.13: Feature progression (residual r)

End of Discharge Voltage [V]	U_{EoD}	2.65	2.70
End of Charge Voltage [V]	U_{EoC}	4.20	4.25
Charge Current [A]	I_{C}	15	20
Normalized Factors	x_i	-1	$+1$

Table 5.2: Operational parameters and assignment to normalized factors

on observed field-relevant usage profiles (accumulation of parameter constellations). These constellations are depicted in Figure 5.16 as red points within the cuboid.

As no field data are available, it is assumed that the accumulator will be charged as fast as possible (high charging current I_{C}) to the maximum possible end of charge voltage U_{EoC} and discharged as far as possible to the minimum possible end of discharge voltage U_{EoD}. Thus, the region of densest accumulation of relevant operational parameter constellations is limited and given in Table 5.2.

This relevant partial sub-space is depicted in detail in Figure 5.17. Within this sub-sub-space, it is assumed that the deterioration behavior can be approximated by deterioration information from measurement results at boundary values $x_i = -1$ and $x_i = +1$.

The designed test sequence consists of the measurement of relevant deterioration information and the subsequent aging of the cell. The primer information are the nominal capacity C_{n} (before first aging cycle) and actual capacities C_{a} (after each aging cycles), respectively. Furthermore, the physical parameters C_{p}, R_{p}, and R_{o} are determined by appropriate measurements as described in Section 5.2.3. The aging cycles are realized by 30 complete discharge and subsequent charge profiles.

Each cell is tested with constant operational parameters for the complete sequence. The test procedure is performed five times in order to age each cell with 150 discharge-charge profiles. Accordingly, six measurements of relevant deterioration information are obtained.

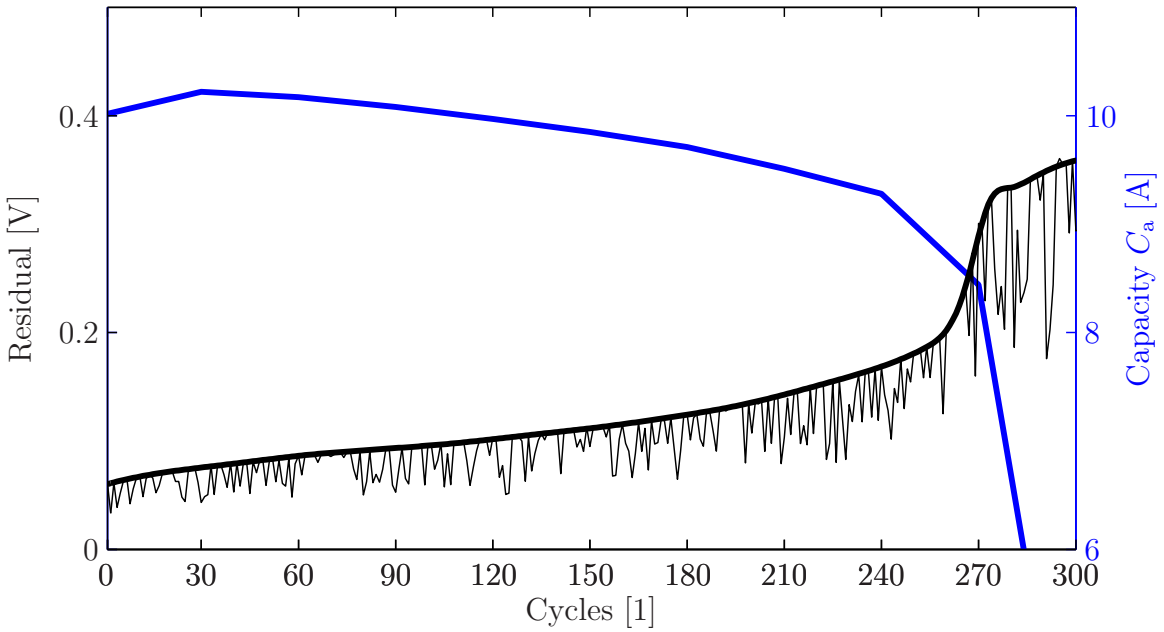

Figure 5.14: Correlation of calculated model-based fault detection result (residual) and measured capacity loss

As three independent operational parameters are chosen, eighth cells are tested for their deterioration behavior due to the individual operation. The test matrix with the cell number assignment (according to Figure 5.17) and normalized factors is given in Table 5.3.

5.5.2 Results

First results for three cells of the test procedure are depicted in Figure 5.18, namely for cell 2 (minimal degradation), cell 6 (average degradation), and cell 7 (maximum degradation).

In accordance with Figure 5.14, the blue curve corresponds the progression of the actual capacity C_a. Here, the capacity is expressed in terms of the state of charge (see Section 5.1.1) and thus, as a ratio of the actual and the nominal capacity in percent. The bold black curve denotes the envelope of the feature progression, adjusted by the individual, initial value, Figure 5.15.

The deterioration behavior of all cells reveals a similar behavior. First, the formation phase takes place (SEI film, see Section 5.1.3) and the actual capacity slightly increases (during first 30 aging cycles). Subsequently, a constant capacity loss is obtained. In dependency on the chosen operational parameters, the wear-out phase is entered (cell 7) and the capacity fades rapidly and thus, fails.

The results for all tested cell are given in Table 5.4.

In the second column, the nominal capacity before aging is listed, followed by the actual capacity after aging. The resulting state of charge after aging is given in the forth column. Finally, the adjusted feature for deterioration estimation is listed in the last column.

The table entries with more than 100% of capacity signify an increased actual capacity for the particular cell. Thus, these cells are not significantly aged by the corresponding

Cell Number	Operational Parameters			Normalized Factors		
	U_{EoD} [V]	U_{EoC} [V]	I_{C} [A]	x_1	x_2	x_3
1	2.65	4.20	15	-1	-1	-1
2	2.70	4.20	15	$+1$	-1	-1
3	2.65	4.25	15	-1	$+1$	-1
4	2.70	4.25	15	$+1$	$+1$	-1
5	2.65	4.20	20	-1	-1	$+1$
6	2.70	4.20	20	$+1$	-1	$+1$
7	2.65	4.25	20	-1	$+1$	$+1$
8	2.70	4.25	20	$+1$	$+1$	$+1$

Table 5.3: Test matrix with cell number assignment, operational parameters, and normalized factors

Cell Number	$C_{\mathrm{n}}(0)$ [Ah]	$C_{\mathrm{a}}(150)$ [Ah]	SoC [%]	Δr [10^{-2}V]
1	9.97	10.07	105.02	4.92
2	9.83	9.96	106.61	4.79
3	10.01	9.85	92.01	6.01
4	10.03	9.62	79.56	11.79
5	10.01	9.83	71.21	6.13
6	9.90	9.80	94.95	5.85
7	10.45	8.61	11.96	22.84
8	10.24	10.18	97.07	5.64

Table 5.4: Results of test procedure

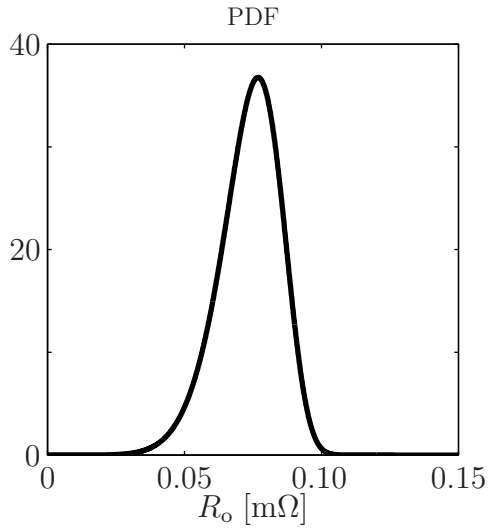

Figure 5.15: Distribution of initial ohmic resistance

operational parameters but formed a stable SEI film. These cells deteriorate much slower than the other tested cells.

A graphical overview about the test results is depicted in Figure 5.19. The values at the tested operational parameter sets correspond to the state of charge after aging.

5.5.3 Discussion

Following the RSM methodology, introduced in Section 2.6.2, the operational parameters are normalized in order to estimate the response surface

$$x_1 = \frac{U_{\mathrm{EoD}} - 2.675\mathrm{V}}{0.025\mathrm{V}}\,, \qquad x_2 = \frac{U_{\mathrm{EoC}} - 4.225\mathrm{V}}{0.025\mathrm{V}}\,, \text{and} \qquad x_3 = \frac{I_{\mathrm{C}} - 17.5\mathrm{A}}{2.5\mathrm{A}}\,. \tag{5.11}$$

A first-order polynomial relation from Equation (2.33) is applied and parameterized by the algorithm of least squares. The resulting response is hence obtained as

$$y = 82.30 + 12.25x_1 - 12.15x_2 - 13.50x_3\,. \tag{5.12}$$

For the maximization of the response, the x_1 (end of discharge voltage U_{EoD}) should be increased. The factors x_2 (charge current I_{C}) and x_3 (end of charge voltage U_{EoC}) should be decreased. The greatest impact on the deterioration is realized by factor x_3. For practical purpose, high charge currents at a high state of charge should be avoided as these may occur during energy harvesting (recuperation).

5.6 Summary and Discussion

The amount of energy that can be fed to or withdrawn from an accumulator decreases with time and usage (cycle number). The chemical processes are various and stochastically distributed in time and space. A common simplification is to observe the irreversible change

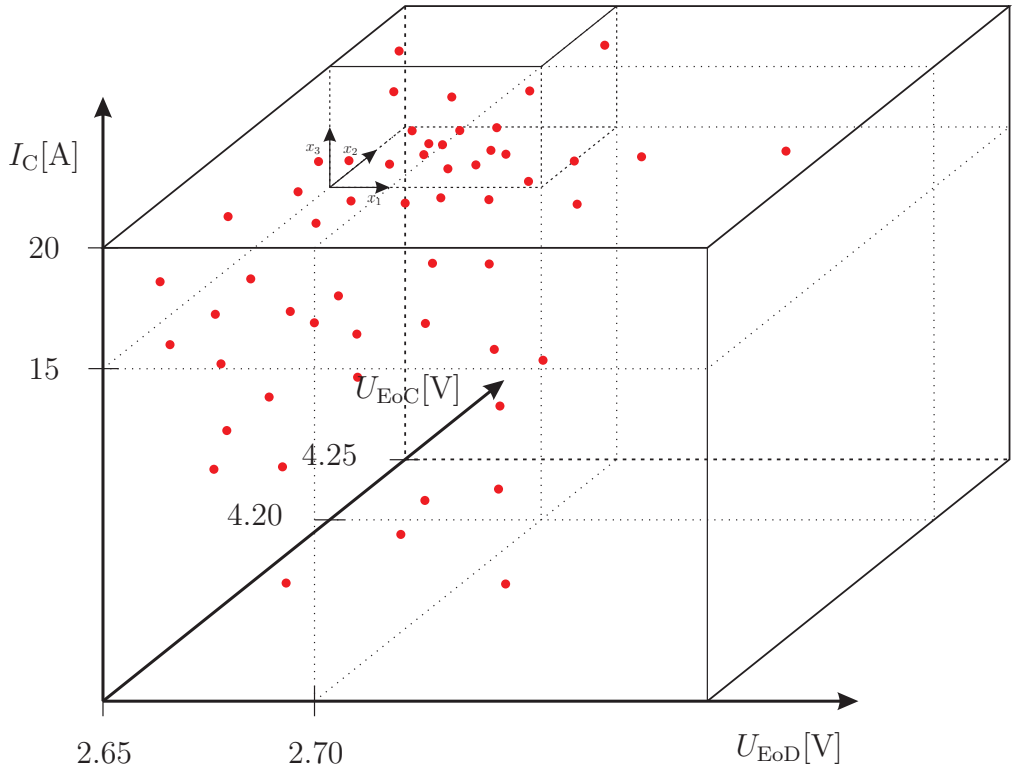

Figure 5.16: Graphical representation of investigated parameter sub-space, spanned by U_{EoD}, U_{EoC}, and I_C

of the ohmic resistance, as this property corresponds to the degree and rate of deterioration [SHWG05]. This phenomenon was observed experimentally by the developed test rig and used for a deterioration estimation algorithm. By using an observer for fault detection in combination with measured, deterioration-effected physical parameters, a simple but effective method was found that describes the effect of individual operational parameters on the deterioration progression.

Relevant information about tested and non-tested operational parameter sets and their contribution to the deterioration within the considered sub-space of possible constant operational parameters were found. The method is so far validated for constant operational parameters. The particular contribution of composed loading will need to be investigated in future research work by taking into account varying additional relevant operational parameters, different/additional parameters, etc. The idea is to derive information about switching (varying) operational parameters on the aging and hence further information about varying operation. Here, further investigations with decreased maximum charging current can be processed, as this factor was found to have the greatest impact on deterioration. By enlarging the database and thus the heuristic knowledge about accumulator aging, the accuracy of the optimal operational parameter set is refined.

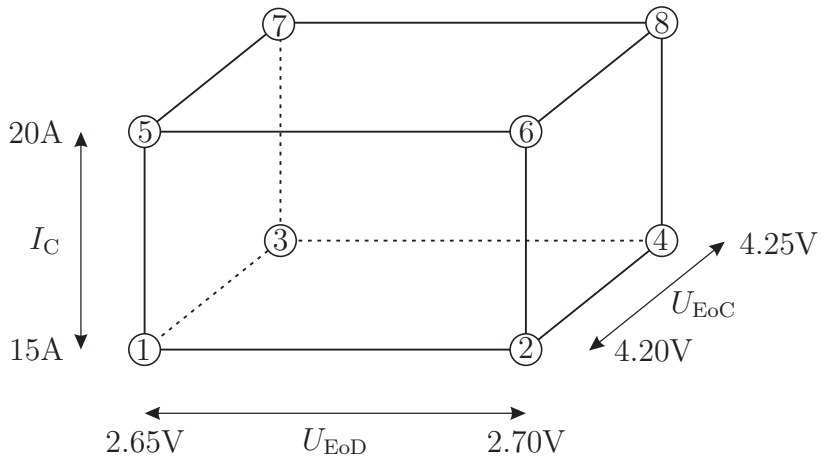

Figure 5.17: Partial sub-space of operational parameters

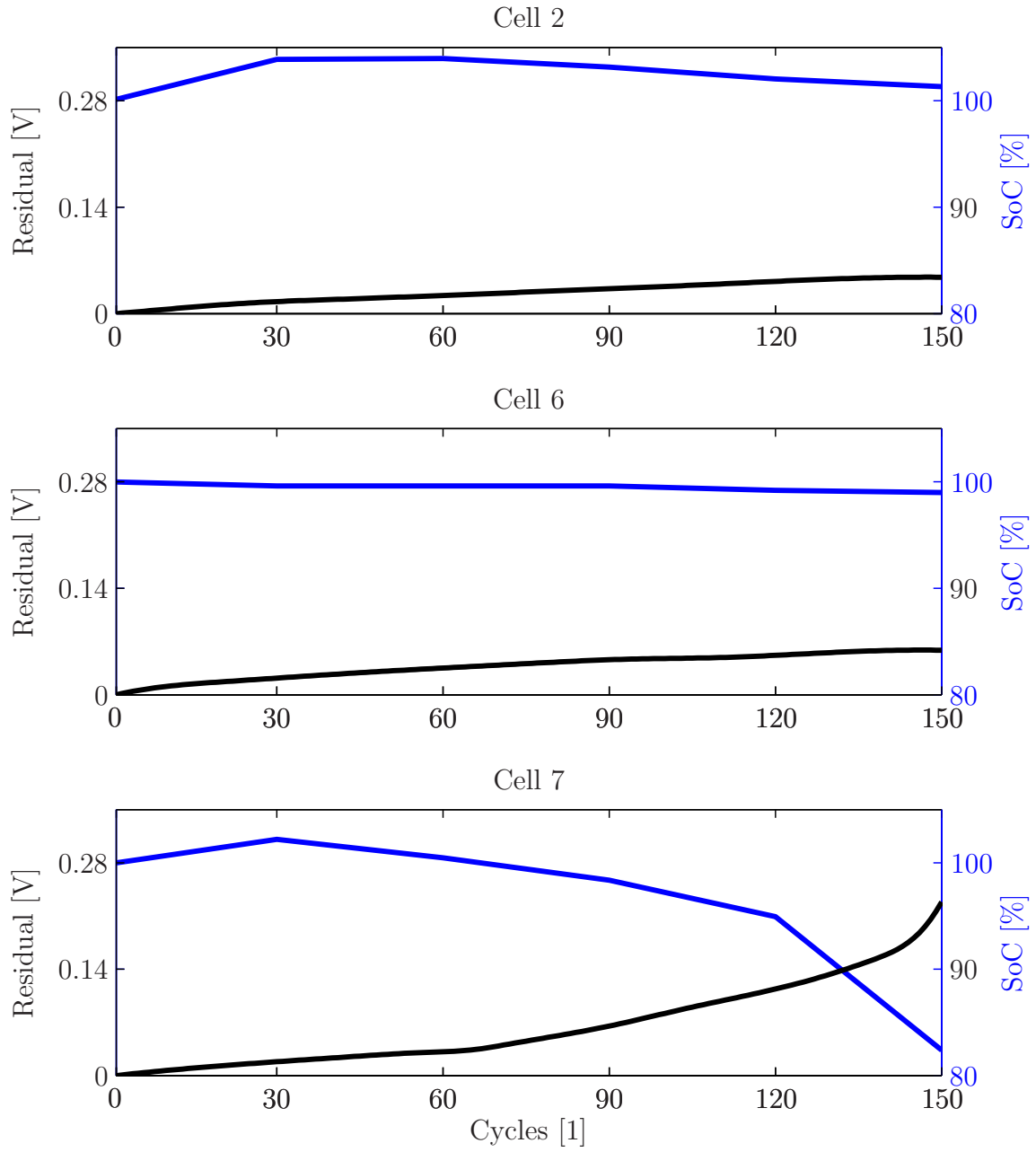

Figure 5.18: Capacity fade due to different operational parameter sets

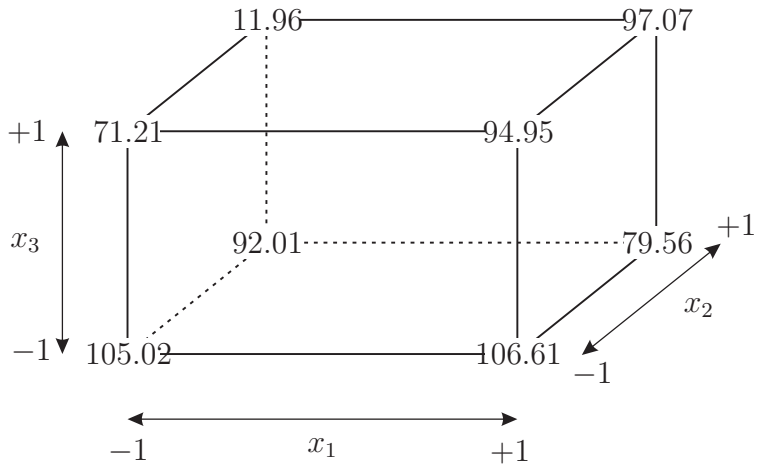

Figure 5.19: Partial sub-space of operational parameters

6 Summary and Outlook

The goal of this thesis was to realize and detail the descriptive Safety and Reliability Control Engineering Concept (SRCE), developed in [RS96, SR97], as there is a demand for an adaptive compromise between safety and reliability. After introducing reliability-related, relevant definitions with a special focus on probabilistic aspects, common ideas on fault detection, fault diagnosis, and fault prognosis are briefly discussed. Based on the SRCE concept and preliminary works on that [Wol08], the single modules for a reliability-centered operation of an arbitrary system are developed and discussed in detail.

The application of the developed modules constitutes the core of this thesis; application examples are introduced and discussed in Chapter 4 for a mechanical system failing due to mechanical wear (abrasive wear) and in Chapter 5 for an electro-chemical system failing due to capacity fade. In Chapter 4, the main focus is on the novel, developed measurement chain and the related evaluation of deterioration-inherent quantities. As the deterioration process is highly non-linear, solely signal-based fault detection and diagnosis approaches are discussed and appropriate, deterioration-specific countermeasures for reliability improvements are shown. In Chapter 5, a model-based fault detection and diagnosis strategy is developed and novel aspects for appropriate deterioration countermeasures are detailed.

6.1 Summary

The central scientific contributions of this thesis are summarized in the following:

- In order to operate the system within a required (minimum) reliability margin, the deterioration progression due to prospective operation has to be quantified. In addition with the actual state-of-deterioration, various scenarios for remaining useful life can be derived and used for appropriate lifetime control strategies. Therefore, traditional and novel SHM approaches are briefly introduced at the beginning of this thesis. The research goes on to describe the so far missing step towards using health information for controlling the remaining lifetime by changing specific operation parameters. Based on the Safety and Reliability Control Engineering concept and preliminary works on that, a novel method, which extends the strategies known from literature, is introduced. The single modules are introduced in detail. In particular, the challenging aspect of using deterioration-affected measurands to draw conclusions about the actual state-of-deterioration is detailed. Furthermore, the adaptive, probabilistic-based deterioration model realizes the continuously adaptive, time-variant, probabilistic correlation between deterioration-proportional information and the most probable deterioration. From this correlation, information about the remaining useful life can be derived. As a direct consequence of the obtained deterioration estimations, appropriate strategies can be developed to modify the operation of the systems (by limiting disproportionately high damaging situations, proposing alternative strategies, etc.).

- The adaptive probabilistic-based deterioration model realizes the continuously adaptive, time-variant, probabilistic correlation between deterioration-proportional information and the most probable deterioration. As a direct consequence of the obtained deterioration estimations, appropriate strategies for modifying the operation of the systems (by limiting disproportionately high damaging situations, proposing alternative strategies, etc.) are derived and proposed.

- The failure due to wear of an industrial machine is investigated. According to the results of a detailed material analysis, three main tribological mechanisms which lead to failure were identified. For investigation purposes, a test rig which reproduces the main wear effects was presented and a novel measuring chain based on the direct piezoelectric effect for acoustic emission sensing was developed and operated. The FPGA compatible filter, which realizes the signal analysis, was introduced and an adequate visualization method was developed to indicate regions and severeness of stochastically occurring wear. Several comparable wear tests were performed for the most typical material and lubrication combination, and the result was presented. A high correlation between the point of failure and the measured deterioration-equivalent signal was shown. Under normal operation conditions, the deterioration can be estimated within sufficient probabilistic limits.

- The challenge of estimating the accumulator deterioration and proposing optimal usage (in terms of phase-specific operational parameters) with the help of independent parameters and non-stationary operation in field usage is demonstrated and solved by appropriate on-line capable methods. The developed database is realized with a minimum number of required test runs. A common simplification is to observe the irreversible change of the ohmic resistance, as this property corresponds to the degree and rate of deterioration. This phenomenon was observed experimentally by the developed test rig and used for a deterioration estimation algorithm. By using an observer for fault detection in combination with measured, deterioration-effected physical parameters, a simple but effective method was found that describes the effect of individual operational parameters on the deterioration progression. Relevant information about tested and non-tested operational parameter sets and their contribution to the deterioration within the considered sub-space of possible constant operational parameters were found. The method is so far validated for constant operational parameters.

This thesis widens the preliminary work by novel aspects of appropriate strategies for addressing and improving systems' reliability. Additionally, the conceptual ideas of the SRCE concept are brought into practice for the first time.

6.2 Outlook on Future Work

Further research should focus on

- the application of the developed algorithms and approaches on further test specimens. The development of a comprehensive data base for both test systems (considering variable operational conditions, etc.) is required in order to further detail and validate the proposed correlations.
- the further improvement of the acoustic emission sensor by developing a housed piezoelectric ceramic in order to reduce the effort of calibration and impedance measurement. The integration of the proposed admittances (piezoelectric ceramic, impedance converter, transmission lines, etc.) in the FPGA ensures the signal quality and facilitates the correlation of characteristic frequency contents with individual failure modes.
- the variable operation of accumulators, especially depending on the actual state-of-deterioration. It is with a view to this proposed application in particular that the possible improvement realized by the Response Surface Model-based module 3 can be demonstrated. The goal is to obtain information about the effect of varying operational parameters on the aging process and, in turn, further information about the effect varying operation modes have on the lifetime. Here, further investigations with decreased maximum charging current may be useful, as this factor was found to have the greatest impact on deterioration.

References

[AB09] D. Astapenko and L. M. Bartlett. System design optimisation involving phased missions. *International Journal of Reliability and Safety*, 3(4):331–344, 2009.

[Abe05] R. B. Abernethy. *The new Weibull handbook. Reliability & statistical analysis for predicting life, safety, survivability, risk, cost and warranty claims.* Abernethy, North Palm Beach, Florida, USA, 4th edition, 2005.

[ACL+01] K. Amine, C. H. Chen, J. Liu, M. Hammond, A. Jansen, D. Dees, I. Bloom, D. Vissers, and G. Henriksen. Factors responsible for impedance rise in high power lithium ion batteries. *Journal of Power Sources*, 97–98:684–687, 2001.

[Arc53] J. F. Archard. Contact and rubbing of flat surfaces. *Journal of applied physics*, 24(8):981–988, 1953.

[AST90] American society for testing and materials. Standard terminology for nondestructive examinations. E 1316-90, 1990.

[Aus96] D. M. Auslander. What is mechatronics? *IEEE/ASME Transaction on Mechatronics*, 1(1):5–9, 1996.

[Ban09] D. Banjevic. Remaining useful life in theory and practice. *Metrika*, 69(2–3):337–349, 2009.

[Bar05] E. Barsoukov. *Impedance spectroscopy. Theory, experiment, and applications.* Wiley-Interscience, Hoboken, New Jersey, 2nd edition, 2005.

[BB10] K. G. Budinski and M. K. Budinski. *Engineering materials: properties and selection.* Pearson, Upper Saddle River, NJ u.a., 9. edition, 2010.

[BBB+05] M. Broussely, P. Biensan, F. Bonhomme, P. Blanchard, S. Herreyre, K. Nechev, and R. J. Staniewicz. Main aging mechanisms in Li ion batteries. *Journal of Power Sources*, 146(1-2):90–96, 2005.

[BBHF07] M. Barbezat, A. J. Brunner, C. Huber, and P. Flüeler. Integrated active fiber composite elements: characterization for acoustic emission and acousto-ultrasonics. *Journal of Intelligent Material Systems and Structures*, 18:515–525, 2007.

[BCL+05] H. Bindner, T. Cronin, P. Lundsager, J. F. Manwell, U. Abdulwahid, and I. Baring-Gould. Lifetime modelling of lead acid batteries. Technical report, Risø National Laboratory, 2005.

[BCS+01] I. Bloom, B. W. Cole, J. J. Sohn, S. A. Jones, E. G. Polzin, V. S. Battaglia, G. L. Henriksen, C. Motloch, R. Richardson, T. Unkelhaeuser, D. Ingersoll, and H. L. Case. An accelerated calendar and cycle life study of Li-ion cells. *Journal of Power Sources*, 101(2):238–247, 2001.

[BDHH07] G. E. P. Box, N. R. Draper, W. G. Hunter, and J. S. Hunter. *Response surfaces, mixtures and ridge analyses*. Wiley series in probability and statistics. J. Wiley & Sons, Hoboken, NJ, 2nd edition, 2007.

[Bel98] D. E. Bell. *Decision making: descriptive, normative, and prescriptive interactions*. Cambridge University Press, Cambridge, 1998.

[Bes05] H. W. Bester. Untersuchung des Verschleißes von Riffelblechen - UB 050905-1. Technical report, Institute of Product Engineering, University of Duisburg-Essen, 2005.

[Bes07] H. W. Bester. Untersuchung des Verschleißes von Riffelblechen - UB 230407-1. Technical report, Institute of Product Engineering, University of Duisburg-Essen, 2007.

[BFG06] D. Balageas, C. P. Fritzen, and A. Guemes. *Structural health monitoring*. ISTE, London, 2006.

[BHH05] G. E. P. Box, J. S. Hunter, and W. G. Hunter. *Statistics for experimenters: design, innovation, and discovery*. Wiley series in probability and statistics. Wiley-Interscience, Hoboken, New Jersey, 2nd edition, 2005.

[BIMP04] C. Bonivento, A. Isidori, L. Marconi, and A. Paoli. Implicit fault tolerant control: Application to induction motors. *Automatica*, 40(3):355–371, 2004.

[Bis94] C. M. Bishop. Neural networks and their applications. *Review of scientific instruments, RSI*, 65(6):1803–1832, 1994.

[BKLS06] M. Blanke, M. Kinnaert, J. Lunze, and M. Staroswiecki. *Diagnosis and Fault-Tolerant Control*. Springer-Verlag Berlin Heidelberg, 2nd edition, 2006.

[BM91] R. J. Boness and S. L. McBride. Adhesive and abrasive wear studies using acoustic emission techniques. *Wear: an international journal on the science and technology of friction, lubrication and wear*, 149(1–2):41–53, 1991.

[BMFF11] S. Bashash, S. J. Moura, J. C. Forman, and H. K. Fathy. Plug-in hybrid electric vehicle charge pattern optimization for energy cost and battery longevity. *Journal of Power Sources*, 196(1):541–549, 2011.

[BMS90] R. J. Boness, S. L McBride, and M. Sobczyk. Wear studies using acoustic emission techniques. *Tribology International*, 23(5):291–295, 1990.

[BSM+07] R. Bornatico, A. Storti, L. Mandrioli, A. Zappavigna, Y. Guezennec, and G. Rizzoni. NiMH battery characterization and state-of-charge estimation for HEV applications. *ASME Conference Proceedings*, 2007(43106):205–214, 2007.

[BSMM05] I. N. Bronstein, K. A. Semendjajew, G. Musiol, and H. Mühlig. *Taschenbuch der Mathematik*. Harri Deutsch, 6th edition, 2005.

[BW51] G. E. P. Box and K. B. Wilson. On the experimental attainment of optimum conditions. *Journal of the Royal Statistical Society. Series B (Methodological)*, 13(1):1–45, 1951.

[CH10] H. Czichos and K.-H. Habig. *Tribologie-Handbuch. Tribometrie, Tribomaterialien, Tribotechnik*. Vieweg Teubner, Wiesbaden, 3. edition, 2010.

[CFC06] E. Castillo and A. Fernández-Canteli. A parametric lifetime model for the prediction of high-cycle fatigue based on stress level and amplitude. *Fatigue & Fracture of Engineering Materials & Structures*, 29(12):1031–1038, 2006.

[Coi01] D. W. Coit. Cold-standby redundancy optimization for nonrepairable systems. *IIE Transactions*, 33(6):471–478, 2001.

[CSGR06] Z. Chehab, L. Serrao, Y. Guezennec, and G. Rizzoni. Aging characterization of nickel metal hydride batteries using electrochemical impedance spectroscopy. In *ASME International Mechanical Engineering Congress and Exhibition*, 2006.

[CT65] J. W. Cooley and J. W. Tukey. An algorithm for the machine calculation of complex fourier series. *Mathematicas of Computation*, 19:297–301, 1965.

[CV05] J. Chiasson and B. Vairamohan. Estimating the state of charge of a battery. *IEEE Transactions on Control Systems Technology*, 13(3):465–470, 2005.

[DAS06] D. Doerffel and S. Abu Sharkh. A critical review of using the peukert equation for determining the remaining capacity of lead-acid and lithium-ion batteries. *Journal of Power Sources*, 155(2):395–400, 2006.

[DIN 1313] Fundamental technical standards committee. Quantities (DIN 1313:1998), 1998.

[DIN 1319] Fundamental technical standards committee. Fundamentals of metrology - Part 1: Basic terminology (DIN 1319-1), 1995.

[DIN 6344] Tools and clamping devices standards committee. Coated abrasives - grain size analysis - Part 3: Determination of grain size distribution of microgrits P 240 to P 2500 (ISO 6344-3:1998), 2000.

[DIN 50321-1] German commission for electrical, electronic and information technologies of DIN and VDE. piezoelectric properties of ceramic materials and components - Part 1: Terms and definitions; German version EN 50324-1:2002, 2002.

[DIN 50321-3] German commission for electrical, electronic and information technologies of DIN and VDE. piezoelectric properties of ceramic materials and components - Part 3: Methods of measurement; high power; German version EN 50324-3:2002, 2002.

[DIN EN 1330] Materials testing standards committee. Non-destructive testing - Terminology DIN EN 1330, 1998-2010.

[DIN EN 60254] German commission for electrical, electronic and information technologies of DIN and VDE. Lead-acid traction batteries - Part 1: General requirements and methods of tests (IEC 60254-1:2005); German version EN 60254-1:2005, 2006.

[DIN EN 61078] CES-TK 56 dependability, fiabilité et maintenabbilité. Analysis techniques for dependability - Reliability block diagram and boolean methods (IEC 61078:2006), 2006.

[DS82] S. D. Downing and D. F. Socie. Simple rainflow counting algorithms. *International Journal of Fatigue: Materials, Structures, Components*, 4(1):31–40, 1982.

[DS09] K.-U. Dettmann and D. Söffker. Classification of wear phenomena by specific ultrasonic emission detection for prognostic purposes. In *Annual Conference of the Prognostics and Health Management Society, PHM*, San Diego (CA, USA), 2009.

[DW92] S.-H. Dai and M.-O. Wang. *Reliability analysis in engineering applications*. Van Nostrand Reinhold (NY, USA), 1992.

[EN 13306] Fundamental technical standards committee. Maintenance terminology; trilingual version EN 13306:2010, 2010.

[FCGC01] A. Fei, J. Cui, M. Gerla, and D. Cavendish. A dual-tree scheme for fault-tolerant multicast. In *IEEE International Conference on Communications, ICC*, volume 3, pp. 690–694, 2001.

[FK01] S. Fouvry and P. Kapsa. An energy description of hard coating wear mechanisms. *Surface & coatings technology*, 138(2–3):141–148, 2001.

[FK06] C.-P. Fritzen and M. Klinkov. Online force identification with robust observers. In *VDI-Berichte, Band 1941*, pp. 303–312, 2006.

[FK09] C.-P. Fritzen and P. Krämer. Self-diagnosis of smart structures based on dynamical properties. *Mechanical systems and signal processing (MSSP)*, 23(6):1830–1845, 2009.

[FLK+03] S. Fouvry, T. Liskiewicz, Ph. Kapsa, S. Hannel, and E. Sauger. An energy description of wear mechanisms and its applications to oscillating sliding contacts. *Wear: an international journal on the science and technology of friction, lubrication and wear*, 255(1):287–298, 2003.

[Fra10] J. Fraden. *Handbook of modern sensors. Physics, designs, and applications.* AIP Press, Melville, (NY, USA) 3rd edition, 2010.

[Fri05] C.-P. Fritzen. Vibration-based structural health monitoring - concepts and applications. *Key Engineering Materials*, Damage Assessment of Structures VI (Volumes 293–294):3–20, 2005.

[Fri10] C.-P. Fritzen. *Structural health monitoring*, volume 1, chapter 2, pp. 45–224. ISTE Publishing Company, London, U. K., 2010.

[GfT] Gesellschaft für Tribologie e. V. (GfT). Tribologie Definitionen, Begriffe, Prüfung. Technical Report 7, Aachen, 2002.

[GGQ] Deutsche Gesellschaft für Qualität e. V. (DGQ). *Das Lebensdauernetz - Leitfaden zur grafischen Bestimmung von Zuverlässigkeitskenngrößen der Weibull-Verteilung.* Band 17–26. Beuth Verlag; Berlin, Wien, Zürich, 1st edition, 1995.

[GLGP08] F. García Lorca and M. García-Posada. *Obra completa.* Universidad Pontificia De Salamanca, Tres Cantos, 2nd edition, 2008.

[GR10] J. Gausemeier and F. Rammig. *Entwurf mechatronischer Systeme.* Number 272 in HNI-Verlagsschriftenreihe. Heinz-Nixdorf-Institut, Paderborn, 2010.

[Gro11] Group Five - Advanced Materials & Technology. Actual list of industrial cells. online, http://kokamdirect.com/, July 2011.

[Gue08] R. M. Guedes. Creep and fatigue lifetime prediction of polymer matrix composites based on simple cumulative damage laws. *Composites, Part A: Applied Science and Manufacturing*, 39(11):1716–1725, 2008.

[HDS10] D. Hockmann, K.-U. Dettmann, and D. Söffker. Merkmalsbasierte Zustandsbeschreibung werkstoffseitiger Verschleißzustände. In *3. Tagung des DVM-Arbeitskreises: Zuverlässigkeit mechatronischer und adaptronischer Systeme*, pp. 93–102, Darmstadt (Germany), 2010.

[Hen55] D. L. Henry. A theory of fatigue-damage accumulation in steel. *Transaction of the ASME*, 77(6):913–917, 1955.

[HH86] W. Hwang and K. S. Han. Cumulative damage models and multi-stress fatigue life prediction. *Composite Materials*, 20(2):125–153, 1986.

[HH09] L. Hollmotz and M. Hackmann. Lithium-Ionen Batterien: Anforderungen und Risiken beim Einsatz aus dem Blickwinkel der Kraftfahrzeugsicherheit. *Innovativer Kfz-Insassen- und Partnerschutz - VDI-Tagung Fahrzeugsicherheit*, 7:101–114, 2009.

[HK91] J. Hanchi and B. E. Klamecki. Acoustic emission monitoring of the wear process. *Wear: an international journal on the science and technology of friction, lubrication and wear*, 145(1):1–27, 1991.

[Hol79] J. O. Holmen. *Fatigue of concrete by constant and variable amplitude loading*. University of Trondheim, Institute of Technology, Norway, 1979.

[Hol82] J. O. Holmen. Fatigue of concrete by constant and variable amplitude loading. In S. P. Shah, editor, *Fatigue of concrete structures*, volume 75, pp. 71–110, 1982.

[HS09] F. Heidtmann and D. Söffker. Virtual sensors for diagnosis and prognosis purposes in the context of elastic mechanical structures. *Sensors Journal, IEEE*, 9(11):1577–1588, 2009.

[HWHB09] S. O. Han, K. Wolf, H. Hanselka, and T. Bein. Sensitivity evaluation of adaptive systems with respect to scattering design and environment parameters. In *VDI-Berichte 2065*, pp. 145–155. Fraunhofer-Institut für Betriebsfestigkeit und Systemzuverlässigkeit (LBF), Darmstadt, VDI-Verlag, 2009.

[IEC 60050-191] German commission for electrical, electronic and information technologies of DIN and VDE. International electrotechnical vocabulary - chapter 191: Dependability and quality of service (IEC 50(191):1990), 1994.

[IEC 60050-486] German commission for electrical, electronic and information technologies of DIN and VDE. International electrotechnical vocabulary - part 486: Secondary cells and batteries (IEC 50(486):1991), 1994.

[Ike90] T. Ikeda. *Fundamentals of piezoelectricity*. Oxford science publications. Oxford University Press, 1990.

[Ise99] R. Isermann. *Mechatronische Systeme: Grundlagen*. Springer, Berlin [u. a.], 1999.

[Ise06] R. Isermann. *Fault diagnosis systems: an introduction from fault detection to fault tolerance*. Springer Berlin Heidelberg, 2006.

[IVA90] *Journal of Vibration and Acoustics*. American Society of Mechanical Engineers (ASME) and American Institute of Physics (AIP), since 1990.

[JBS+04] H. Janocha, S. Butzmann, H. D. Stölting, W. Backé, and A. Klein. *Actuators: basics and applications*. Springer, Berlin, 1st edition, 2004.

[Jon09] K. Jonas. *Online-Alterungsdiagnose und belastungsabhängige Lebensdauerprognose von Polymerelektrolyt-Brennstoffzellen*. Dissertation, Technische Universität Dresden, Professur für Energiesystemtechnik und Wärmewirtschaft, Düsseldorf, VDI-Verlag, 2009.

[JW06] A. Jossen and W. Weydanz. *Moderne Akkumulatoren richtig einsetzen*. Reichardt, Untermeitingen, 1st edition, 2006.

[Kal60] R. E. Kalman. On the general theory of control systems. *IRE Transactions on Automatic Control*, 4(3):481–493, 1960.

[Kas06] K. Kashi. *Development of a Fault Diagnosis System for an Active Roll Control System using Observers and Virtual Sensors*. Dissertation, Chair of Dynamics and Control (SRS), Department of Mechanical Engineering, Faculty of Engineering Sciences, University of Duisburg-Essen, Duisburg, Germany, 2006.

[KBSM09] M. Keller, P. Birke, M. Schiemann, and U. Möhrstädt. Lithium ion battery development for hybrid and electrical vehicle. *ATZ-Elektronik*, 4(2):16–23, 2009.

[Kha02] H. K. Khalil. *Nonlinear systems*. Prentice Hall, Upper Saddle River, NJ, 3rd edition, 2002.

[Kim10] I.-S. Kim. A technique for estimating the state of health of lithium batteries through a dual-sliding-mode observer. *IEEE Transactions on Power Electronics*, 25(4):1013–1022, 2010.

[KRC+10] U. Krupp, I. Roth, H. J. Christ, M. Kübbeler, and C.-P. Fritzen. In situ SEM observation and analysis of martensitic transformation during short fatigue crack propagation in metastable austenitic steel. *Advanced Engineering Materials*, 12(4):255–261, 2010.

[LLO11] H. Li, J. Liu, and J. Ou. Seismic response control of a cable-stayed bridge using negative stiffness dampers. *Structural Control and Health Monitoring*, 18:265–288, 2011.

[LMWK01] J. Li, E. Murphy, J. Winnick, and P. A. Kohl. Studies on the cycle life of commercial lithium ion batteries during rapid charge-discharge cycling. *Journal of Power Sources*, 102(1–2):294–301, 2001.

[LSSM10] A. Ling, C. Shantz, S. Sankararaman, and S. Mahadevan. Stochastic characterization and update of fatigue loading for mechanical damage prognosis. In *Annual Conference of the Prognostics and Health Management Society*, 2010.

[Lue64] D. G. Luenberger. Observing the state of a linear system. *IEEE Transactions on Military Electronics*, 8(2):74–80, 1964.

[Lun08] J. Lunze. *Regelungstechnik 2: Mehrgrößensysteme, Digitale Regelung*. Springer-Verlag Berlin Heidelberg, 5th edition, 2008.

[LYY93] S. Lingard, C. W. Yu, and C. F. Yau. Sliding wear studies using acoustic emission. *Wear: an international journal on the science and technology of friction, lubrication and wear*, 162–164(1):597–604, 1993.

[ME68] M. Matsuishi and T. Endo. Fatigue of metals subjected to varying stress. *Japan Society of Mechanical Engineering*, 1968.

[MEC02] Q. W. Meeker, L. A. Escobar, and V. Chan. *Using accelerated tests to predict service life in highly variable environments*, chapter 19, pp. 396–413. American Chemical Society, 2002.

[MFSF09] S. J. Moura, J. Forman, J. L. Stein, and H. K. Fathy. Control of film growth in lithium ion battery packs via switches. 2nd Annual Dynamic Systems and Control Conference, DSCC, 2009.

[MIL-HDBK] Military handbook - Reliability prediction of electronic equipment MIL-HDBK-217F. U. S. Department of Defense. Technical report, 1991.

[MIL-STD] Military handbook - Standard practice for system safety MIL-STD-882D. U. S. Department of Defense. Technical report, 2000.

[MIL-NSWC] Handbook of reliability prediction procedures for mechanical equipment NSWC-06. Logistics technology support group, carderock division, naval surface warfare center (CDNSWC). Technical report, 2006.

[Min45] M. A. Miner. Cumulative damage in fatigue. *Journal of Applied Mechanics*, 12(3):159–164, 1945.

[MM10] H. Ma and W. Q. Meeker. Strategy for planning accelerated life tests with small sample sizes. *IEEE Transactions on Reliability*, 59(4):610–619, 2010.

[MMS+03] N. K. Myshkin, L. V. Markova, M. S. Semenyuk, H. Kong, H.-G. Han, and E.-S. Yoon. Wear. *14th International Conference on Wear of Materials*, 255(7-12):1270–1275, 2003.

[Mon09] D. C. Montgomery. *Design and analysis of experiments*. Wiley, Hoboken, NJ, 7th edition, 2009.

[Mor05] C. Moraga. *Data Driven Fuzzy Modelling with Neural Networks*, volume 179 of *Studies in Fuzziness and Soft Computing*, chapter 1, pp. 153–164. Springer Berlin Heidelberg, 2005.

[MS54] S. M. Marco and W. L. Starkey. A concept of fatigue damage. *Transaction of the ASME*, 76(4):626–662, 1954.

[MvKM05] R. K. Miller, E. v. Kill, and P. O. Moore. *Acoustic emission testing*. American Society for Nondestructive Testing, 2005.

[MXJ04] D. N. P. Murthy, M. Xie, and R. Jiang. *Weibull models*. New York: Wiley, 2004.

[MZD03] B. Moreno, J. Zapatero, and J. Domínguez. An experimental analysis of fatigue crack growth under random loading. *International Journal of Fatigue*, 25(7):597–608, 2003.

[Nac05] J. A. Nachlas. *Reliability engineering. probabilistic models and maintenance methods*. Taylor & Francis, Boca Raton u. a., 2005.

[Nel01] O. Nelles. *Nonlinear System Identification*. Springer, Berlin, 2001.

[NF99] M. Nagode and M. Fajdiga. The influence of variable operating conditions upon the general multi-modal weibull distribution. *Reliability engineering & system safety*, 64(3):383, 1999.

[Oza09] K. Ozawa. *Lithium ion rechargeable batteries*. Wiley-VCH, 2009.

[Özb10] M. Özbek. *Modeling, Simulation, and Concept Studies of a Fuel Cell Hybrid Electric Vehicle Powertrain*. Dissertation, Chair of Dynamics and Control (SRS), Department of Mechanical Engineering, Faculty of Engineering Sciences, University of Duisburg-Essen, Duisburg, Germany, 2010.

[Pal24] A. Palmgren. Die Lebensdauer von Kugellagern. *VDI-Z*, 68(14):339–341, 1924.

[PFKN09] C. Papadimitriou, C. P. Fritzen, P. Kraemer, and E. Ntotsios. Fatigue lifetime estimation in structures using ambient vibration measurements. In M. Papadrakakis, N. D. Lagaros, and M. Fragiadakis, editors, *ECCOMAS Thematic Conference on Computational Methods in Structural Dynamics and Earthquake Engineering (COMPDYN)*, 2009.

[PI11] PI Ceramic. Typical parameters of piezoelectric ceramics. Internet resource http://www.piceramic.com/, 2011.

[Pic07] N. Picciano. Battery aging and characterization of nickel metal hydride and lead acid batteries. Master's thesis, Center for Automotive Research, Department of Mechanical Engineering, Ohio State University, 2007.

[Poh03] J. Pohl. *Zerstörungsfreie Charakterisierung adaptiver CFK-Piezokeramik-Verbunde: konventionelle Verfahren und health monitoring*. Habilitation, Fakltät für Maschinenbau, Institut für Werkstoff- und Fügetechnik, Otto-von-Guericke-Universität Magdeburg, 2003.

[Rai09] G. B. Raines, editor. *Electric vehicles. technology, research, and development*. Nova Science Publishers Inc, New York, 2009.

[Ram03] P. Ramadass. Mathematical modeling of the capacity fade of Li-ion cells. *Journal of Power Sources*, 123(2):230–240, 2003.

[Ran47] J. E. Randles. Kinetics of rapid electrode reactions. *Discussions Of The Faraday Society*, 1:11–19, 1947.

[RBM+10] J. Remmlinger, M. Buchholz, M. Meiler, P. Bernreuter, and K. Dietmayer. State-of-health monitoring of lithium-ion batteries in electric vehicles by on-board internal resistance estimation. *Journal of Power Sources*, 196(12):5357–5363, 2010.

[RDS10] J. Ravelin, K.-U. Dettmann, and D. Söffker. Examinations classifying wear states using signal-based approaches. In *Gordon Reserarch Conference on Tribology - Challenges at the Buried Interface*, 2010.

[RH04] M. Rausand and A. Høyland. *System reliability theory. Models, statistical methods, and applications*. Wiley series in probability and statistics applied probability and statistics. Wiley-Interscience, Hoboken, NJ, 2nd edition, 2004.

[RHG+04] P. Ramadass, B. Haran, P. M. Gomadam, R. White, and B. N. Popov. Development of first principles capacity fade model for Li-ion cells. *Journal of The Electrochemical Society*, 151(2):A196–A203, 2004.

[RLB+01] A. G. Ritchie, B. Lakeman, P. Burr, P. Carter, P. N. Bames, and P. Bowles. *Battery degradation and ageing*, chapter 5, pp. 523–527. New York: Kluwer Academic/Plenum Publishers, 2001.

[RMC+07] M. R. Raupach, G. Marland, P. Ciais, C. Le Quéré, J. G. Canadell, G. Klepper, and C. B. Field. Global and regional drivers of accelerating CO_2 emissions. In *Proceedings of the National Academy of Sciences of the United States of America*, volume 104, pp. 10288–10293, 2007.

[RS96] U. K. Rakowsky and D. Söffker. Verknüpfung von Methoden der Regelungstheorie und der Technischen Zuverlässigkeit zur Modellierung dynamischer Systeme. *VDI Berichte*, 1282:753–763, 1996.

[Run10] A. Runge. Modellierung der Lebensdauer von Systemen. Master's thesis, Institut für Mathematik, Universität Potsdam, 2010.

[San08] M. Sander. *Sicherheit und Betriebsfestigkeit von Maschinen und Anlagen. Konzepte und Methoden zur Lebensdauervorhersage*. Springer, Berlin u. a., 2008.

[SCGR05] L. Serrao, Z. Chehab, Y. Guezennee, and G. Rizzoni. An aging model of Ni-MH batteries for hybrid electric vehicles. pp. 78–85, 2005.

[SCW+09] M. Sternad, M. Cifrain, D. Watzenig, G. Brasseur, and M. Winter. Condition monitoring of lithium-ion batteries for electric and hybrid electric vehicles. *e & i. Elektrotechnik und Informationstechnik*, 126(5):186–193, 2009.

[SFH+04] H. Sohn, C. R. Farrar, F. M. Hemez, D. D. Shunk, S. W. Stinemates, B. R. Nadler, and J. J. Czarnecki. A Review of Structural Health Monitoring Literature form 1996-2001. Report. Los Alamos National Laboratory report LA-13976-MS (2004).

[SG08] B. Saha and K. Goebel. Uncertainty management for diagnostics and prognostics of batteries using bayesian techniques. pp. 1–8, 2008.

[SG09] B. Saha and K. Goebel. Modeling Li-ion battery capacity depletion in a particle filtering framework. In *Annual Conference of the Prognostics and Health Management Society, PHM*, 2009.

[SGPC09] B. Saha, K. Goebel, S. Poll, and J. Christophersen. Prognostics methods for battery health monitoring using a bayesian framework. *IEEE Transactions on Instrumentation and Measurement*, 58(2):291–296, 2009.

[SH87] T. Shimokawa and Y. Hamaguchi. Statistical evaluation of fatigue life and fatigue strength in circular-hole notched specimens of a carbon eight-harness-satin/epoxy laminate. *Statistical research on fatigue and fracture*, A88-51351 22–39:159–176, 1987.

[Shu02] P. J. Shull. *Nondestructive evaluation: theory, techniques, and applications*. Mechanical engineering; 142. Marcel Dekker, Inc., New York, Basel, 2002.

[SHWG05] A. T. Stamps, C. E. Holland, R. E. White, and E. P. Gatzke. Analysis of capacity fade in a lithium ion battery. *Journal of Power Sources*, 150:229–239, 2005.

[SLWW02] J. Y. Song, H. H. Lee, Y. Y. Wang, and C. C. Wan. Two- and three-electrode impedance spectroscopy of lithium-ion batteries. *Journal of Power Sources*, 111(2):255–267, 2002.

[SR97] D. Söffker and U. K. Rakowsky. Perspectives of monitoring and control of vibrating structures by combining new methods of fault detection with new approaches of reliability engineering. In *12th ASME Conference on Reliability, Stress Analysis and Failure Prevention*, pp. 671–682, April 1997.

[SRA+08] A. Saltelli, M. Ratto, T. Andres, F. Campolongo, J. Cariboni, D. Gatelli, M. Saisana, and S. Tarantola. *Global sensitivity analysis. The primer*. John Wiley & Sons, Chichester, England; Hoboken, NJ, 2008.

[SSB+07] J. Schiffer, D. U. Sauer, H. Bindner, T. Cronin, P. Lundsager, and R. Kaiser. Model prediction for ranking lead-acid batteries according to expected lifetime in renewable energy systems and autonomous power-supply systems. *Journal of Power Sources - 10th European Lead Battery Conference*, 168(1):66–78, 2007.

[SW08] D. U. Sauer and H. Wenzl. Comparison of different approaches for lifetime prediction of electrochemical systems - using lead-acid batteries as example. *Journal of Power Sources*, 176(2):534–546, 2008.

[Sye10] A. Syed. Limitations of Norris-Landzberg equation and application of damage accumulation based methodology for estimating acceleration factors for pb free solders. In *11th International Conference on Thermal, Mechanical Multi-Physics Simulation, and Experiments in Microelectronics and Microsystems, (EuroSimE)*, pp. 1–11, 2010.

[TEKP10] J. Tichý, J. Erhart, E. Kittinger, and J. Prívratská. *Fundamentals of Piezoelectric Sensorics. Mechanical, Dielectric, and Thermodynamical Properties of Piezoelectric Materials*. Springer-Verlag, Berlin, Heidelberg, 2010.

[TSG08] U. Tietze, C. Schenk, and E. Gamm. *Electronic circuits: Handbook for design and application*. Springer, Berlin, 2nd edition, 2008.

[VDI 3452] VDI/VDE-society measurement and automation. Safety terms for automation systems - Qualitative terms and definitions VDI/VDE 3542 Blatt 1, 2000.

[VDI 4008] VDI society product and process design. Conditions and applicational preferences of reliability analyses VDI 4008, 1998.

[Vez10] A. Vezzini. Elektrofahrzeuge: Mobilität und erneuerbare Energie. *Physik in unserer Zeit*, 41:36–42, 2010.

[VNW+05] J. Vetter, P. Novák, M. R. Wagner, C. Veit, K.-C. Möller, J. O. Besenhard, M. Winter, M. Wohlfahrt-Mehrens, C. Vogler, and A. Hammouche. Ageing mechanisms in lithium-ion batteries. *Journal of Power Sources*, 147(1–2):269–281, 2005.

[VPB07] A. Vasebi, M. Partovibakhsh, and S. M. Taghi Bathaee. A novel combined battery model for state-of-charge estimation in lead-acid batteries based on extended Kalman filter for hybrid electric vehicle applications. *Journal of Power Sources*, 174(1):30–40, 2007.

[WDB04] K. Worden and J. M. Dulieu-Barton. An overview of intelligent fault detection in systems and structures. *Structural Health Monitoring, SHM*, 3(1):85–98, 2004.

[Wei51] W. Weibull. A statistical distribution function of wide applicability. *Journal of Applied Mechanics*, 18(3):239–297, 1951.

[Whi87] R. M. White. A sensor classification scheme. *Ferroelectrics and Frequency Control, IEEE Transactions on Ultrasonics*, 34(2):124–126, 1987.

[WM04] M. Wohlfahrt-Mehrens. Aging mechanisms of lithium cathode materials. *Journal of Power Sources*, 127(1–2):58–64, 2004.

[Wöh70] A. Wöhler. Über die Festigkeitsversuche mit Eisen und Stahl. *Zeitschrift für Bauwesen XX*, 20:73–106, 1870.

[Wol08] K. Wolters. *Formalismen, Simulation und Potenziale eines nutzungsoptimierenden Zuverlässigkeitskonzepts*. Dissertation, Chair of Dynamics and Control (SRS), Department of Mechanical Engineering, Faculty of Engineering Sciences, University of Duisburg-Essen, Duisburg, Germany, 2008.

[WS04] K. Wolters and D. Söffker. The SRCE concept - a probabilistic avoidance of failures. In *Proceedings of the IAR Annual Meeting*, pp. 229–234, 2004.

[WS05] K. Wolters and D. Söffker. The potential of the safety and reliability control engineering concept as framework for reliability based utilization strategies. In F. K. Chang, editor, *Proceedings of the 5th International Workshop on Structural Health Monitoring, SHM*, pp. 1353–1360, 2005.

[WZX09] X. Wei, B. Zhu, and W. Xu. Internal resistance identification in vehicle power lithium-ion battery and application in lifetime evaluation. In *Proceedings of the 2009 International Conference on Measuring Technology and Mechatronics Automation*, volume 3, pp. 388–392, Washington, D.C., USA, 2009.

[YPL96] P. Young, S. Parkinson, and M. Lees. Simplicity out of complexity in environmental modelling - Occam's razor revisited. *Journal of applied statistics*, 23(2–3):165–210, 1996.

[ZHD+00] D. Zhang, B. S. Haran, A. Durairajan, R. E. White, Y. Podrazhansky, and B. N. Popov. Studies on capacity fade of lithium-ion batteries. *Journal of Power Sources*, 91(2):122–129, 2000.

[ZW08] Q. Zhang and R. E. White. Capacity fade analysis of a lithium ion cell. *Journal of Power Sources*, 179(2):793–798, 2008.

Im Rahmen von Forschungs- und Projektarbeiten im Lehrstuhl SRS wurden von Dr.-Ing. Kai-Uwe Dettmann und Univ.-Prof. Dr.-Ing. Dirk Söffker die nachstehenden Studien-, Diplom-, Bachelor-, Projekt- und Masterarbeiten inhaltlich betreut, wobei Bestandteile und Ergebnisse aus den Forschungs- und Projektarbeiten sowie den studentischen Qualifikationsarbeiten wechselseitig in die jeweiligen Arbeiten und somit auch in diese Promotionsarbeit eingeflossen sind.

[Don08] F. Dong. Design and comparison of nonlinear control methods for a hydraulic servo system with simulation study of force tracking. Master thesis, Chair of Dynamics and Control (SRS), Department of Mechanical Engineering, Faculty of Engineering Sciences, University of Duisburg-Essen, Duisburg, Germany, 2008.

[EJ09] B. Egenolf Jonkmanns. Grundlagenbetrachtung für die Erfassung verschleißcharakteristischer Ultraschallsignale mittels geeigneter Piezokeramiken. Master thesis, Chair of Dynamics and Control (SRS), Department of Mechanical Engineering, Faculty of Engineering Sciences, University of Duisburg-Essen, Duisburg, Germany, 2009.

[Esc09] S. Esch. Signalanalyse von Ultraschallsignalen zur Extraktion von Schädigungsphänomenen. Projektarbeit, Chair of Dynamics and Control (SRS), Department of Mechanical Engineering, Faculty of Engineering Sciences, University of Duisburg-Essen, Duisburg, Germany, 2009.

[Jin11] X. Jin. Parametrierung von Akkumulatoralterungsmodellen mittels experimentell bestimmter Kenngrößen. Diplomarbeit, Chair of Dynamics and Control (SRS), Department of Mechanical Engineering, Faculty of Engineering Sciences, University of Duisburg-Essen, Duisburg, Germany, 2011.

[Rav11] J. Ravelin. Klassifikation von Schleißblechzuständen anhand der auftretenden Verschleißerscheinungsformen. Bachelor thesis, Chair of Dynamics and Control (SRS), Department of Mechanical Engineering, Faculty of Engineering Sciences, University of Duisburg-Essen, Duisburg, Germany, 2011.

[Sac10] O. Sacher. Programmierung von Auswertealgorithmen auf einer FPGA-Messdatenanalysehardware mittels Matlab/Simulink und toolboxen. Studienarbeit, Chair of Dynamics and Control (SRS), Department of Mechanical Engineering, Faculty of Engineering Sciences, University of Duisburg-Essen, Duisburg, Germany, 2010.

[Xu10] X. Xu. Simulation von Batterielebensdauermodellen. Diplomarbeit, Chair of Dynamics and Control (SRS), Department of Mechanical Engineering, Faculty of Engineering Sciences, University of Duisburg-Essen, Duisburg, Germany, 2010.

[Zha08] M. Zhang. Identification of time-invariant discrete and continuous mathematical systems in Matlab/Simulink. Master thesis, Chair of Dynamics and Control (SRS), Department of Mechanical Engineering, Faculty of Engineering Sciences, University of Duisburg-Essen, Duisburg, Germany, 2008.